UNIVERSITY OF PARDUBICE

FACULTY OF CHEMICAL TECHNOLOGY

Doctoral Dissertation

2023 MSc. Hamza Aboelanin

UNIVERSITY OF PARDUBICE

FACULTY OF CHEMICAL TECHNOLOGY

INSTITUTE OF CHEMISTRY AND TECHNOLOGY OF MACROMOLECULAR MATERIALS

Synthesis and Characterization of Branched Polymers

PhD DISSERTATION

Author: M.Sc. Hamza Mahmoud Ahmed Mahmoud Aboelanin

Supervisor: Prof. Ing. Štěpán Podzimek, CSc.

2023

AUTHOR'S DECLARATION

I declare:

The thesis entitled Synthesis and Characterization of Branched Polymers is my own work. All literary sources and information that I used in the thesis are referenced in the bibliography.

I have been acquainted with the fact that my work is subject to the rights and obligations arising from Act No. 121/2000 Sb., On Copyright, on Rights Related to Copyright and on Amendments to Certain Acts (Copyright Act), as amended, especially with the fact that the University of Pardubice has the right to conclude a license agreement for the use of this thesis as a school work under Section 60, Subsection 1 of the Copyright Act, and that if this thesis is used by me or a license to use it is granted to another entity, the University of Pardubice is entitled to request a reasonable fee from me to cover the costs incurred for the creation of the work, depending on the circumstances up to their actual amount.

I acknowledge that in accordance with Section 47b of Act No. 111/1998 Sb., On Higher Education Institutions and on Amendments to Other Acts (Higher Education Act), as amended, and the Directive of the University of Pardubice No. 7/2019 Rules for Submission, Publication and Layout of Theses, as amended, the thesis will be published through the Digital Library of the University of Pardubice.

In Pardubice on ……...

Hamza Aboelanin

ACKNOWLEDGEMENT

Supporting of Faculty of Chemical Technology, University of Pardubice are gratefully acknowledged.

Here I would like to express my deepest and sincere gratitude to my supervisor Prof. Ing. Štěpán Podzimek, CSc., for professional guidance of my work. I have to thank him for the continuous scientific advice and life experience. I would thank all colleagues from Department Material Analytics and Characterization group under supervision Dr. Robert Brüll at Fraunhofer Institute for Structural Durability and System Reliability LBF, Darmstadt, Germany.

I would like to thank, of course my parents for everything that I am and other friends who gave me during my studies constantly help and support. Thanks to my wife Samah Asharf for her immense patience and emotional support.

Special thanks go to Dr. Tibor Macko who learned and helped me a lot during my training and work at the Fraunhofer Institute for Structural Durability and System Reliability LBF in Darmstadt, Germany. Also special thanks to Ing. Vladimír Špaček, CSc., head of Testing and Evaluation department in SYNPO, CZ, for supporting and guiding me in the preparation of all-star-like samples.

It was an honour to be granted this opportunity to work in UPCE, I am thankful for all that was given and for all that I have taken. I thank you all for the support and generosity that had helped me so much.

SUMMARY

This thesis is concerned with the separation and characterization of the molar mass and molar mass distribution and molecular structure in details of different types of branched polymers (methacrylate branched polymers and polyolefins). It is divided into two basic chapters. Each chapter contains the synthetic route and characterization methods for all obtained branched polymers.

Chapter 1 focuses on the preparation of two types of methacrylate's branched polymers. The first type is star-branched methacrylate polymer which was prepared by group transfer polymerization in tetra hydro furan (THF) as a solvent. While the second type linear methacrylate's short chain branching polymers was prepared by solution-free radical polymerization in toluene as solvent. The specific refractive index increment for some of the prepared star-branched and linear methacrylate samples were determined in THF at 25 °C using a refractive index (RI) detector Optilab T-rEX operating at 660 nm. The molar mass and molar mass distributions, and branching studies for all the prepared methacrylate's branched polymers were determined by size exclusion chromatography with a multi-angle light scattering detector DAWN NEON, an RI detector Optilab NEON and an online viscometer ViscoStar NEON.

Chapter 2 is mainly dedicated to the monitoring of the chemical composition distribution of polyolefins. The separation and monitoring methyl (CH_3–) and methylene (–CH_2–) groups of series of ethylene/1-alkene and ethylene-propylene-diene copolymers (polyolefins) by high temperature-size exclusion chromatography with a filter-based infrared detector (IR5). Many plots of ratio of CH_3/CH_2 against the molar masses were created and investigated. The correlation between the ratio of CH_3– to –CH_2– groups and the average chemical composition of the investigated series of polymer samples as well as the reproducibility of the measurements and the limit of detection of the SEC-IR5 measurements are evaluated.

Table of Contents

LIST OF TABLES

LIST OF FIGURES

LIST OF ABBREVIATIONS AND SYMBOLS

MMA	Methyl methacrylate
BMA	Butyl methacrylate
BZMA	Benzyl methacrylate
LMA	Lauryl methacrylate
2-EHMA	2-Ethyle hexyl methacrylate
EGDMA	Ethylene glycol dimethacrylate
THF	Tetra hydro furane
AIBN	Azobisisobutyronitrile
TMS	Trimethylsilyl
SKA	Silyl ketone acetal
t-BuAAc	Tertiary butylammonium acetate
PO	Polyolefins
LDPE	Linear density polyethylene
HDPE	High density polyethylene
PE	Polyethylene
PP	Polypropylene
EPDM	Ethylene-propylene-diene-monomer
ENB	Ethylidene norbornene
TCB	1,2,4-trichlorobenzene
PS	Polystyrene
EP	Ethylene propylene
ZN	Ziegler-Natta
EH	Ethylene/Hexene copolymer
EB	Ethylene/Butene copolymer
GTP	Group Transfer Polymerization
MI	Macroinitiator
GPC	Gel Permeation Chromatography
SEC	Size Exclusion Chromatography
HT SEC	High-temperature Size Exclusion Chromatography
A4F	Asymmetric flow field-flow fractionation
MALS	Multi-angle light scattering
Visco	Viscosity detector

RI	Refractive index
IR	Infrared
TREF	Temperature Rising Elution Fractionation
CRYSTAF	Crystallization Analysis Fractionation
CEF	Crystallization Elution Fractionation
FTIR	Fourier-transform infrared
NMR	Nuclear Magnetic Resonance
M	Molar mass
M_w	Weight average molar mass
M_n	Number average molar mass
$Đ$	Dispersity
$[\eta]$	Intrinsic viscosity
$[\eta]_w$	Weight-average intrinsic viscosity
RMS	Root mean square
MMD	Molar mass distribution
CCD	Chemical composition distribution
dn/dc	Refractive index increment
lin	Linear
br	Branched
SCB	Short chain branching
LCB	Long-chain branching
f	Number of arms
f_n	Number-average arms per molecule
f_w	Weight-average arms per molecule
e	Draining parameter
g	Branching ratio based on root mean square radius
g'	Branching ratio based on intrinsic viscosity
CFRP	Carbon fibre reinforced polymer

INTRODUCTION: TARGETS OF DISSERTATION

This thesis focused on the determination and studying the molecular structure of synthesized different branched methacrylate polymers via group transfer polymerization and solution free radical polymerization and different polyolefin samples. During its elaborating, it was necessary to accomplish the following tasks to achieve the planned targets:

- Introduction and literature review about synthesis of branched polymer and different characterization methods of branched polymers and their importance and applications in our life.
- Laboratory preparation of star-like polymers with different molar masses and lengths of arms by group transfer polymerization and preparation of linear polymethacrylates with different lengths of branches by solution-free radical polymerization.
- Description of chromatographic methods (SEC-MALS-Visco and HT SEC-IR5) used for characterization and investigation of prepared branched polymers.
- Determination of molar mass and molar mass distributions.
- Studying in detail the molecular structure of the prepared star-like polymers and the effect of short chain branching length for linear polymethacrylate polymers using SEC-MALS-Visco.
- Carbon fibre reinforced polymer (CFRP) composites.
- Monitoring the chemical composition distribution of a series of ethylene/1-alkene and ethylene-propylene-diene copolymers as polyolefins examples using HT SEC-IR5.
- Repeatability and limit of detection of filter-based IR (IR5) detector.

CHAPTER 1

SYNTHESIS AND CHARACTERIZATION OF MOLECULAR STRUCTURE AND DILUTE SOLUTION PROPERTIES OF METHACRYLATE POLYMERS

1.1. Introduction

Branched polymers have attracted increasing interest due to their numerous and various applications originating from a large variety of available polymer topologies, compositions, or morphologies for phase separating systems, as emulsifier and interfacial compatibilizers, enhancing mechanical properties of composites, or for surface modification properties. Branching can be also used for modifying properties used for drug delivery as the branched structure is capable of incorporating better the active pharmaceutical ingredients and the degree of branching also affects the rate of biodegradation. Star-like polymers (as a type of branching polymers) have been widely studied because of their unique topological structures and attractive physical and chemical properties. Therefore, a number of researchers have focused on star polymers to design various advanced materials for biomedical applications, including drug and gene delivery, diagnosis, antibacterial and antifouling coatings, and implanted medical devices [1–5].

Branching can affect various chemical and physical properties of polymers, such as thermodynamic interactions between the polymer and the solvent [6–8], rheological properties [9,10], glass transition temperature [11], melting behavior and crystallization [12], phase separation of polymer blends [13,14], mechanical properties, solubility, chemical stability, and solution viscosity. In some cases, branching can have opposite effects; for example, the change in glass transition temperature with increasing degree of branching is the result of two effects: The increased number of end groups increases chain mobility and free volume, while the introduction of branching points decreases chain mobility and free volume. Typical features of randomly branched polymers are the broadening of the molecular mass distribution compared to the corresponding distribution without branching and a significant fraction of linear molecules even in highly branched samples [15]. In randomly branched polymers, the number of branching units in a polymer chain increases with increasing molar mass, and branching leads to a high molecular weight tail of the molar mass distribution [16].

The classical branching paper by Zimm and Stockmayer [17] offers the following equations relating the number of arms (f) with the branching ratio (g):

$$g = \frac{6f}{(f+1)(f+2)} \tag{1}$$

$$g = \frac{3f-2}{f^2} \tag{2}$$

Equation 1 was derived for star polymers where the arm length is polydisperse, i.e., the arms are not of equal length, whereas Equation 2 was derived for the stars with equal arm length. The branching ratio (contraction factor) is defined as the ratio of the mean square radii of branched (*br*) and linear (*lin*) molecules of the same molar mass (M):

$$g = \left(\frac{R_{br}^2}{R_{lin}^2}\right)_M \tag{3}$$

Where R is the root means square (RMS) radius (radius of gyration), and the subscript M indicates that the comparison is performed for the macromolecules of equal molar mass. A general limitation of the above equations is that they are valid for theta conditions, whereas the SEC measurements are typically performed in thermodynamically good solvents. As the thermodynamic quality of the solvent decreases with increasing degree of branching, the expansion of the branched macromolecules in thermodynamically good solvent is less than that of linear polymer chains. Consequently, the experimental values of g become smaller compared to the theta state.

Alternative branching ratio based on the intrinsic viscosity ($[\eta]$) was suggested by Zimm and Kilb [18]:

$$g' = \left(\frac{[\eta]_{br}}{[\eta]_{lin}}\right)_M \tag{4}$$

The two branching ratios are related by a simple equation:

$$g' = g^e \tag{5}$$

The main limitation is given by the fact that the relation of g' to the number of arms in star polymers or number of branch units in randomly branched macromolecules is less certain as it is via the parameter e which is related to the drainability of polymer chains. The draining parameter e is supposed to fall in the range of 0.5–1.5, yet the exact value is mostly unknown. The detailed discussion of hydrodynamic properties of branched polymers can be found in papers by Kurata et. al. [19,20] and Lederer et. al. [21].

Literature offers several equations relating the number of arms directly with the intrinsic viscosity-based branching ratio [18,22,23]:

$$g' = \frac{(2/f)^{1.5}[0.396(f-1)+0.196]}{0.586} \quad (6)$$

$$g' = \left(\frac{3f-2}{f^2}\right)^{0.58} \frac{0.724-0.015(f-1)}{0.724} \quad (7)$$

$$log\, g' = 0.36 - 0.8\, log\, f \quad (8)$$

The importance of short chain branching (SCB) in the properties of polymers is well-known. Stiffness, ductility, tear strength, clarity, and softening temperature are among the many performance characteristics affected profoundly by structure, frequency, and distribution SCB [24, 25]. Sun et al. [26] the short branch effect in α-olefin copolymers on root mean square (RMS) radius and intrinsic viscosity [η] in trichlorobenzene at 135 °C. This study of the effect of SCB on series of homopolymers of methacrylate and their copolymers with different alkyl groups was inspired by Sun et al. [26].

1.2. Theoretical part and literature review

1.2.1. Branched polymers and their structure

Branched polymers have side chains or branches growing out from the main chain as shown in Figure 1. The side chains or branches are made of the same repeating units as the main polymer chains. The branches may result from side reactions during polymerization or are created purposefully. For a polymer to be classified as a branched polymer the side chains or branches should comprise of a minimum of one complete monomer unit, but typically this work talks about branching when the branch includes at least four monomer units. One of the most common examples is low-density polyethylene (LDPE) which has applications ranging from plastic bags, containers, textiles, and electrical insulation to coatings for packaging materials. Branched polymers display lower density as a consequence of reduced ability to crystallize. The length of the side chains or branches differentiates between long-chain or short-chain branched polymers. In the case of long chain branching (LCB) the length of branches is comparable with the main chain. Long branches can have comb-like, random, or star-like structures. The branches may be further branched (branch on branch), yet they do not connect to another polymer chains [27–29]. Some examples of branched polymers are listed below and represented in Figure 1.

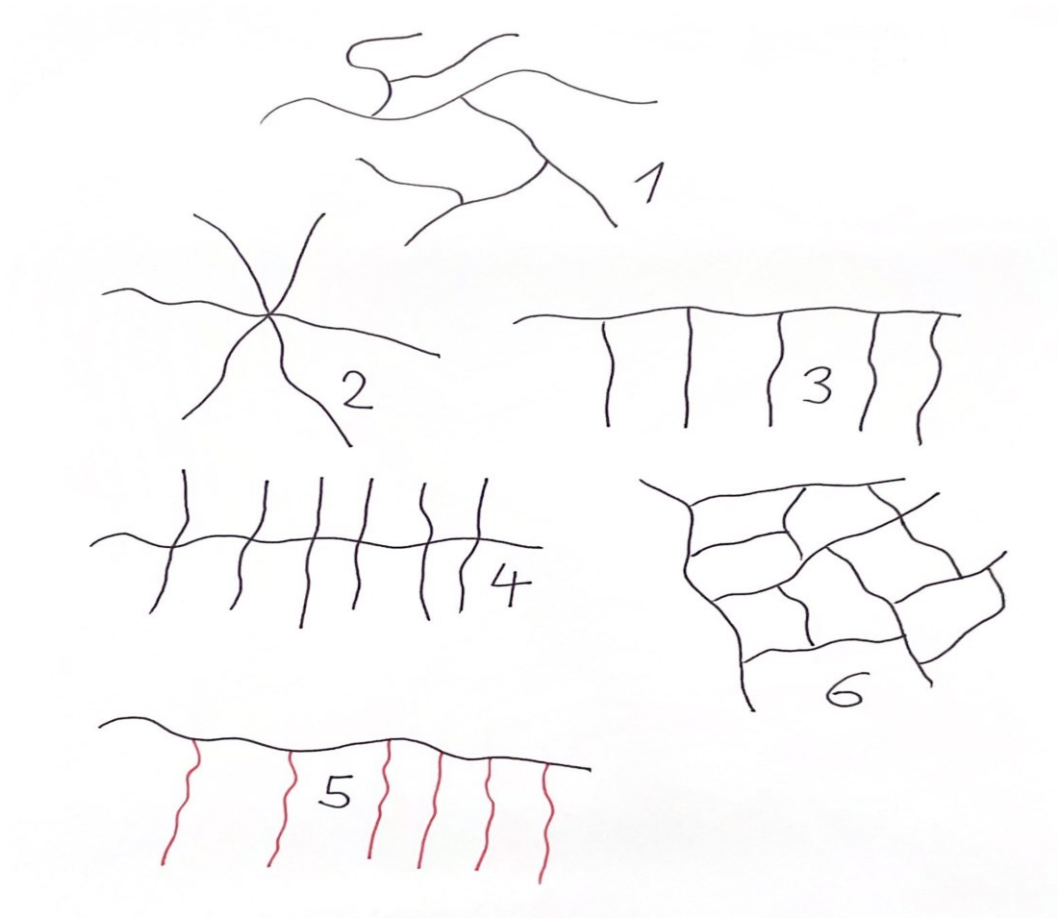

Figure 1 Branched polymer and different types of branched polymers (1) branched polymer, (2) star-like polymer, (3) comb polymer, (4) brush polymer, (5) graft polymer and (6) network polymer.

1.2.2. Star-like polymer

Star polymers are branched polymers consisting of several linear chains attached to a central core and can be subclassified depending on the nature of the different branches. If the branches are identical linear chains they are named “symmetric stars” and if the branches have different molecular weights or topology they are named “asymmetric stars”, or “miktoarm stars” if the branches are chemically different. In all cases, these arms can be constituted by one-block or multiblock copolymers. This special category of polymers has become popular in different research areas (chemistry, physics, biochemistry, and engineering) due to their unique mechanical, rheological, as well as biomedical properties that are unattainable for linear polymers [30–32]. In general, star polymers are characterized by a compact structure, presumably with a globular shape, with a large surface area, and increased concentrations of functional end groups when compared to polymers of similar molar mass (*M*).

Two major strategies have been widely applied for the synthesis of star polymers: the core-first approach and the arm-first approach [32]. The "core-first" approach is based on the use of a multifunctional initiator as a core that initiates the polymerization of several arms simultaneously. Equally reactive initiating sites are crucial to control polymerization and to synthesize homogeneous constructs, and this also requires that the initiation step must be always faster than the propagation step. Historically, the major disadvantage of this methodology is the difficulty in the characterization of the polymers obtained, as the arm molar mass cannot be directly measured. Nevertheless, advances in characterization techniques are progressively solving this problem and this strategy is the most widely used in the synthesis of star polypeptides [33]. Alternatively, the "arm-first" approach consists of the reaction of living macroinitiators (MI) (also named macromonomers) with multifunctional molecules acting as cross-linkers giving rise to stars-like architectures known as core cross-linked star polymers. The main advantage of the "arm-first" approach is the relative ease of characterization since the living arms can be characterized in a previous step before linkage [34,35].

1.2.3. Synthesis of branched polymers

In polymer chemistry, branching occurs by the replacement of a substituent, e.g., a hydrogen atom, on a monomer subunit, by another covalently bonded chain of that polymer; or, in the case of a graft copolymer, by a chain of another type. Branched polymers have more compact and symmetrical molecular conformations and exhibit intra-heterogeneous dynamical behaviour with respect to unbranched polymers.

Branched polymers can be synthesized through various routes such as free radical polymerization, group transfer polymerization, ring opening polymerization, condensation polymerization, etc.

1.2.3.1. Free radical polymerization

Branching occurs in some free-radical polymerizations of monomers like ethylene, vinyl chloride, acrylates, and vinyl acetate in which the macroradicals are very reactive. So-called self-branching can occur in such polymerizations because of atom transfer reactions between such radicals and polymer molecules. In the chain transfer mechanism, the active center of the growing chain is transferred to another molecule. The transferred active center is not terminated during migration and has the potential to initiate either another polymer chain or a branch on an existing polymer chain. Chain transfer is a chain breaking step and decreases the average

length of the propagating chain, significantly applicable to biomedical drug delivery applications. The molecule receiving the active center may or may not initiate the growth of another polymer chain depending on its reactivity [36]. The chain transfer mechanism is very helpful in the formation of graft copolymers.

1.2.3.2. Condensation or Step-Growth Polymerization

Condensation polymerization is the second most common mechanism for polymerization. In this mechanism, the reaction between the repeating units and the growing chain results in the release of a small molecule (condensate) such as water or hydrochloric acid as a byproduct [37,38]. Branching can be produced by condensation bi-functional monomer (e.g., dicarboxylic acids) with another polyfunctional monomer (polyamines). Branching also occurs naturally during enzymatically catalyzed polymerization of glucose to form polysaccharides such as glycogen (animals), and amylopectin, a form of starch (plants).

1.2.3.3. Group Transfer Polymerization (GTP)

Group transfer polymerization (GTP) was invented at DuPont over 30 years ago [39]. It is a popular method to control the molecular weight and molecular weight distribution of acrylic polymers during chain growth. Like other living polymerization methods, GTP allows for the preparation of polymers with low polydispersity and with well-defined architecture such as block copolymers and star-like polymers. However, unlike conventional anionic polymerization, methyl methacrylate (MMA) can be polymerized at above ambient temperature. Thus, the temperature can be controlled with simple water-cooled reflux condensers, rather than with more expensive refrigeration units. Furthermore, the process typically uses initiators and catalysts of low toxicity which can be readily removed from the product by filtration,[39] and thus can be reused and are not a source of undesirable discoloration or odor. A major drawback of GTP is the sensitivity of the catalysts to protonic impurities (moisture, alcohol etc.) which renders the initiator inactive and causes loss of molecular weight control. Thus, to achieve low dispersity and high molecular weights, all ingredients including monomer, solvent and catalyst have to be carefully purified [40, 41].

Chain growth is started by intermolecular Michael's addition of the ester enolate group of a silyl ketene acetal (SKA) to the vinyl group of a monomer catalyzed by a nucleophilic anion or Lewis acid [42]. Early studies indicated that the trimethylsilyl group (TMS) remains with the growing chain centre during polymerization which is only possible if the TMS group is

transferred to the incoming monomer [43–45]. A possible mechanism of TMS transfer is shown below in Scheme 1. The TMS transfer can be explained by a concerted rearrangement of double bonds. The process is repeated in each vinyl addition step.

Although GTP was developed for living polymerization of methacrylates, other monomers such as alkyl acrylates, N,N-dimethylacrylamide, acrylonitrile, methacrylonitrile, and vinyl ketones can be polymerized as well [41,44].

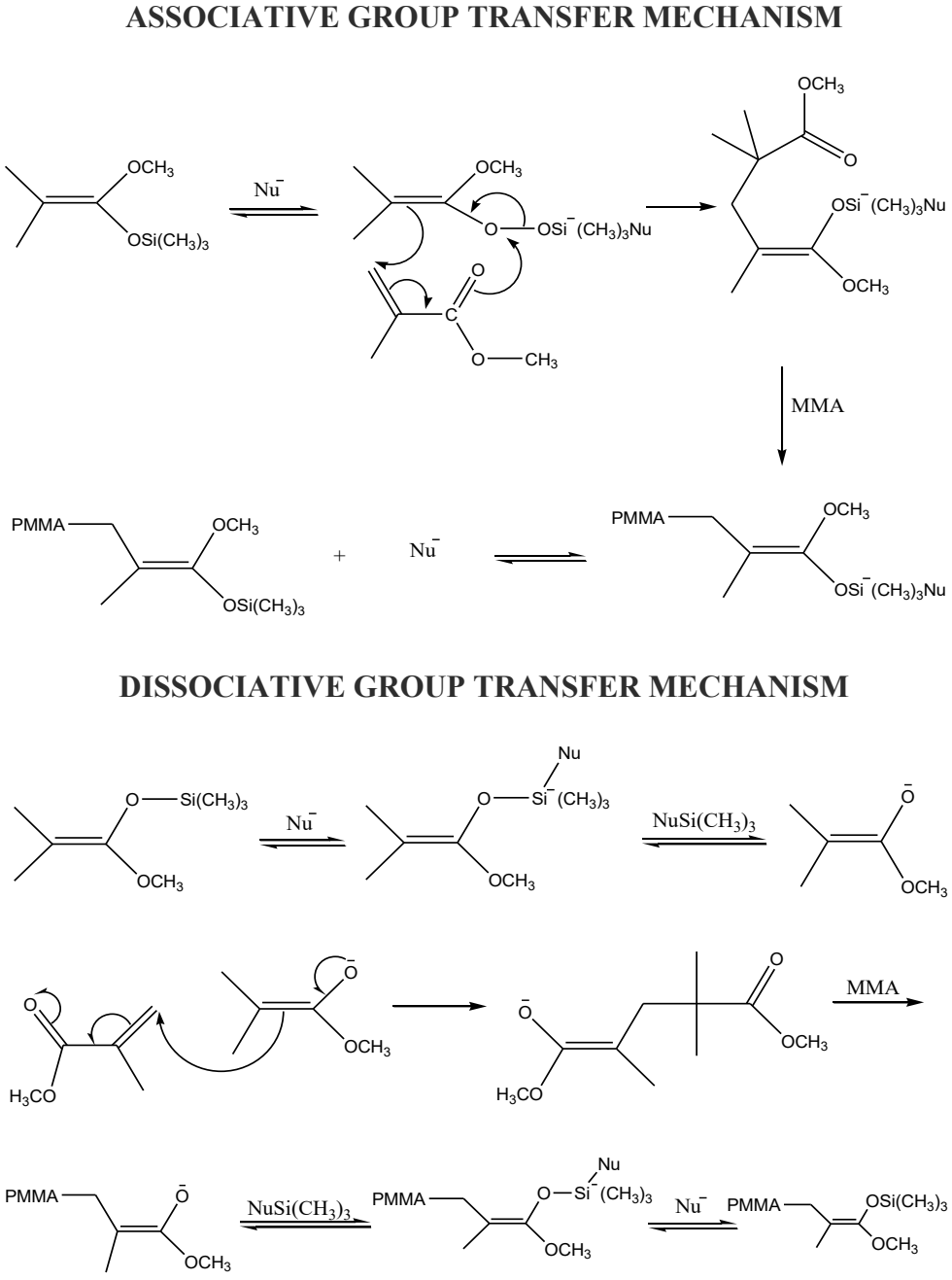

Scheme 1 A possible mechanism for group transfer polymerization technique.

1.2.4. Application of branched polymers with the focus on star-like polymer

While many studies have been published regarding star-like polymers, their commercial applications are limited, but growing constantly as research expands. Some commercial applications of star-like polymers include:

Asymmetrical star-like polymers have been found to be effective thermoplastic elastomers [46]. Their morphologies contribute favourably to mechanical properties such as toughness, stretch recovery, transparency, and thermostability.

Use as viscosity index improvers in car engine lubricating oils [47]. Star-like polymers generally have lower internal viscosities than their linear analogues due to their smaller hydrodynamic radii and radii of gyration. This makes them favourable for use in fluids that require low viscosity such as lubricating oils in car engines.

The architecture of photoresists has typically been dominated by linear polymers. Star-like polymers, however, have been shown to display more advantageous properties when compared to their linear analogues. They are able to decrease roughness of photoresist sidewalls without a decrease in sensitivity or resolution. This is due to star-like polymers' decreased tendency to form chain entanglements relative to their linear analogues of similar molecular weights, which leads to insolubility and increased roughness [48].

Miktoarm polymers that form core-shell-corona micellar structures have been proved to uptake and release small molecules in different biological conditions [49]. Small molecules associate with certain polymer arms that form the interior of the micellar structure during transport. When they are exposed to conditions that cause the interior arms to become solvated, the small molecules are released. Specifically, successful encapsulation of the anti-cancer agent doxorubicin hydrochloride has been achieved [50].

The low gelation concentration of telechelic and semitelechelic star-like polymers has made them useful in the development of new hydrogels for biomaterial applications [50]. This low gelation concentration is caused by an increased number of intermolecular interactions relative to linear analogues due to star-like polymers' increased number of functional groups in a given volume.

1.2.5. Characterization of branched polymers

Branching is an important structural parameter of many synthetic and natural polymers. It can influence the mechanical and thermodynamic properties of polymers, and also affect the viscosity and rheological behaviour of polymer solutions and melts.

It is well known that the dilute solution properties of a branched polymer are influenced by its molecular weight distribution and branching distribution thus the characterization of branched polymers are very important to utilize the molecular structure of branched polymers. There are several methods used for separation and characterization of branched polymers.

1.2.5.1. Basic principles of branching characterization

Branching is widely recognized as relevant to synthetic polymers but has more recently become relevant to natural polymers. For example, hyaluronic acid, an important biopolymer with numerous medical and pharmaceutical applications, was believed to have a linear structure until multi-angle light scattering (MALS) analysis proved otherwise [51]. The most common method of separating polymers in solution is size-exclusion chromatography, also called gel permeation chromatography (SEC/ GPC) coupled with different detectors. For example, SEC–MALS is a well-established technique for the absolute characterization of typical polymers; however, large and highly branched polymers can exhibit abnormal conformation plots in SEC [23].

1.2.5.2. Separation techniques

SEC and asymmetrical flow field-flow fractionation (A4F) are the most common separation techniques used for the characterization of polymers. Coupling these separation techniques with different advanced detectors such as multi-angle light scattering, viscometer, and infra-red detector, provides full characterization of polymers, specially branched polymers.

Size Exclusion Chromatography (SEC)

Size exclusion chromatography (SEC), known also by its original name as gel permeation chromatography (GPC), represents undoubtedly one of the most frequently used analytical methods for the characterization of synthetic and natural polymers. The history of SEC/GPC in the area of synthetic polymers started by a paper by Moore [52] who described for the first time the separation of polystyrene samples of various molar mass on columns packed with a porous swollen styrenedivinylbenzene gel. From its inception, the main application of SEC was the determination of molar mass distribution and molar mass moments. The main limitation of SEC

has always been given by limited availability of narrow well characterized polymer standards and by the dependency of the obtained results on various operational conditions [53]. Narrow polystyrene standards prepared by anionic polymerization represent the most frequently used standards in the case of synthetic polymers.

Asymmetric Flow Field Flow Fractionation (A4F)

Although SEC can separate many synthetic and natural polymers with very sufficient resolution, it may fail in the case of some polymers such as: 1) branched polymers when the steric separation is affected by the anchoring of the branches in the pores of column packing [23]; 2) polymers containing polar functional groups when the steric separation is affected by enthalpic interactions of polymer molecules with column packing [53]; 3) polymers containing ultra-high molar mass fractions that can be degraded by shearing forces in the SEC columns [54]; and 4) polymers containing aggregates and nanogels that can be completely retained by the packed columns.

All these polymers can be mostly well separated by asymmetric flow field flow fractionation (A4F), which currently represents the most instrumentally developed type of field flow fractionation with readily available instrumentation and numerous applications covering synthetic polymers, natural polymers, colloidal particles, proteins, vaccines, various biological materials, and environmental samples. Due to the recent development of a new generation of A4F instruments, the method has finally achieved the mature state where it can be used as routinely as SEC [55,56].

Combination of SEC with multi-angle light scattering detector (SEC-MALS)

Combination of SEC with the multi-angle light scattering (MALS) detectors not only free SEC from the column calibration completely but allow the determination of true molar mass, and the root mean square (RMS) radius, often called radius of gyration, as another important parameter characterizing the size of macromolecules in solution. The simultaneous measurement of molar mass and RMS radius provides information about the polymer chain conformation and allows detection and characterization of long chain branching. Here, without any further details, let us briefly mention that the intensity of light scattered by macromolecules in dilute solution is directly proportional to the product of molar mass and concentration according to Equation (9) [57]:

$$\frac{R_\theta}{K^* c} = MP(\theta) + \cdots \quad (9)$$

Where R_θ is the intensity of scattered light related to the intensity of the incident light and geometry of the instrument; K^* is the optical constant including the refractive index of the solvent, wavelength of the incident light in vacuum and specific refractive index increment of a given polymer in a given solvent, c is the concentration of polymer molecules eluting in a given elution volume from SEC columns; M is their molar mass; and $P(\theta)$ is the particle scattering function describing the decrease of the scattered light intensity with angle of measurement θ Equation (10):

$$\lim_{\theta \to 0} P(\theta) = 1 - \frac{16\pi^2}{3\lambda^2} R^2 sin^2(\theta/2) \quad (10)$$

where R is the RMS radius and λ is the wavelength of the incident light in a given solvent. At low concentrations typical for SEC analysis the other terms in Equation (9) can be neglected and thus the molar mass equals the left side of Equation (9) at zero angle where $P(\theta)$ becomes unity, and the RMS radius is obtained from the slope of the angular variation at zero angle.

Combination of SEC with multi-angle light scattering detector and viscosity detector (SEC-MALS-Visco)

Most applications of viscometric detection have involved one of two topics: Either the determination of absolute, calibrant-independent molar mass averages and distributions, based on applying Benoit's concept of universal calibration, and/or the use of online viscometry to establish the presence of long-chain branching in macromolecules. The realized potential of viscometry, however, greatly exceeds just these two applications.

The intrinsic viscosity $[\eta]$ represents one of the most important variables describing the behavior of a dilute polymer solution as it offers exceptional insight into the structure of synthetic and natural polymer molecules. It is a measure of the hydrodynamic volume occupied by a macromolecule in solution and therefore a reflection of its size. The relation between the intrinsic viscosity and molar mass (called Mark-Houwink or Mark-Houwink-Kuhn-Sakurada relation):

$$[\eta] = K \times M^a$$

provides direct information about the configuration and conformation of polymer chains in a dilute solution under given conditions (i.e., solvent and temperature). The Mark-Houwink

plots of linear polymers are linear over the entire molar mass range while curved plots indicate branched structure.

A reliable and fast way to generate the Mark-Houwink plot is to couple an SEC instrument to MALS and a viscosity detector. The coupling SEC-MALS-Visco technique yields molar masses and intrinsic viscosities for narrow fractions eluting from SEC columns with the limitations discussed in relation to complex polymers [58].

1.3. Experimental

1.3.1. Materials

n-butyl methacrylate (BMA), Methyl methacrylate (MMA), Benzyl methacrylate (BZMA), Ethylene Glycol Dimethacrylate (EGDMA), Lauryl methacrylate (LMA) and 2-ethyl hexyl methacrylate (2-EHMA) were purchased from Sigma-Aldrich, United States. Tetrahydrofuran (THF) (99.8%) and *n*-hexane were purchased from VWR Chemicals, United States. Methyl trimethylsilyl dimethyl ketene acetal (Me initiator), azobisisobutyronitrile (AIBN) and tetrabutylammonium acetate (tBuAAc) were purchased from Sigma-Aldrich.

1.3.2. Synthesis of star-like polymers

Before starting the polymerization process all monomers and solvents were purified by passing through a column filled with alumina to remove inhibitors (see Figure 2) while the initiator and catalyst were used without further purification.

Figure 2 Drying system for solvent and monomers.

The polymerizations were carried out in 250 mL round-bottom flasks, fitted with rubber septa (see Figure 3). The reactions were carried out at ambient temperature (25 °C) without thermostatic polymerization reactor. The polymerization exotherm was monitored by thermometer and was used to follow the progress of the reaction. A scavenger (N,N-Diethyltrimethylsilylyamine) was transferred to the flask, which was purged with dry nitrogen.

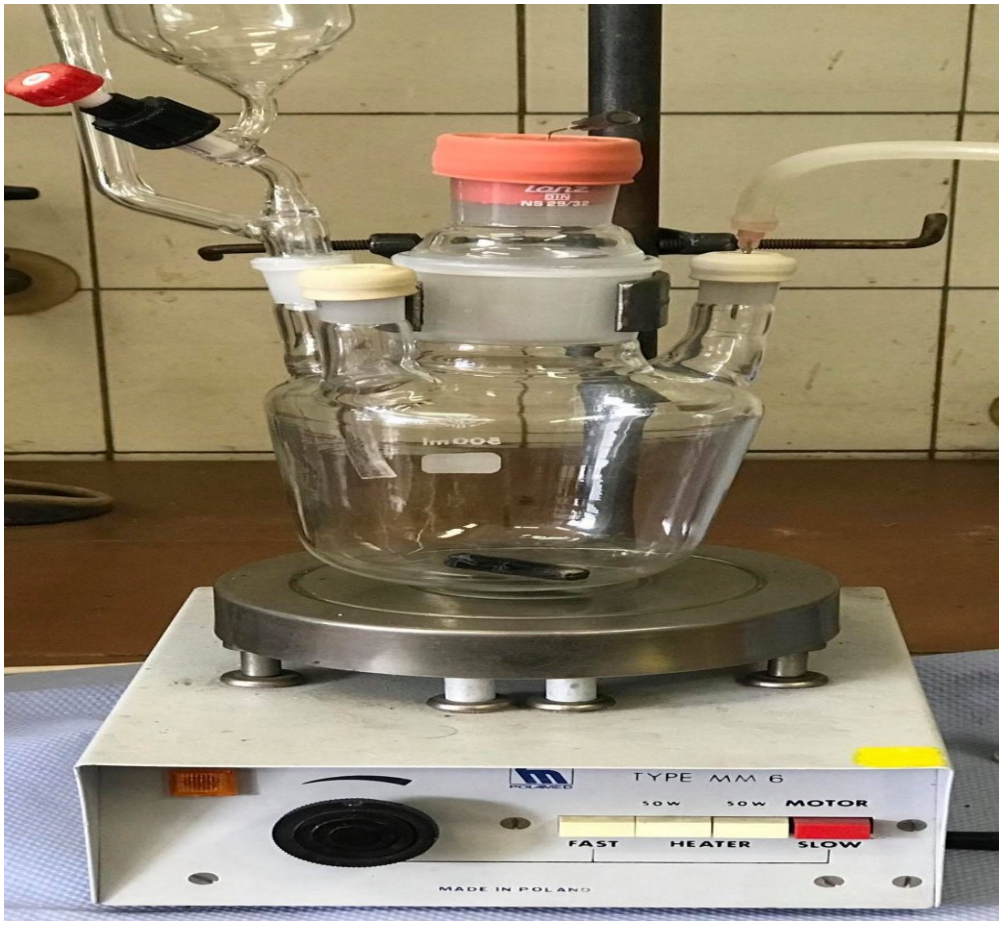

Figure 3 Three neck bottom flask system for star-like polymer synthesis.

Freshly distilled THF was subsequently transferred directly from the still into the flask via a syringe. Then, the methyl trimethylsilyl dimethylketene acetal initiator (Me initiator) and Tetrabutylamonium acetate catalyst were added, followed by the slow addition of monomer to form the arm or macromolecular initiator. After finishing the addition of monomer, arm solution let stirring for 20 min. then a 10 mL of arm solution was removed for further characterization. After that, the synthesis was completed by the addition of EGDMA cross-linker. Finally, the polymerization was terminated by adding commercial methanol (see scheme 2). The molar ratios of particular reagents for all prepared star-like samples are listed in Tables 1–3.

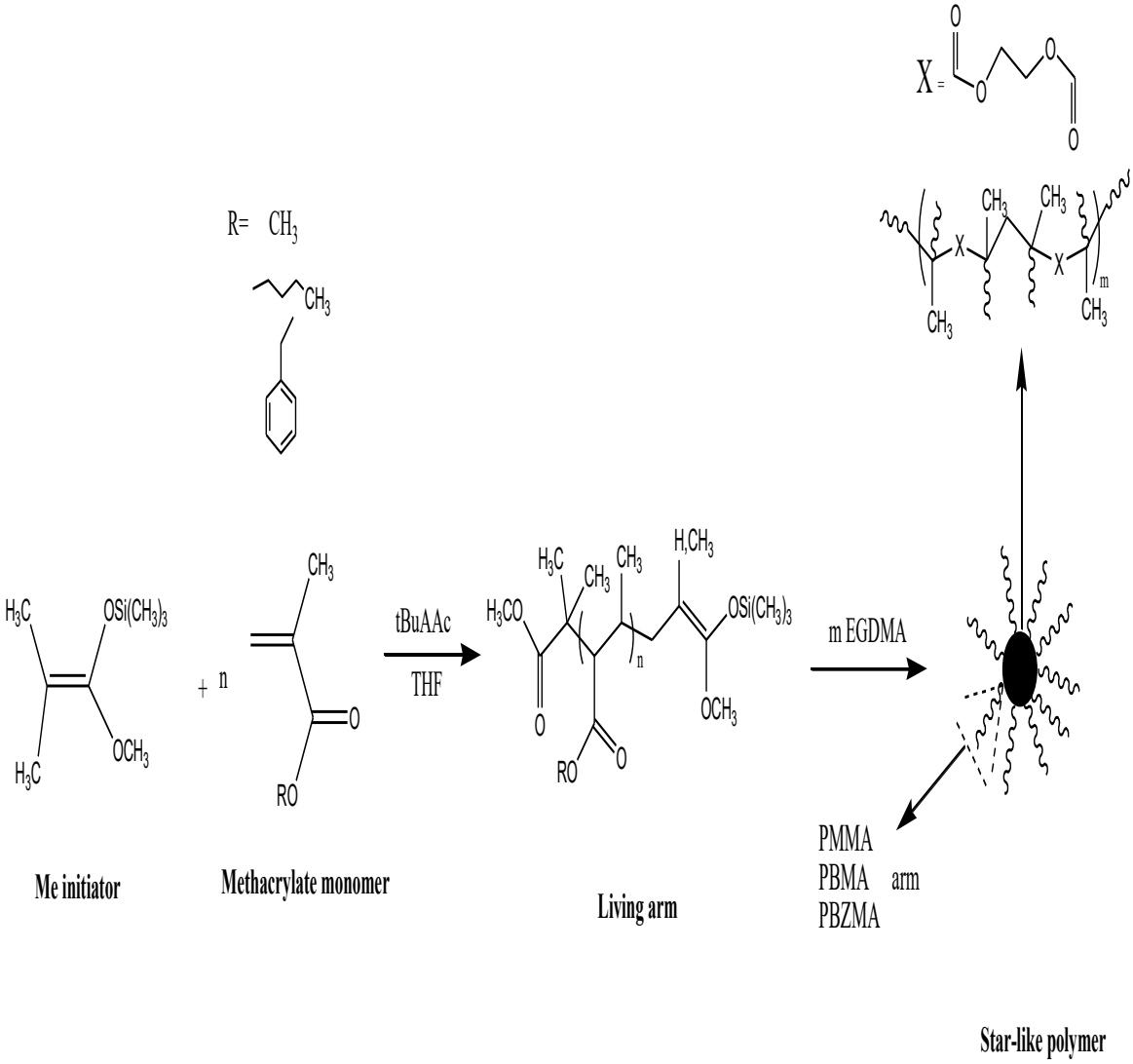

Scheme 2 Synthesis procedures of methacrylate star-like polymers.

Table 1 Molar ratios of reagents used for PBMA star-like synthesis.

Sample	Monomer	Molar ratio		
		Initiator	Monomer	EGDMA
B1	BMA	1	49	2.3
B2	BMA	1	49	3.7
B3	BMA	1	49	2.8
B4	BMA	1	49	1.7
B5	BMA	1	49	3.3
B6	BMA	1	49	2.5
B7	BMA	4	49	3.8
B8	BMA	4	49	6.9
B9	BMA	4	49	6.4
B10	BMA	4	49	9.3
B11	BMA	4	49	8.4

Table 2 Molar ratios of reagents used for PMMA star-like synthesis.

Sample	Monomer	Molar ratio		
		Initiator	Monomer	EGDMA
M1	MMA	1.0	30	1.3
M2	MMA	1.0	30	1.8
M3	MMA	1.0	30	1.5
M4	MMA	1.0	30	1.0
M5	MMA	2.5	30	1.2
M6	MMA	2.5	30	1.6
M7	MMA	2.5	30	2.3
M8	MMA	2.5	30	2.0
M9	MMA	2.5	30	2.7
M10	MMA	2.5	30	4.0

Table 3 Molar ratios of reagents used for PBZMA star-like synthesis.

Sample	Monomer	Molar ratio		
		Initiator	Monomer	EGDMA
BZ1	BZMA	1.7	17	1.4
BZ2	BZMA	1.7	17	2.0
BZ3	BZMA	1.7	17	2.5
BZ4	BZMA	1.7	17	1.5

1.3.3. Synthesis of linear homo and co polymethacrylates

Linear homo- and co-polymethacrylates were prepared by solution free radical polymerization using azobisisobutyronitrile (AIBN) as initiator. About 50 mL of 50% solution of monomer in toluene was placed into a 100 mL closed vial and heated at 80 °C for 8 hr. (Tables 4 and 5). Scheme 3 shows the preparation steps of Linear methacrylate polymers. After completing the polymerization, the polymer solution was left to cool overnight. The polymers were precipitated by *n*-hexane and dried in a vacuum oven at 40 °C to a constant weight.

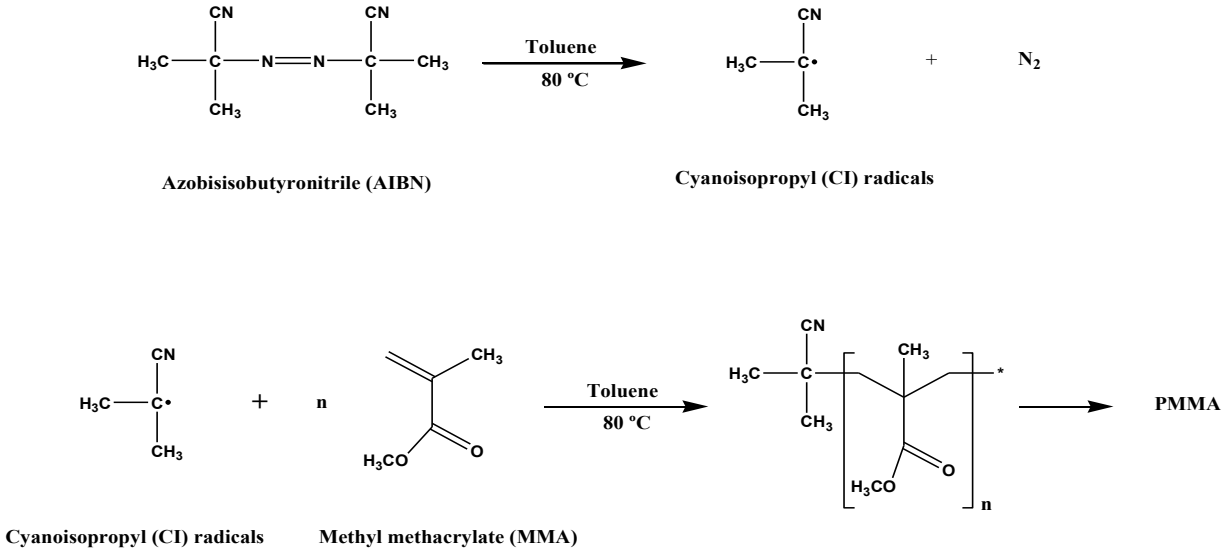

Scheme 3 Preparation of PMMA by free radical polymerization in Toluene.

Table 4 Synthesis of linear homo polymethacrylate samples

Sample	Monomer	Initiator (wt%)	Monomer (mol%)	Solid (%)
PMMA	LMA	0.1	100	40
PBMA	BMA	0.1	100	32
PLMA	LMA	0.5	100	44
P2-EHMA	2-EHMA	0.1	100	32
PBZMA	BZMA	0.1	100	33

Table 5 Synthesis of linear polymethacrylate copolymer samples.

Sample	Monomer	Initiator (wt%)	Monomer (mol%)	Solid (%)
P[MMA/1 BMA]	MMA/BMA	0.1	99/1	36
P[MMA/3 BMA]		0.1	97/3	36
P[MMA/5 BMA]		0.1	95/5	35
P[MMA/10 BMA]		0.1	90/10	31
P[MMA/20 BMA]		0.1	80/20	33
P[MMA/1 2-EHMA]	MMA/2-EHMA	0.1	99/1	32
P[MMA/3 2-EHMA]		0.1	97/3	29
P[MMA/5 2-EHMA]		0.1	95/5	27
P[MMA/10 2-EHMA]		0.1	90/10	28
P[MMA/20 2-EHMA]		0.1	80/20	29
P[MMA/1 LMA]	MMA/LMA	0.1	99/1	27
P[MMA/3 LMA]		0.1	97/3	26
P[MMA/5 LMA]		0.1	95/5	22
P[MMA/10 LMA]		0.1	90/10	10

1.3.4. Instrumentation for SEC-MALS-Visco

The molar mass distributions, the conformation plots (RMS radius versus molar mass), and the Mark-Houwink plots were determined by SEC with a multi-angle light scattering (MALS) detector DAWN NEON, an RI detector Optilab NEON and an online viscometer ViscoStar NEON (all detectors from Wyatt Technology) (Figure 4). The SEC system consisted of a 1200 Series isocratic pump and autosampler with two Mixed-C 300 × 7.5 mm 5 µm columns (all Agilent Technologies) using THF as the mobile phase at a flow rate of 1 mL/min. Samples were

prepared at concentrations of ≈2.5 mg/mL (stars and linear homopolymers), ≈5 mg/mL (long arms), and ≈10 mg/mL (short arms). The samples were filtered with 0.45 µm syringe filters and injected in the amount of 100 µL. The data collection and processing were performed by Wyatt Technology software ASTRA. In addition to the calculations and plots provided by ASTRA, the data were exported from ASTRA as csv files for additional processing in Excel.

Figure 4 Photo of size exclusion chromatography coupled with multi-angle light scattering and an online viscometer.

1.3.5. Determination of specific refractive index increment

The specific refractive index increment (*dn/dc*) was determined in THF at 25 °C using a refractive index (RI) detector Optilab T-rEX operating at 660 nm (Wyatt Technology). The determination was performed off-line by injecting six THF solutions of concentration ranging from ≈0.3 mg/mL to ≈5 mg/mL. Each sample was measured about 4–5 times and then the *dn/dc* average was taken. The stars for the *dn/dc* measurements were isolated from the unreacted arms by the precipitation of THF solutions resulting from GTP by n-hexane and subsequent drying in a vacuum oven at 40 ◦C. The arms were isolated by drying the solutions obtained after the

first polymerization step before addition of EGDM. The star purity was checked by conventional size exclusion chromatography (SEC) with an RI detector. An Alliance e2695 Separation Module with a 2414 RI detector (both Waters) and two Agilent Mixed-C 300 × 7.5 mm 5 μm columns with THF at 1 mL/min were used for this purpose. All stars contained less than ≈2 wt% of remaining arms.

1.4. Results and discussion

This chapter focuses on the preparation of different linear and star-like methacrylate polymers by solution free radical polymerization and group transfer polymerization, respectively. Studying the complete characterization of the molecular structure for all the prepared samples is investigated by using SEC-MALS-Visco system.

1.4.1. Molar mass and molar mass distribution determination

Figures 5–7 depicts typical molar mass versus elution volume plot of one of star-like PBMA, Star-like PMMA with low and high molar mass of arms and Linear homopolymers and copolymers. The data proves the ability of modern MALS detectors to yield sufficient signal to determine the molar mass down to proximity of a thousand g/mol. It must be emphasized at this point that flushing the SEC columns for at least several hours is of utmost importance to minimize the noise caused by the particles bleeding from column packing. Proper flushing is necessary after each restart of the pump since pressure change releases the particles that were trapped in the columns during the previous runs.

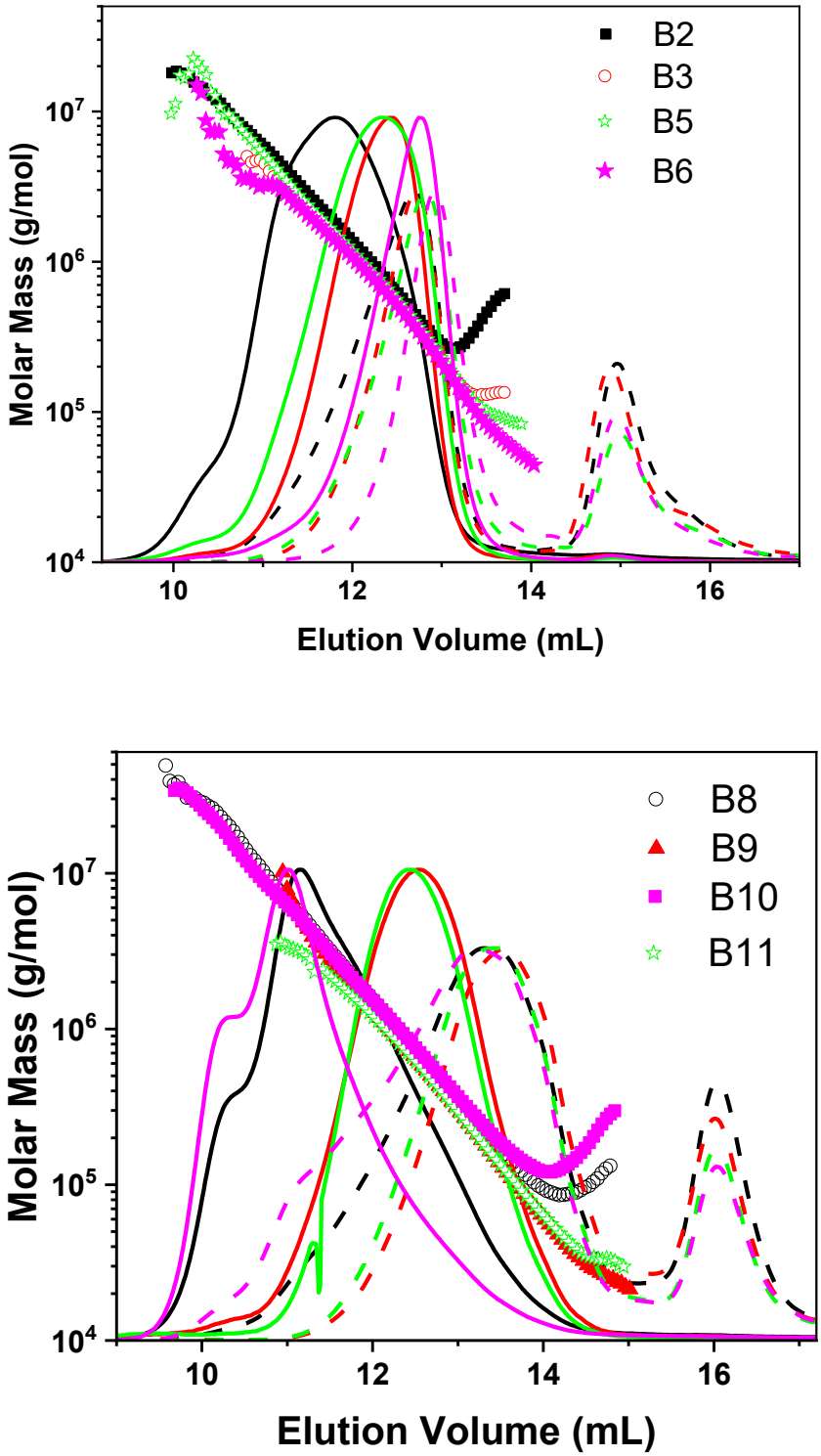

Figure 5 Molar mass versus elution volume plots of star-like PBMA with long arms (top) and with short arms (bottom). MALS @ 90° (—, solid) and RI (---, dashed) chromatograms are overlaid.

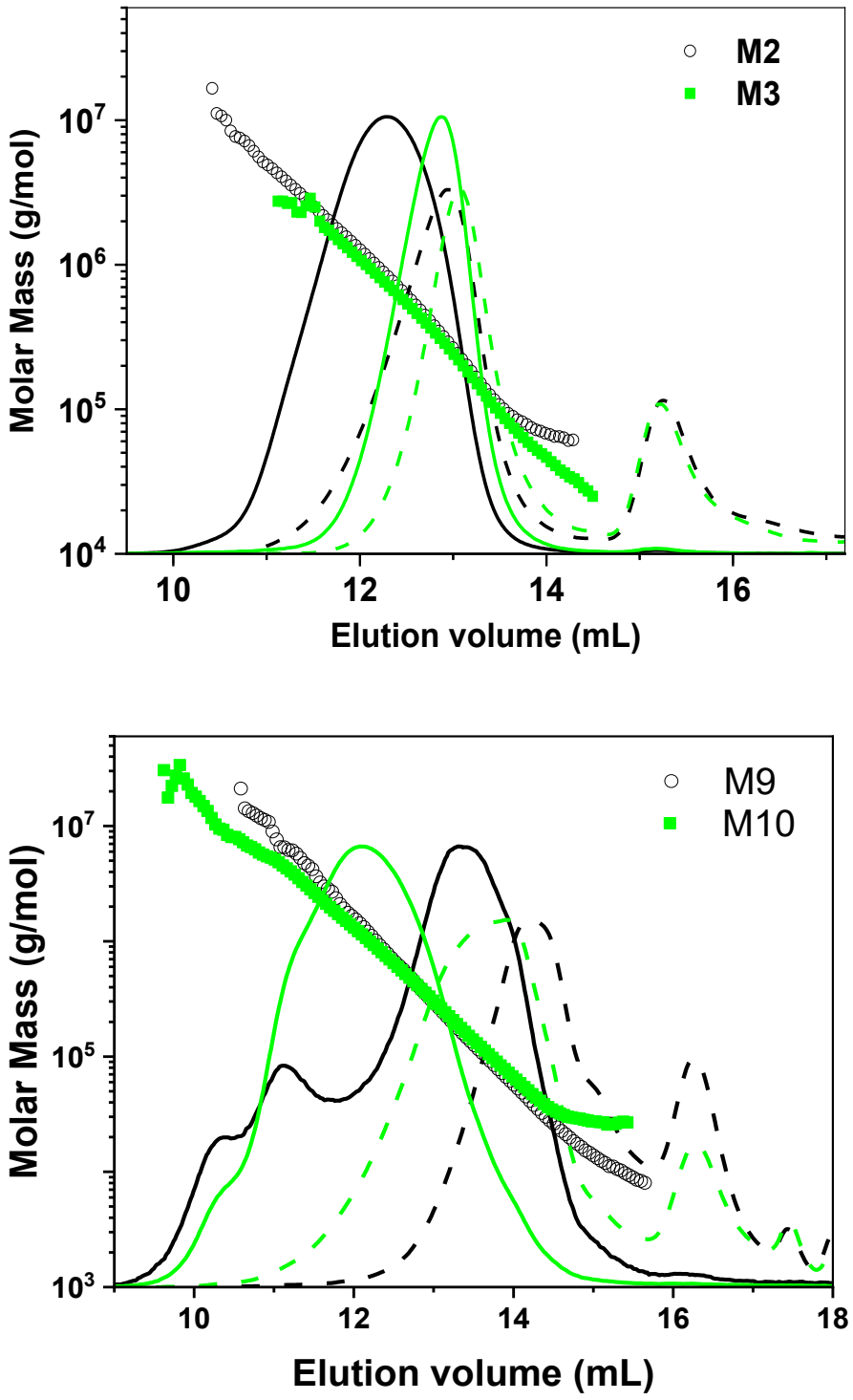

Figure 6 Molar mass versus elution volume plots of star-like PMMA with long arms (top) and with short arms (bottom). MALS @ 90° (—, solid) and RI (---, dashed) chromatograms are overlaid.

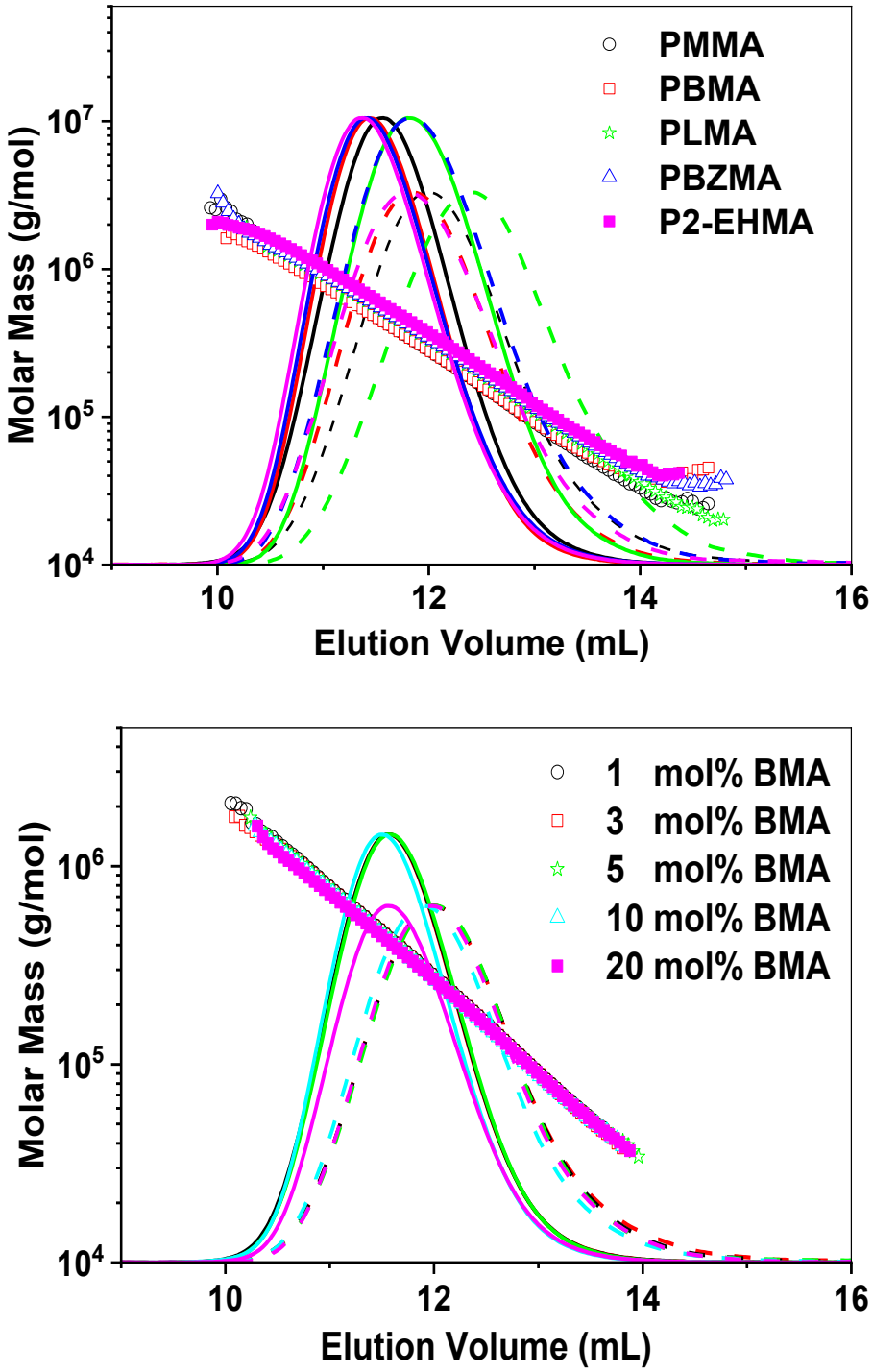

Figure 7 Molar mass versus elution volume plots of linear homopolymers (top) and P[MMA/BMA] copolymers (bottom). MALS @ 90° (—, solid) and RI (---, dashed) chromatograms are overlaid.

The number-average (M_n) and the weight-average (M_w) molar masses, the values of dispersity ($Đ$), and the weight-average intrinsic viscosities ($[\eta]_w$) of arms and stars, and the star fractions in the final polymerization products for all prepared star-like polymers are listed in Tables 6–8. And the same values for linear methacrylate polymers are listed in Table 9.

Table 6 The values of M_n, M_w, $Đ$, $[\eta]_w$, and star fraction for star-like PBMA.

sample	M_n (kg mol^{-1})		M_w (kg mol^{-1})		$Đ$		$[\eta]$ (mL/g)		Star fraction (%)
	arm	star	arm	star	arm	star	arm	star	
B1	6.2	159	6.3	201	1.02	1.45	5.4	10.3	55
B2	8.9	550	9.3	1132	1.05	2.06	6.1	13.6	74
B3	8.8	377	9.9	610	1.12	1.62	6.5	13.0	68
B4	7.3	61	7.7	111	1.06	1.81	5.7	10.7	62
B5	7.7	332	8.3	642	1.07	1.93	6.7	13.4	78
B6	8.3	194	8.7	346	1.05	1.78	6.9	12.9	74
B7	3.1	42	3.3	59	1.07	1.41	4.5	7.7	59
B8	2.3	220	2.5	1029	1.10	4.67	4.1	10.2	79
B9	2.3	94	2.5	305	1.12	3.26	4.2	8.5	78
B10	2.4	237	2.7	1712	1.11	7.22	3.8	12.8	87
B11	2.5	117	2.7	329	1.10	2.83	3.8	9.1	82

Table 7 The values of M_n, M_w, $Đ$, $[\eta]_w$, and star fraction for star-like PMMA.

Code	M_n (kg mol^{-1})		M_w (kg mol^{-1})		$Đ$		$[\eta]$ (mL/g)		Star fraction (%)
	arm	star	arm	star	arm	star	arm	star	
M1	6.5	66	6.9	102	1.07	1.54	6.1	11.2	77
M2	6.4	273	6.9	606	1.08	2.22	6.1	12.4	76
M3	6.5	147	7.0	267	1.08	1.82	6.1	11.7	73
M4	6.1	68	6.6	114	1.08	1.67	6.8	11.3	64
M5	2.1	12	2.2	17	1.08	1.44	4.5	6.9	59
M6	1.5	11	1.7	25	1.15	2.36	4.2	6.0	58
M7	1.9	21	2.1	47	1.09	2.28	3.7	6.6	76
M8	1.6	14	1.8	30	1.09	2.14	4.3	6.4	73
M9	1.6	28	1.8	101	1.09	3.63	4.3	7.2	77
M10	1.9	84	2.1	388	1.07	4.62	3.8	8.9	87

Table 8 The values of M_n, M_w, $Đ$, $[\eta]_w$, and star fraction for star-like PBZMA.

Code	M_n (kg mol^{-1})		M_w (kg mol^{-1})		$Đ$		$[\eta]$ (mL/g)		Star fraction (%)
	arm	star	arm	star	arm	star	arm	star	
BZ1	2.9	69	3.5	123	1.22	1.78	4.1	8.8	50
BZ2	2.4	29	2.8	59	1.19	1.99	4.0	7.1	74
BZ3	2.4	79	2.8	242	1.19	3.08	3.9	9.0	77
BZ4	2.3	75	2.9	275	1.23	3.69	3.9	8.7	71

Table 9 The values of M_n, M_w, $Đ$, $[\eta]_w$ for linear methacrylate polymers.

Polymer	M_n (Kg mol^{-1})	M_w (Kg mol^{-1})	M_w/M_n	$[\eta]_w$ (mL/g)
PMMA	164	310	1.92	70.9
PBMA	215	497	1.68	80.8
PBZMA	234	428	1.83	64.1
P2-EHMA	265	478	1.81	67.5
PLMA	124	260	2.10	43.1
P[MMA/1 BMA]	165	310	1.88	71.1
P[MMA/3 BMA]	155	302	1.96	70.8
P[MMA/5 BMA]	167	305	1.82	72.5
P[MMA/10 BMA]	179	320	1.80	79.4
P[MMA/20 BMA]	164	294	1.80	75.0
P[MMA/1 2-EHAMA]	163	307	1.89	71.2
P[MMA/3 2-EHMA]	169	308	1.83	72.9
P[MMA/5 2-EHMA]	180	321	1.79	75.9
P[MMA/10 2-EHMA]	173	309	1.79	75.5
P[MMA/20 2-EHMA]	177	311	1.76	76.0
P[MMA/1 LMA]	164	311	1.90	72.3
P[MMA/3 LMA]	176	319	1.82	76.3
P[MMA/5 LMA]	179	330	1.84	80.9
P[MMA/10 LMA]	175	350	2.00	86.4

1.4.2. Determination of specific refractive index increment (*dn/dc*)

As the specific refractive index increment is needed for the accurate calculation of molar mass from the combined MALS and RI detection and for the determination of intrinsic viscosity from RI detector and viscometer, its accurate determination is paramount. Figure 8 shows an example for measuring the *dn/dc* plot for star-like polymer where Figure 9 represented example for linear polymer.

The average of *dn/dc* of selected star-like polymers and their corresponding arms with high and low molar masses are listed in Table 9 while the *dn/dc* for linear polymers are listed in Table 10. The values for linear polymers are well comparable with those reported previously [21,22]. The highly dense structure of star-like polymers does not have a significant impact on *dn/dc*. As expected, the *dn/dc* values are lower for the arms as a consequence of their low molar mass. Where the *dn/dc* value of PBZMA star-like polymer is less than the value given in the literature [59. Detailed information on how the literature value was determined is not given and thus the difference can be explained by the experimental uncertainty or by the sample purity in the sense of for instance possible content of residual solvent.

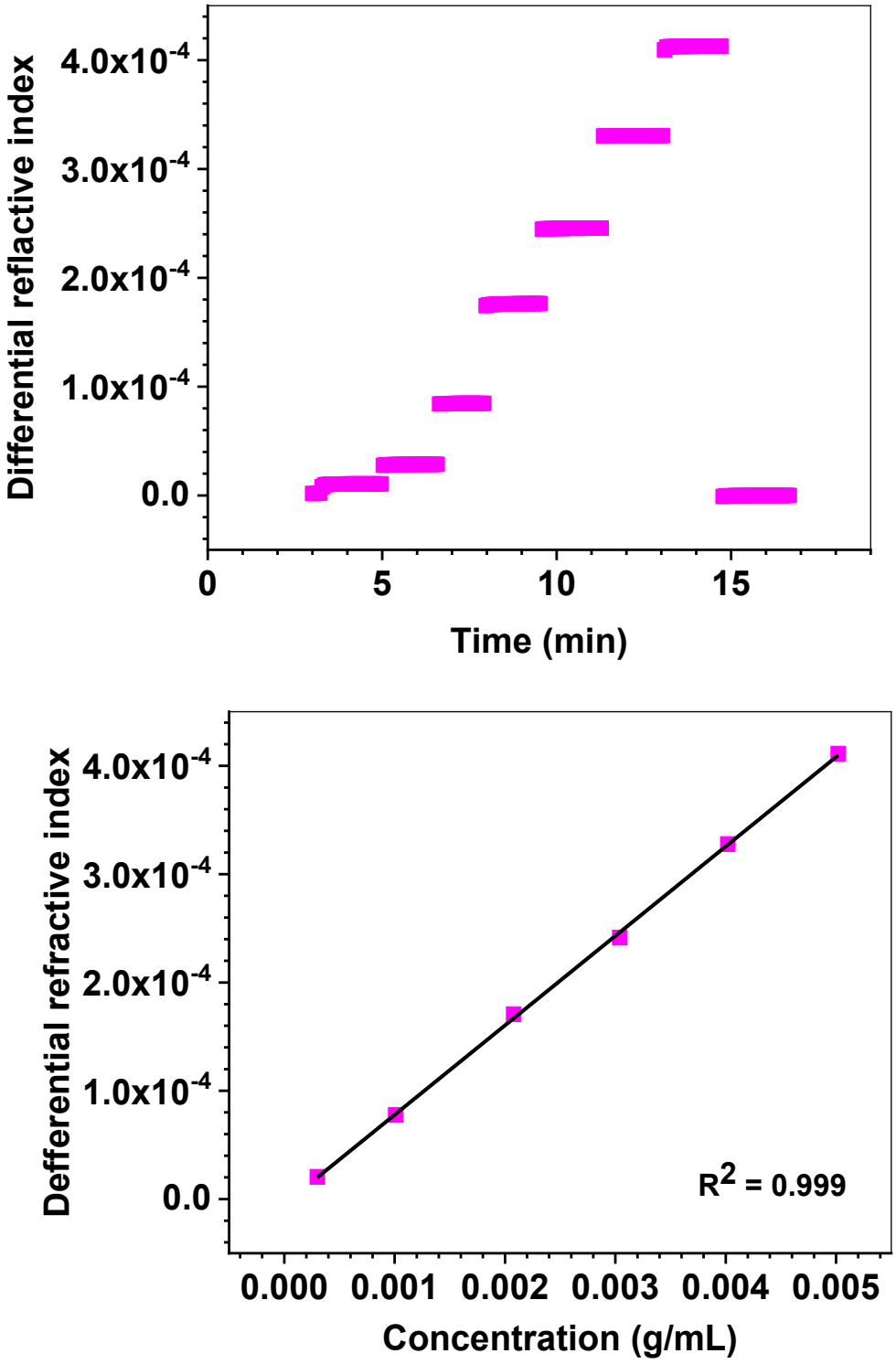

Figure 8 Measuring of specific refractive index increment (*dn/dc*) of B3 pure star-like sample in THF, 25 ˚C, λ 658 nm. Differential refractive index as a function of time (top). The first and last plateaus correspond to solvent without added polymer. Differential refractive index as a function of polymer sample concentration (bottom).

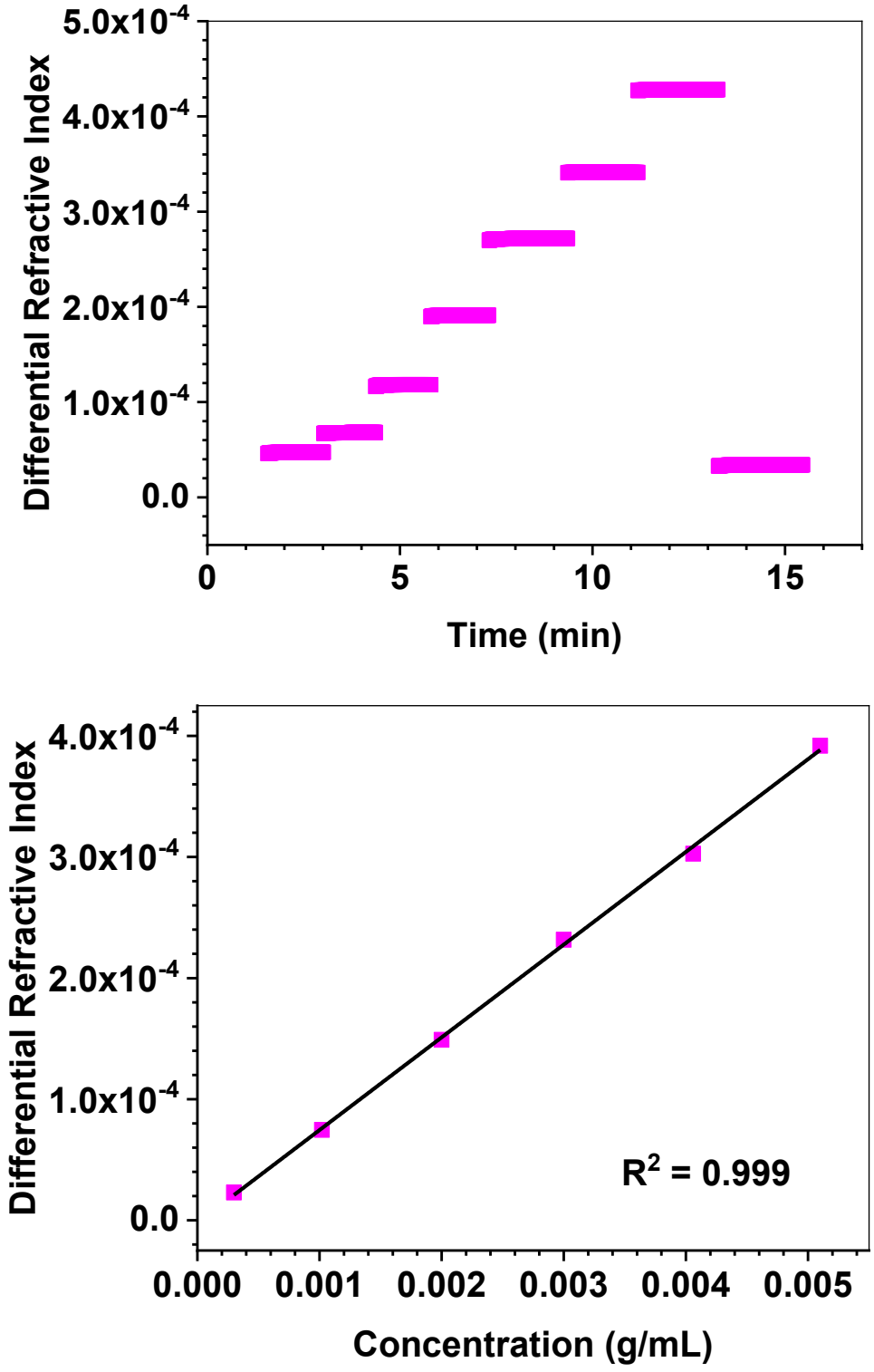

Figure 9 Measuring of specific refractive index increment (*dn/dc*) of linear PBMA in THF, 25 ˚C, λ 658 nm. Differential refractive index as a function of time (top). The first and last plateaus correspond to solvent without added polymer. Differential refractive index as a function of polymer sample concentration (bottom).

Table 10 Specific Refractive Index Increments in THF at 25 °C of pure arm and star polymers.

Polymer	M_w (Kg/mol)	*dn/dc* (mL g^{-1})*
B1 & B3 star	201&610	0.080 ± 0.002
B3 arm	9.9	0.074 ± 0.001
B10 arm	9.3	0.069 ± 0.001
M7 & M10 star	47&388	0.820 ± 0.002
M7 arm	1.8	0.074 ± 0.001
M1 arm	6.9	0.077 ± 0.001
BZ2 & BZ3 star	59&242	0.134 ± 0.001
BZ3 arm	2.8	0.136 ± 0.001

*The uncertainty is based on standard deviation and the uncertainty reported by ASTRA software.

Table 11 Specific Refractive Index Increments in THF at 25 °C of linear polymers.

Polymer	M_w (Kg/mol)	*dn/dc* (mL g^{-1})*
Linear PMMA	310	0.084 ± 0.001
Linear PBMA	497	0.077 ± 0.002
Linear PLMA	260	0.074 ± 0.001
Linear PBZMA	428	0.150 ± 0.002

*The uncertainty is based on standard deviation and the uncertainty reported by ASTRA software.

1.4.3. Solution properties of star-like polymers

The GTP arm-first strategy that is used in the preparation of methacrylate star-like polymers allows the stars to be well separated from the original arms which allows their quantification and characterization without isolation from the remaining arms. The conformation and Mark-Houwink plots of some selected star-like polymer samples are shown in Figures 10–12.

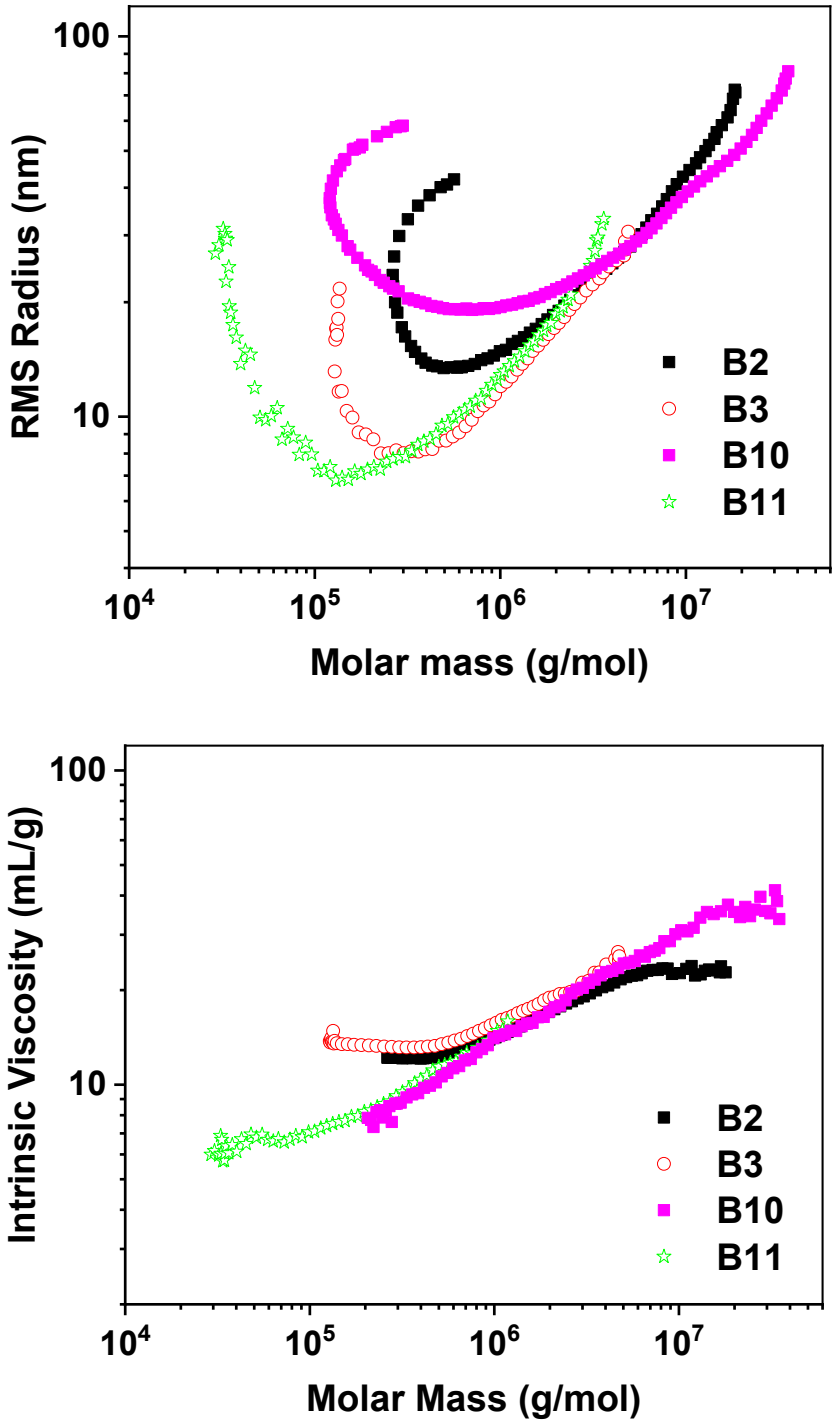

Figure 10 Conformation plot (top) and Mark-Houwink plots (bottom) determined by SEC-MALS-Visco for star-like PBMA with long and short arms.

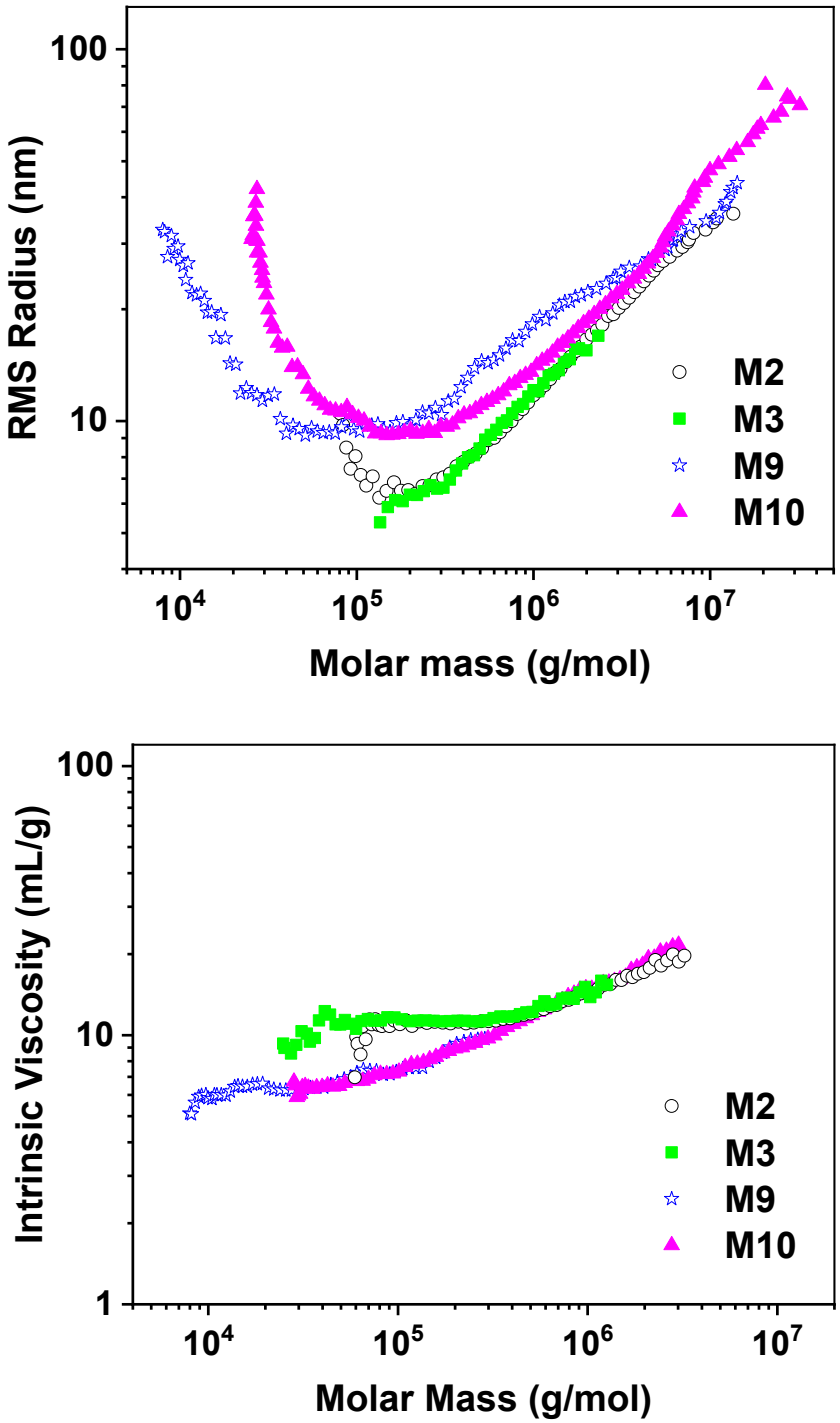

Figure 11 Conformation plot (top) and Mark-Houwink plot (bottom) determined by SEC-MALS-Visco for star-like PMMA with long and short arms.

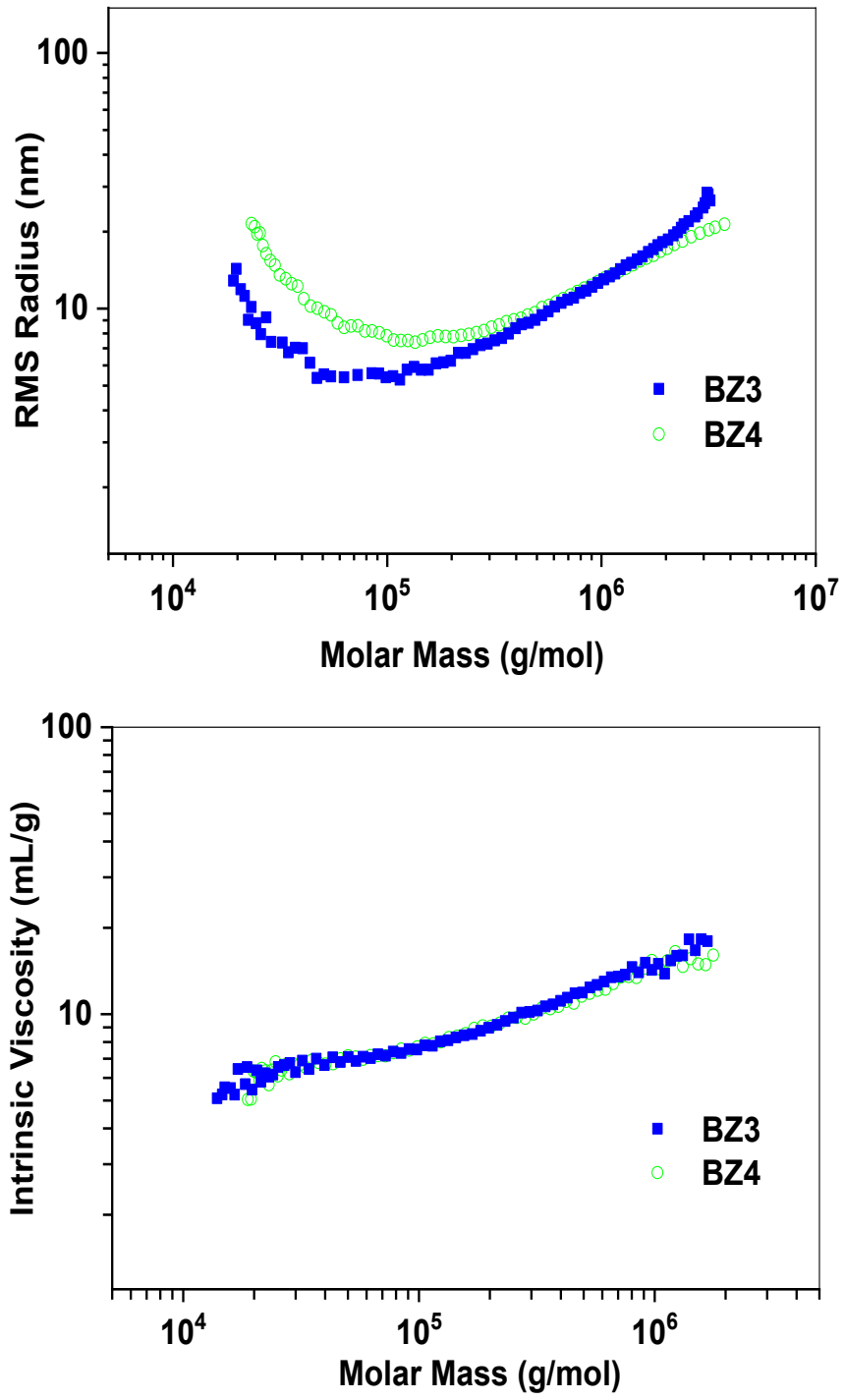

Figure 12 Conformation plot (top) and Mark-Houwink plot (bottom) determined by SEC-MALS-Visco for star-like PBZMA.

Data from Figure 11 as a selected PMMA star-like polymer samples yield the molar mass dependency of the ratios g and g′ shown in Figure 13. The draining parameter *e* can be calculated by comparing the branching ratios *g* and *g′* at the same molar mass. The relation between the parameter *e* and molar mass is described in Figure 14 together with that obtained for one of star-like PBMA. The values of *e* from ≈ 0.5 to ≈ 1.2 fall in the expected range and confirm the dependence of the draining parameter on molar mass. The increase of parameter *e* with molar mass indicates increasing drainability of large star-like macromolecules.

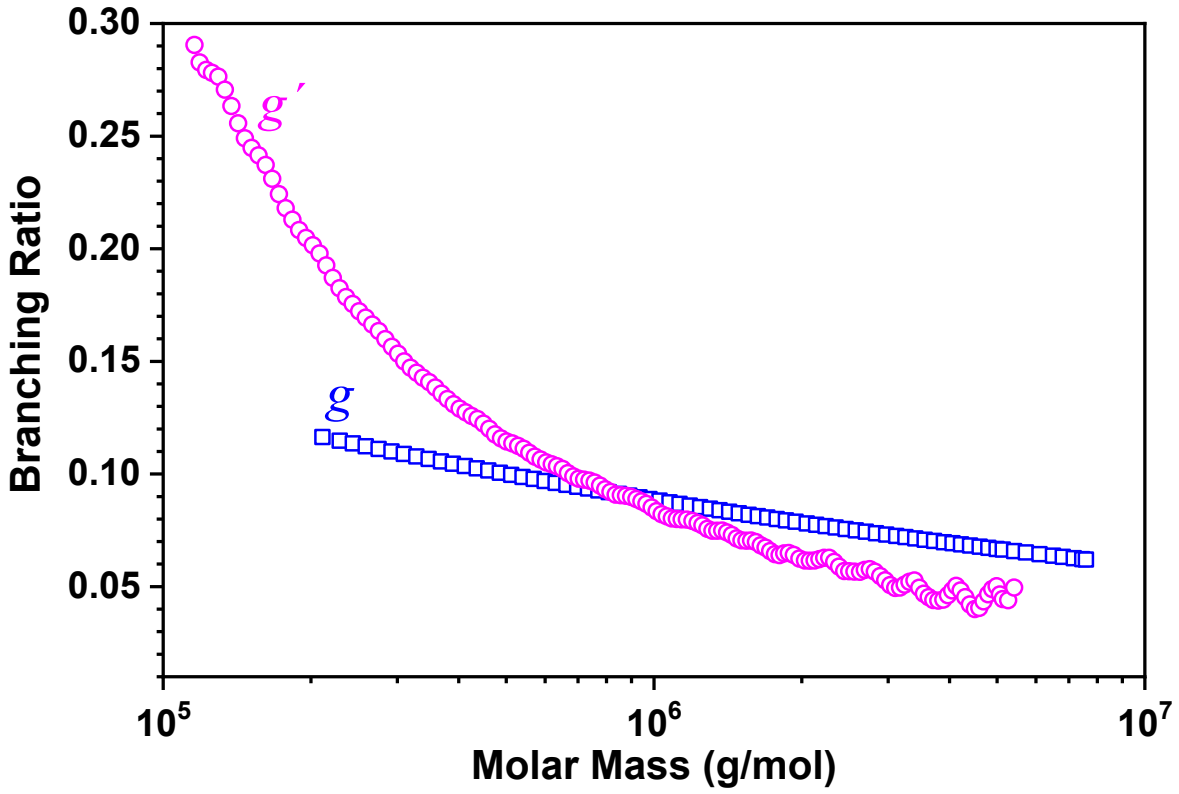

Figure 13 Branching ratios *g* (□, blue) and *g′* (○, magenta) versus molar mass plots of star-like PMMA (sample M2).

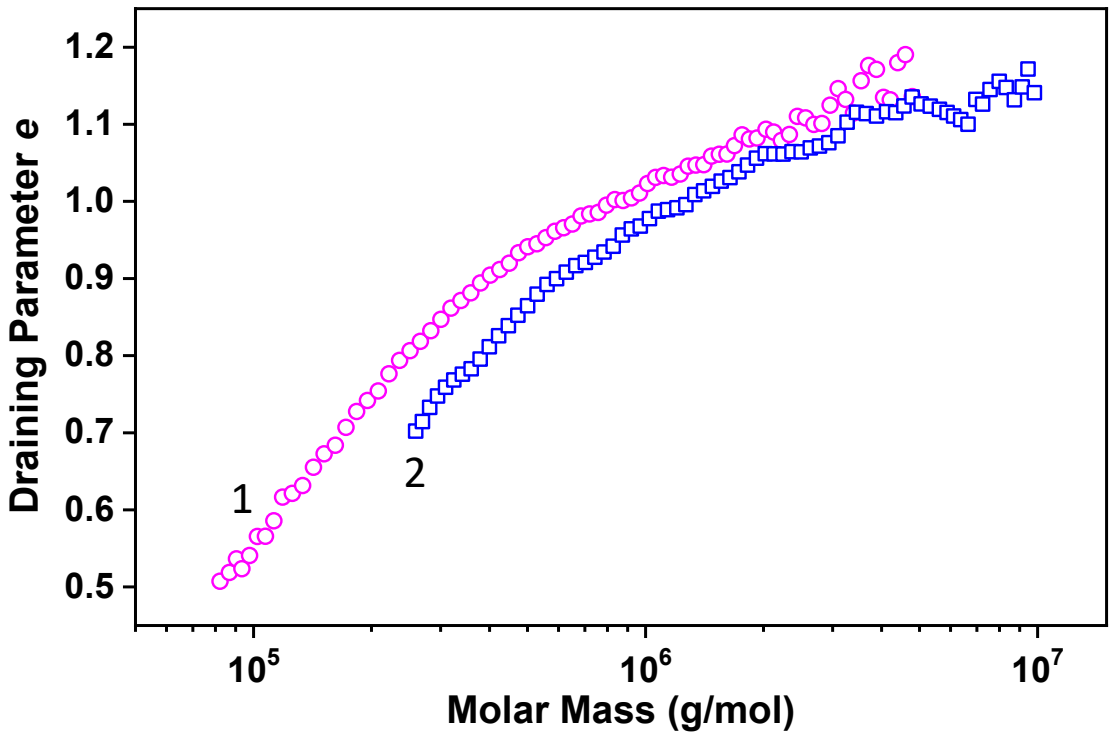

Figure 14 Draining parameter *e* versus molar mass plots of star-like PMMA (1 ○, magenta) and PBMA (2 □, blue) (samples M2 and B2).

The conformation plot is the most direct way to branching information. However, it has two limitations. It cannot be applied to polymers composed of the majority of molecules with RMS radii below ≈ 7 nm. Moreover, for many branched polymers it is strongly affected by the delayed elution of branched macromolecules as described for example in Reference [23].

The size limit applies to most of the prepared samples due to very high molecular compactness. In contrast to the conformation plot, the Mark-Houwink plot can be reliably measured with practically no size limit. In addition, it is markedly less affected by the delayed elution of the branched macromolecules [60].

Mark-Houwink plots of several star-like PMMAs composed of different arm length are compared in Figure 15. The slope (Mark-Houwink exponent) of the plots of star-branched polymers consisting of long arms is close to zero at the region of lower molar masses, which indicates sphere-like structure. Towards the high molar masses, the slope increases to the value of ≈ 0.28. The slope of the plots of samples consisting of short arms starts at ≈ 0.1 and increases to the same value as that of the stars from long arms. At lower molar masses, the plots of stars created by short arms are shifted to lower intrinsic viscosities which can be explained by higher

number of arms at the same molar mass and thus more compact molecular structure. The difference diminishes towards high molar masses. The increase of the Mark-Houwink exponent towards high molar mass suggests the transition of the molecules from sphere-like structures to more expanded structures. One can imagine that the molecules of high molar mass consist of several compact EGDMA cores which are connected by less compact links.

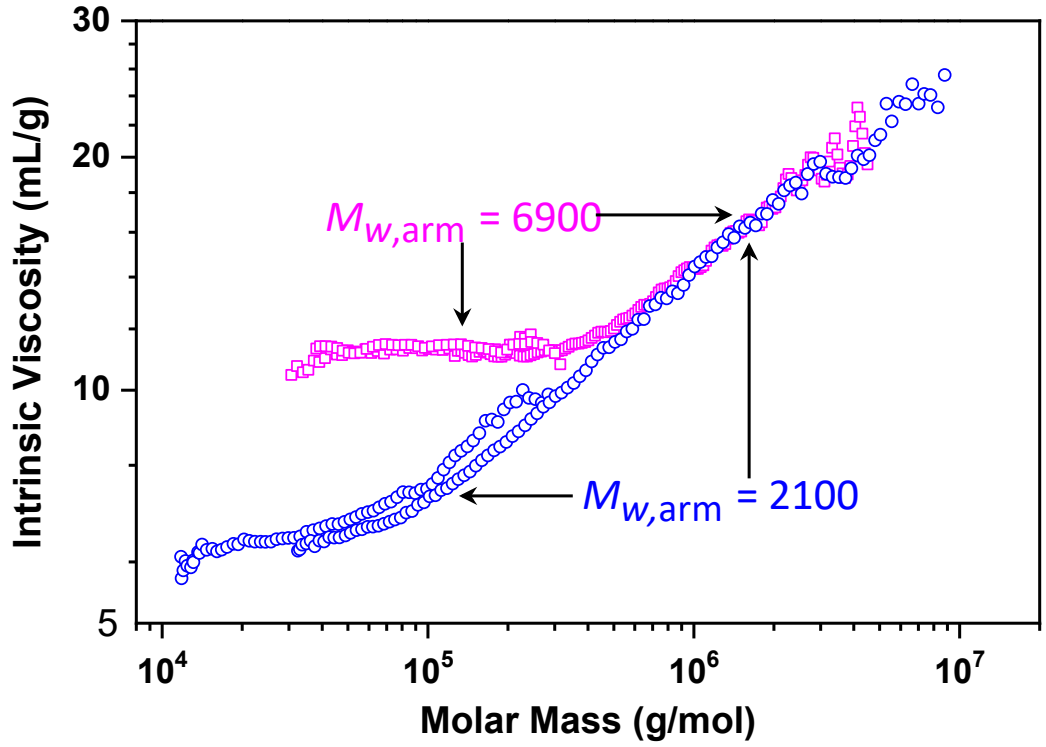

Figure 15 Mark-Houwink plots of star-like PMMAs with arm $M_w \approx 2100$ g/mol (○, blue) and ≈ 6900 g/mol (□, magenta).

The obtained data allow testing various *g*–versus–*f* equations since the true number of arms at each molar mass can be calculated from the slice molar mass and molar mass of the arm prepared in the first reaction step. Instead of explicitly expressing the *f* as a function of *g* or *g*′, Equations 1, 3, 6–8 were entered into Excel, and *g* or *g*′ were calculated for the stepwise increasing *f*, and then the experimental values of *g* or *g*′ were matched in regular intervals with *f*. Figure 16 depicts various plots of the number of arms per molecule against molar mass for star-like PMMA sample for which the determination of the RMS radius was possible and which did not show a significant tendency to the delayed elution and such allowed testing also the Equations 1 and 3. The conclusion from Figure 16 is that none of the equations allow accurate determination of the number of arms from the ratios *g* or *g*′. However, a very good agreement between the plot obtained using Equation 6 and that calculated from the slice molar mass was

obtained for stars created by short arms as shown in Figure 17. The modification of Equation 6 in the sense of using exponent 1.6 instead of 1.5 gives good agreement for the stars consisting of long arms as shown in Figure 18. Similar results are obtained for star-like PBMA, i.e., Equation 6 markedly overestimates the number of arms per molecule in the case of long arms, whereas markedly better agreement is obtained for polymer consisting of short arms as shown in Figure 19. The polymer consisting of long arms requires increasing the exponent to the value of ≈ 1.7 as demonstrated in Figure 20. Comparison of samples M2 (arm M_w ≈ 6900 g/mol) and B2 (arm M_w ≈ 9300 g/mol) indicates that longer arms require higher exponent.

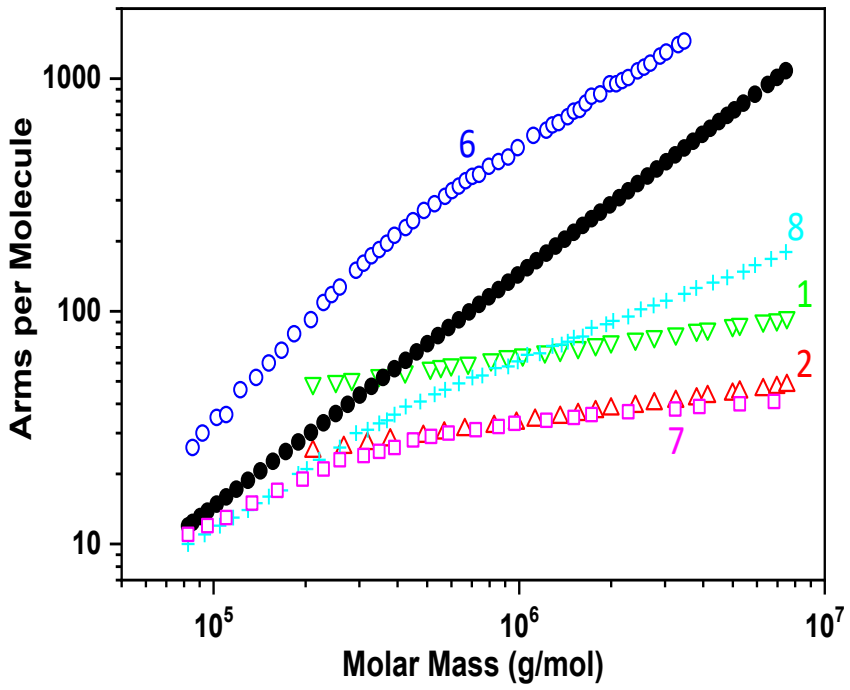

Figure 16 Plots of number of arms per molecules versus molar mass calculated by the division of slice molar mass by M_w of arms (●) and estimated from Equations 1, 2, 6, 7, and 8 for star-like PMMA with arm M_w ≈ 6900 g/mol (sample M2).

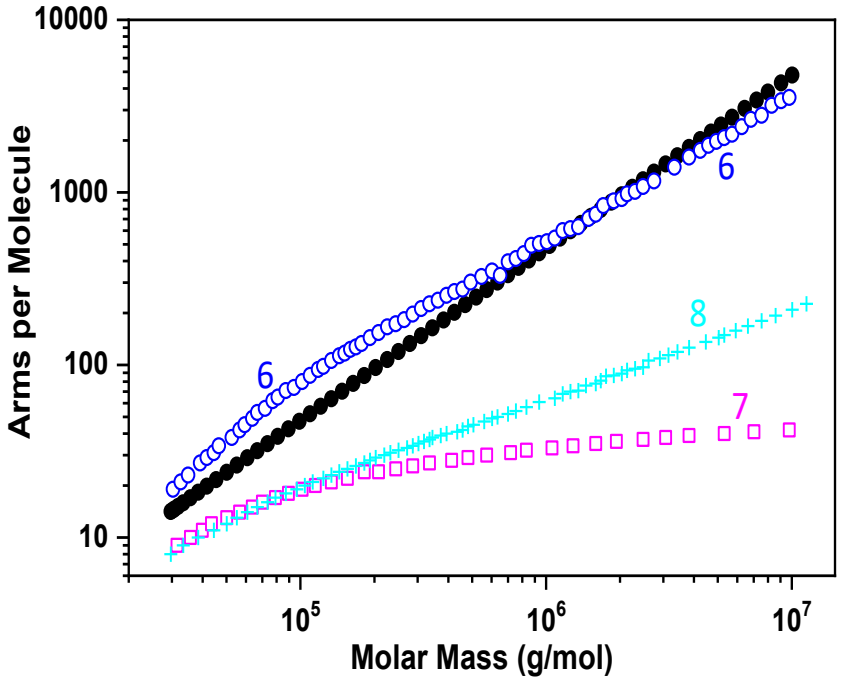

Figure 17 Plots of number of arms per molecule versus molar mass calculated by the division of slice molar mass by M_w of arms (●) and estimated from Equations 6, 7, and 8 for star-like PMMA with arm $M_w \approx 2100$ g/mol (sample M10).

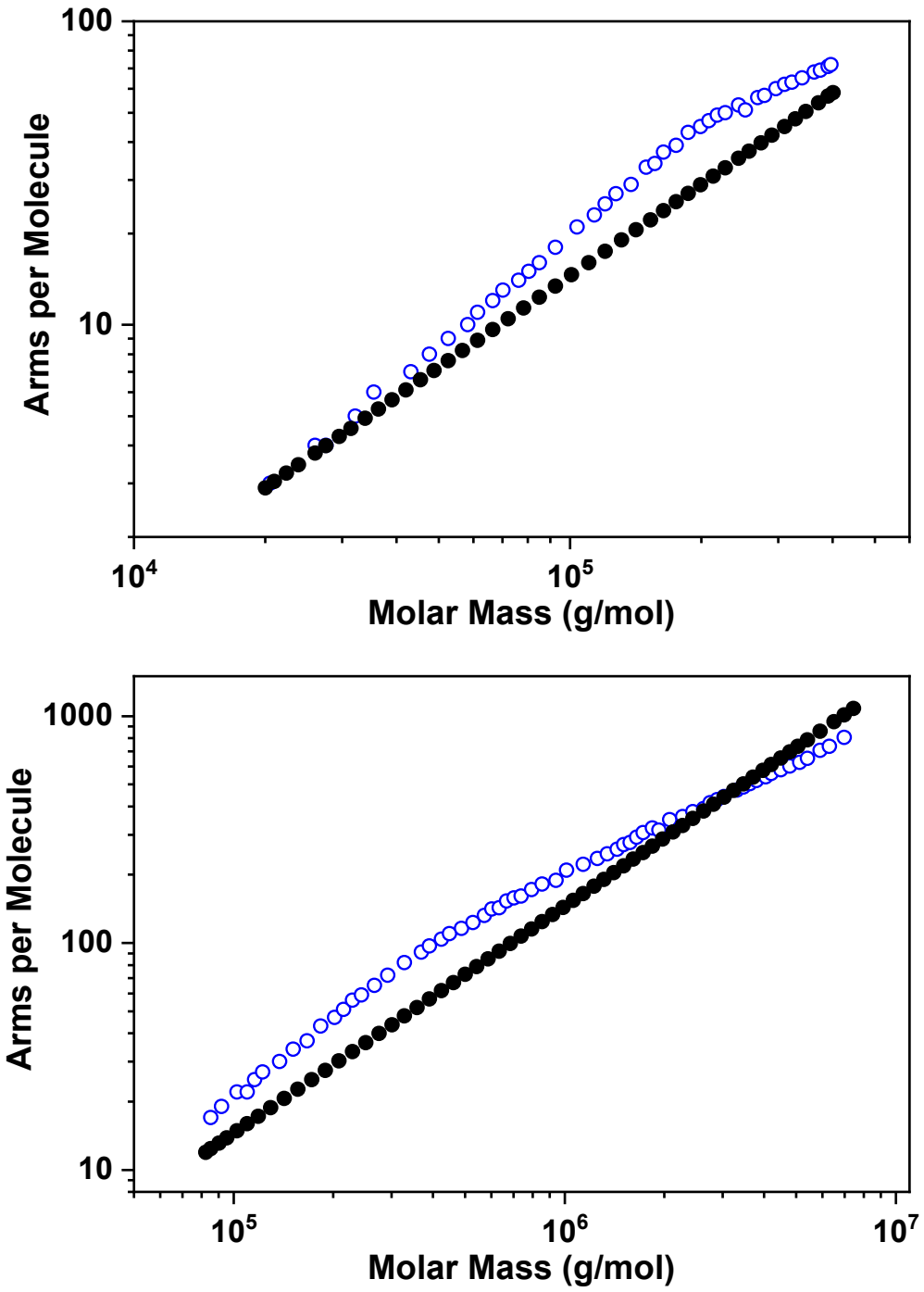

Figure 18 Plots of number of arms per molecule versus molar mass for two star-like PMMAs consisting of arms having $M_w \approx 6900$ g/mol calculated by the division of slice molar mass by M_w of arms (●) and estimated from Equation 6 using the exponent 1.6 instead of 1.5 (○, magenta; samples M1 top and M2 bottom).

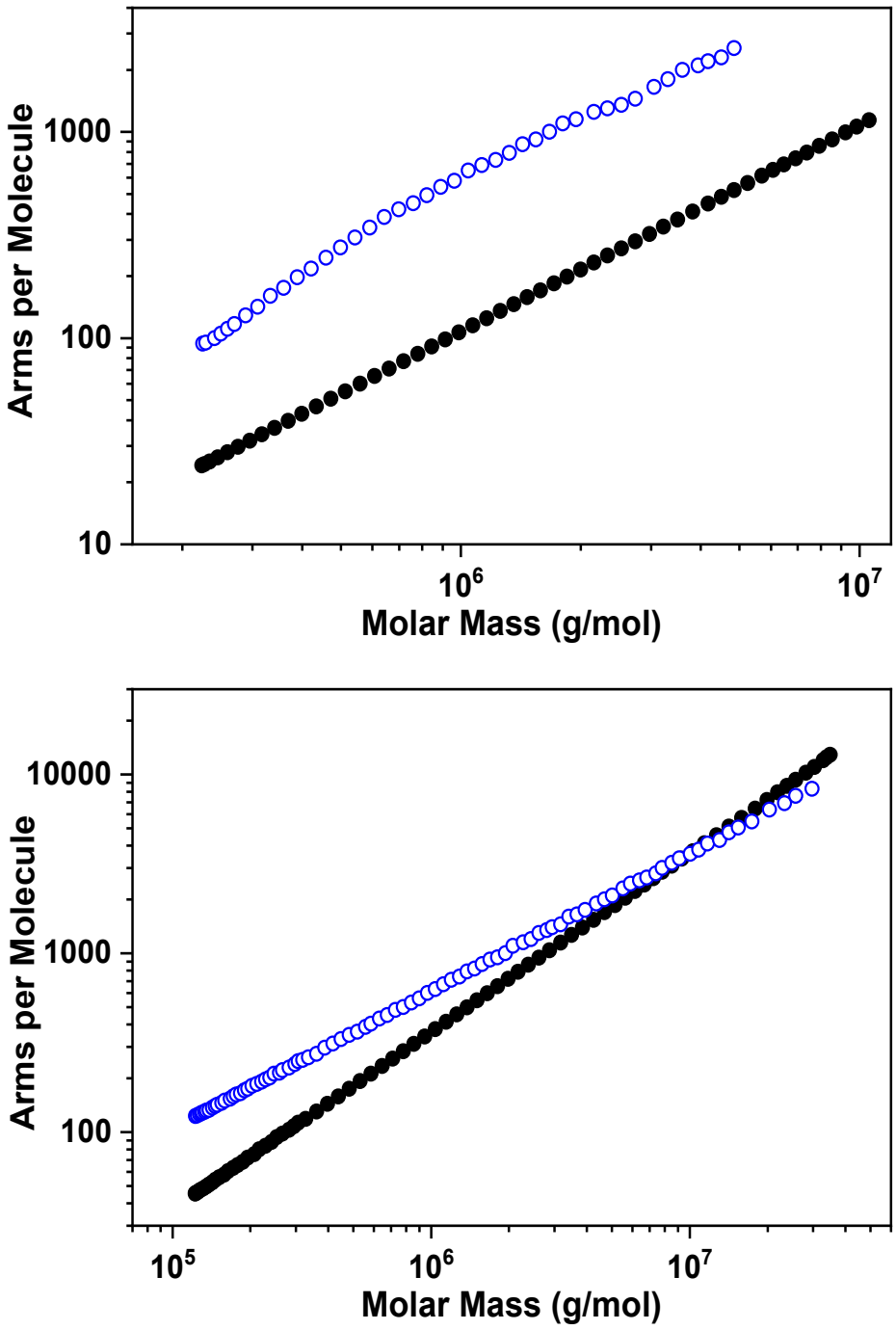

Figure 19 Number of arms per molecule versus molar calculated by the division of slice molar mass by M_w of arms (●) and estimated using Equation 6 for star-like PBMA with arm $M_w \approx 9300$ g/mol (top, sample B2) and $M_w \approx 2700$ g/mol (bottom, sample B10).

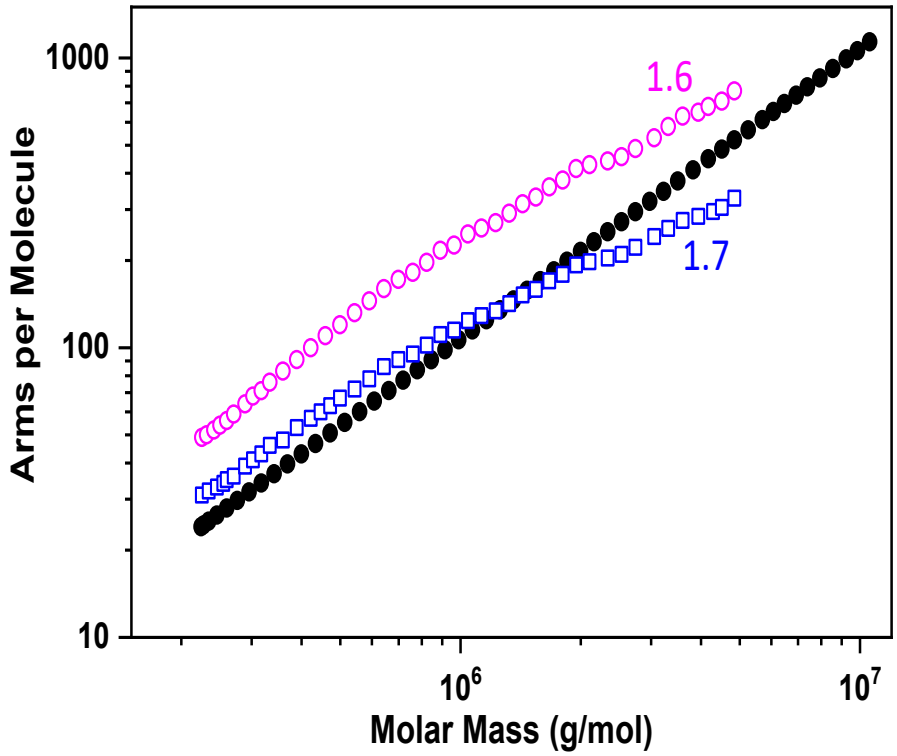

Figure 20 Plots of number of arms per molecule versus molar mass for star-like PBMA consisting of arms having $M_w \approx 9300$ g/mol calculated by the division of slice molar mass by M_w of arms (●) and estimated from Equation 6 using the exponent 1.6 (○, magenta) and 1.7 (□, blue), (sample B2).

The molar mass distribution exported from ASTRA to Excel can be converted to the distribution of arms per molecule by dividing the molar mass axis by the molar mass of arm. The plots obtained for various PMMA and PBMA star-like polymers are shown in Figure 21.

Exporting the slice molar masses and the slice concentrations permits the calculation of the number-average (f_n) and the weight-average (f_w) arms per molecule using the equations equivalent to those for the calculation of molar mass moments:

$$f_n = \frac{1}{\sum \frac{w_i}{f_i}} \tag{11}$$

$$f_w = \sum w_i f_i \tag{12}$$

where f_i is the number of arms in molecules eluting at the *i-th* elution volume V_i and w_i is the weight fraction of molecules eluting at that V_i calculated as the slice concentration c_i divided by the sum $\sum c_i$.

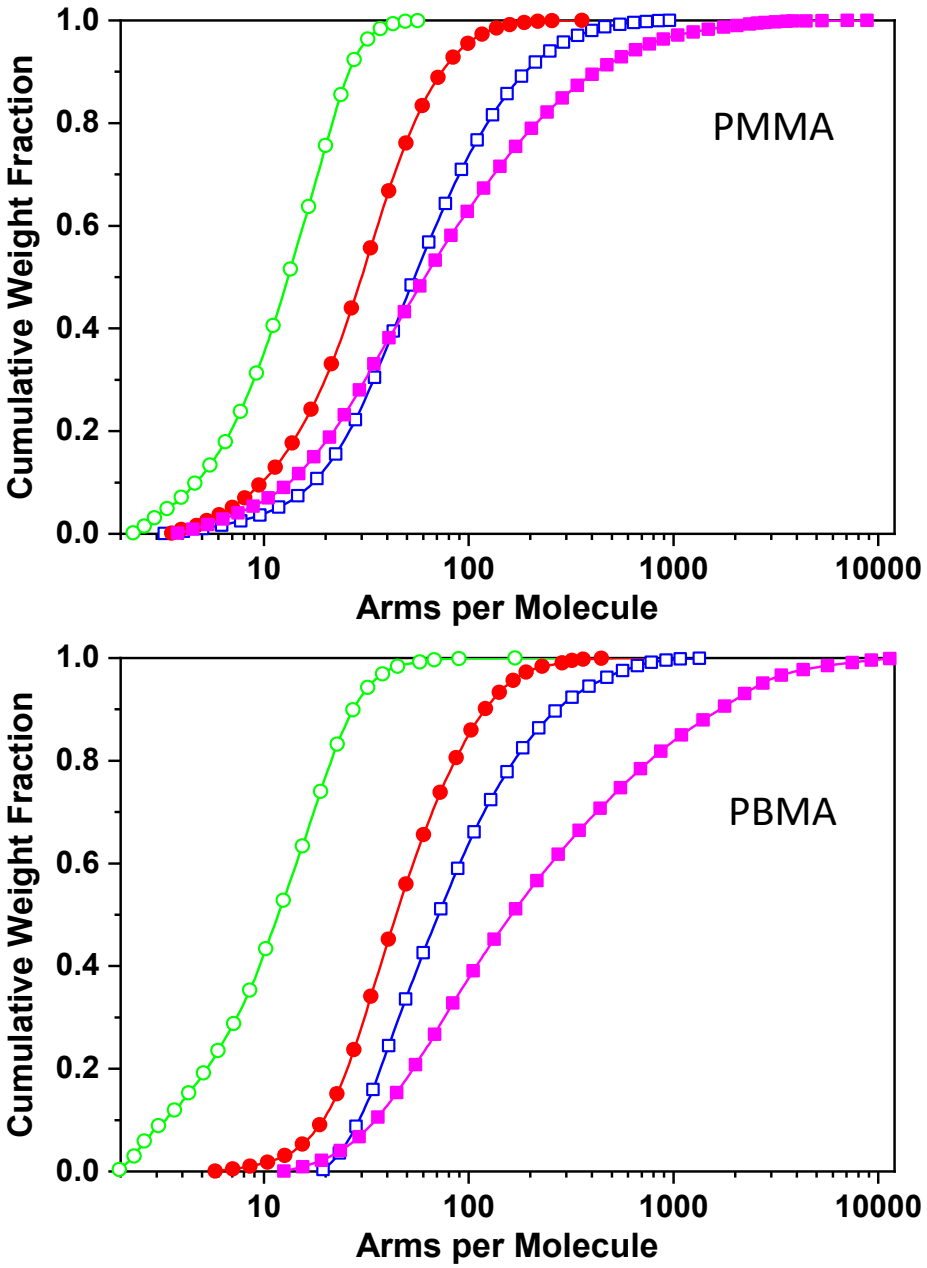

Figure 21 Cumulative distribution of arms per molecule for PMMA star-like polymers with long (samples M1○, green; M2 □,blue and M3 ●, red) and short (sample M10 ■, magenta) arms; and for PBMA star-like polymers with long (samples B2 □, blue; B3 ●, red and B4 ○, green) and short (sample B10 ■, magenta) arms.

The results for samples shown in Figure 21 are listed in Table 11. Table 11 is further completed by the values of $g'(M_w)$. The average branching ratio $g'(M_w)$ is the ratio of the experimental weight-average intrinsic viscosity of the branched polymer divided by the intrinsic viscosity of a hypothetical linear polymer that would have the same M_w as the polymer

requiring analysis. This ratio can be used for mutual comparison of different samples for which the molar mass of arms is unknown.

Table 12 Number-average and weight-average arms per molecule and g′(M_w) for samples shown in Figure 21.

Sample	f_n	f_w	$g'(M_w)$
M1	9	24	0.326
M2	35	80	0.103
M3	19	35	0.173
M10	35	163	0.101
B2	52	110	0.069
B3	33	56	0.105
B4	8	13	0.300
B10	77	582	0.048

1.4.4. Short chain branching of linear methacrylate polymers

The RMS radius conformation plots (i.e., log-log relation RMS radius–molar mass) and Mark-Houwink plots (log-log relation intrinsic viscosity–molar mass) measured by SEC-MALS-Visco give valuable information about the molecular structure and dilute solution properties of the prepared linear homopolymers and PMMA with different comonomers. All conformation plots for homopolymers and copolymers are shown in Figures 22 and 23.

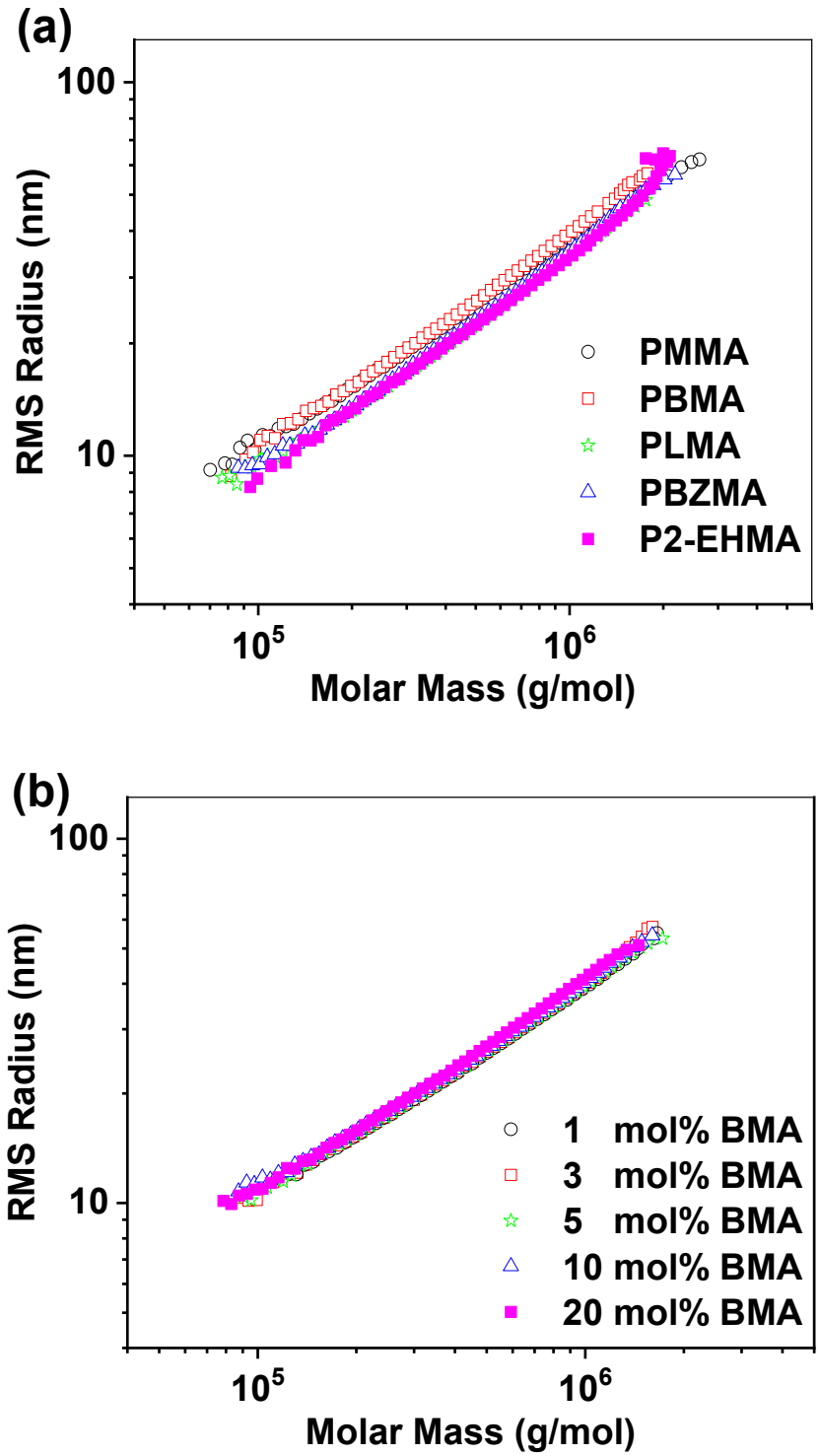
(a)
100
10
RMS Radius (nm)
10^5
10^6
Molar Mass (g/mol)
PMMA
PBMA
PLMA
PBZMA
P2-EHMA
(b)
100
10
RMS Radius (nm)
10^5
10^6
Molar Mass (g/mol)
1 mol% BMA
3 mol% BMA
5 mol% BMA
10 mol% BMA
20 mol% BMA

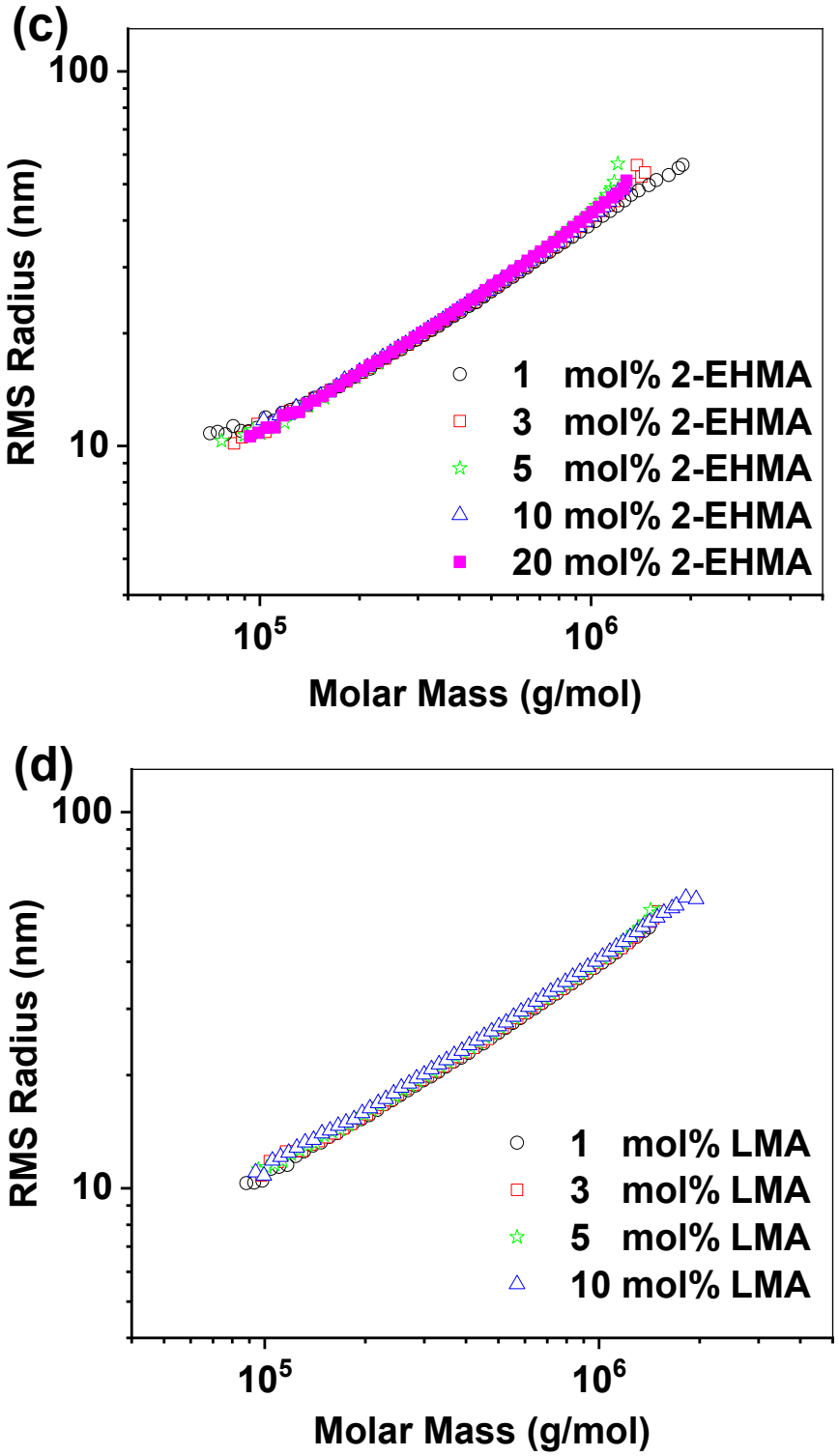

Figure 22 Conformation plots of PMMA, PBMA, PBZMA, PLMA and P2-EHMA homopolymers (a), P[MMA/BMA] copolymers (b), P[MMA/2-EHMA] copolymers (c) and P[MMA/LMA] copolymers (d) with slope ~ 0.6 for all plots.

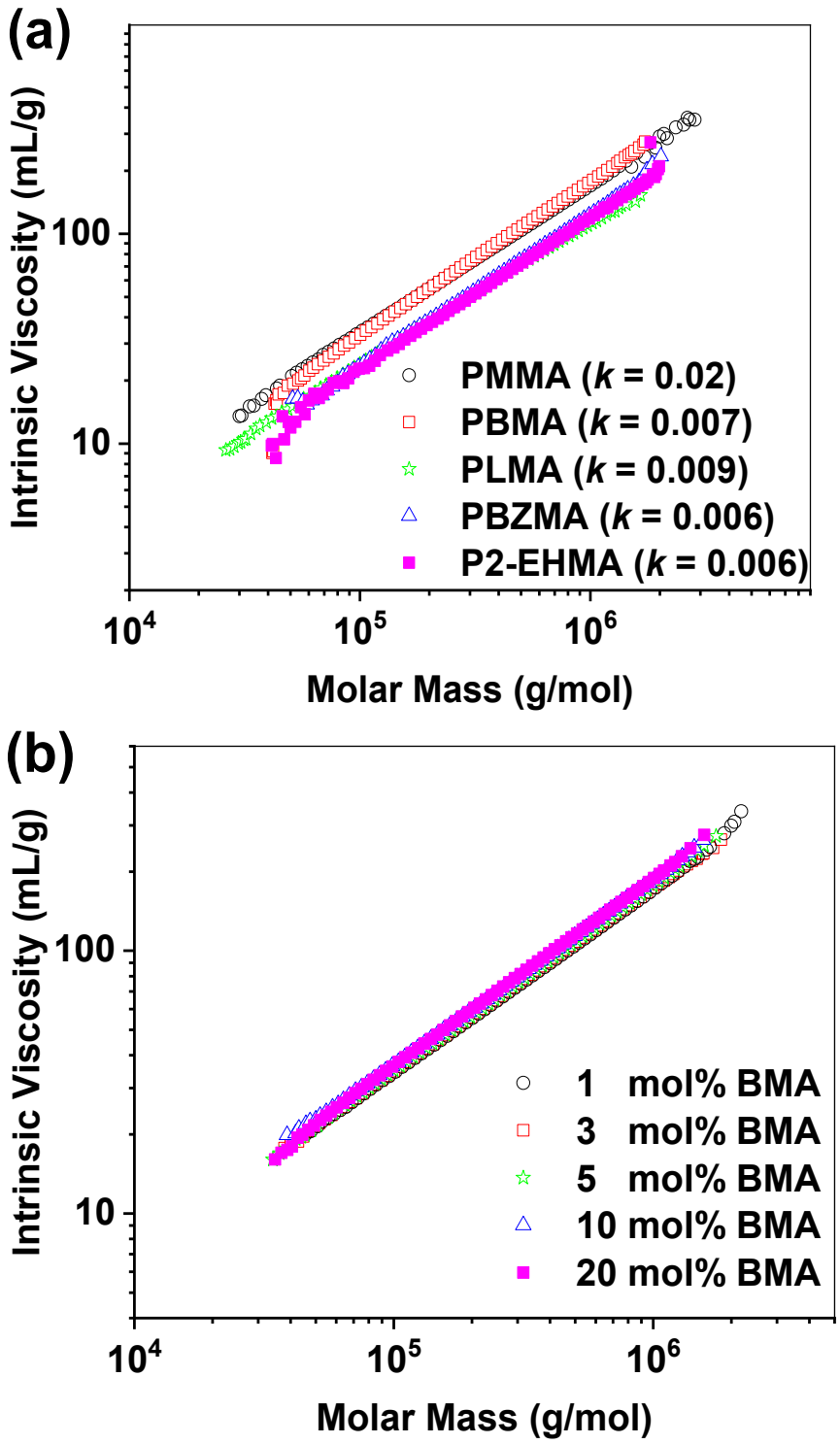
(a)
Intrinsic Viscosity (mL/g)
100
10
10^4
10^5
10^6
Molar Mass (g/mol)
PMMA (k = 0.02)
PBMA (k = 0.007)
PLMA (k = 0.009)
PBZMA (k = 0.006)
P2-EHMA (k = 0.006)
(b)
Intrinsic Viscosity (mL/g)
100
10
10^4
10^5
10^6
Molar Mass (g/mol)
1 mol% BMA
3 mol% BMA
5 mol% BMA
10 mol% BMA
20 mol% BMA

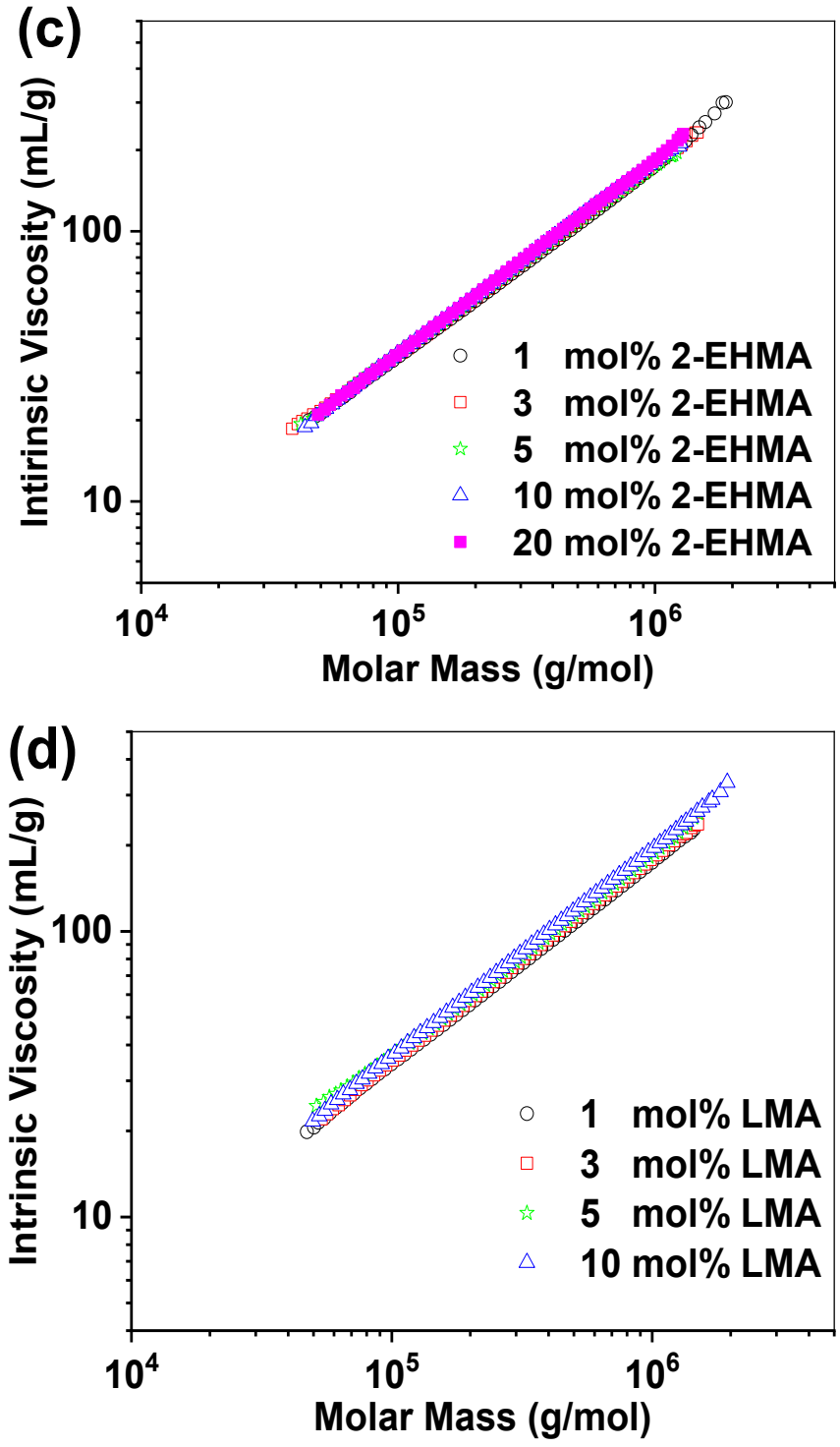

Figure 23 Mark-Houwink plots of PMMA, PBMA, PBZMA, PLMA and P2-EHMA homopolymers (a), P[MMA/BMA] copolymers (b), P[MMA/2-EHMA] copolymers (c) and P[MMA/LMA] copolymers (d) with slope ~ 0.7 for all plots.

The slope of the conformation plots and the Mark-Houwink plots represented in Figure 22 and Figure 23, respectively, of the homopolymers and copolymers are approximately the same ($b \sim 0.6$ slope of conformation plots and $a \sim 0.7$ slope of Mark-Houwink plots) indicating that the power law exponents of each relation are insensitive to the comonomer content. Also, the intercept of the Mark-Houwink plot of PMMA and PBMA homopolymers are very close, and the intercept of PBZMA, P2-EHMA and LMA homopolymers are approximately identical (Figure 22 (a) and Figure 23 (a)). The intercept is slightly shifted only when the side chains increase from C4 to C12, or when they are aromatic rings as evident from comparing PMMA and PBMA with LMA and PBZMA as shown in Figure 22 (a) and Figure 23 (a).

1.4.5. Carbon fibre reinforced polymer (CFRP) composites

Due to the important role of stare-like polymers in the application of automotive composite components related to durability and crashworthiness. Star-like polymers can be used as important components of fiber reinforced composites in the automotive industry. Therefore, some of the prepared star-like polymers were studied as additives to the epoxy matrix (Bisphenol-A) and carbon fibre composites with the cooperation of SYNPO, Czech Republic, and the Department of Mechanical Engineering, Kaunas University of Technology, Kaunas, Lithuania. Tensile and impact tests were performed to analyze the effect of matrix modification. Tensile tests performed on epoxy with various weight fractions of PBMA star-like polymer showed that the addition of 1 wt.% is optimum. The tensile strength was improved from about 35 MPa (for pure epoxy) to about 80 MPa (for 1 wt.% modified epoxy). Carbon fibre was reinforced with 1 wt.% and 3 wt.% star-like polymer-modified epoxy matrixes. By comparing the pure CFRP composites and CFRP composites modified with 1wt% and 3wt% of star-like polymer, it showed that the 1 wt.% star-like polymer sample absorbed more energy while having lower deflection, compared to 3 wt.% star-like polymer samples showing scope for further energy absorption. Both 1 and 3 wt.% modified CFRP composites samples exhibited brittle modes of failure with evident fibre pull out without dimpling. 1 wt.% of star-like polymer CFRP samples showed good adhesion, and wettability and several cases of matrix bridging were observed while CFRP samples modified with 3 wt.% star-like polymers exhibited stiffness and cracks throughout the cured matrix. The details of this study have been already published in reference [61].

1.5. Conclusion

As expected, based on the literature, it is possible to prepare various star-like methacrylate polymers and their corresponding linear polymers.

The arms prepared at the first step were found very narrow. The star-like structures synthetized in the second step are polydisperse as the prepared macromolecules differ in the number of arms. For the first time, the star-like polymers were studied in detail by the combined SEC-MALS-Visco technique. Using the data from commercially available software ASTRA it is possible to determine the distribution of arms in a given sample and to calculate the various averages of the number of arms per molecule. This calculation has not been reported previously.

Most of the literature equations provide values of arms per molecule far from the true ones. The only exception is Equation (6) which is approximately valid for polymers consisting of short arms. In the case of long arms, Equation (6) needs to be slightly modified by increasing the exponent 1.5 to the values of 1.6–1.7. The obtained data suggest that the longer arms require a higher exponent. However, this finding is of limited practical meaning for polymers of unknown arm length that can be only compared mutually using the average ratio $g'(M_w)$. The draining parameter of the star-like methacrylate polymers was found to be molar mass dependent within the expected range of about 0.5–1.2.

Very surprising information is that in contrast to published results for short-chain branched polyethylene, the short chains in PMMA-based copolymers do not affect the intercept of the Mark-Houwink plots as described in reference [26].

The obtained values of *dn*/*dc* were well consistent with the literature data. The *dn*/*dc* of PLMA was reliably determined for the first time as well as the fact that the extremely compact structure of star-like polymers do not affect their *dn*/*dc* compared to linear analogues.

The results of using a selected star-like sample as an additive for epoxy matrix (bisphenol-A) and carbon fiber composites showed the potential of star-like polymers as powerful additives with strong influence on the impact properties of carbon fiber reinforced polymer composites.

It proves that, beside the high energy absorbing of stars, they can also offer good prospects for application in automotive composite components in terms of durability and crashworthiness.

1.6. References

[1] G. Lapienis, Star-shaped polymers having PEO arms, Progress in Polymer Science, 34 (2009) 852.

[2] D. Kuckling, A. Wycisk, Stimuli-responsive star polymers, Journal of Polymer Science Part A: Polymer Chemistry, 51 (2013) 2980.

[3] Z. Iatridi, C. Tsitsilianis, Water-soluble stimuli responsive star-shaped segmented macromolecules, Polymers, 3 (2011) 1911.

[4] Y. Deng, S. Zhang, G. Lu, X. Huang, Constructing well-defined star graft copolymers, Polymer Chemistry 4 (2013) 1289.

[5] L. Mei, Y. Jiang, S.-S. Feng, Star-shaped block polymers as a molecular biomaterial for nanomedicine development, Nanomedicine, 9 (2014) 9.

[6] Y. Lu, L. An, Z.G. Wang, Intrinsic viscosity of polymers: General theory based on a partially permeable sphere model, Macromolecules, 46 (2013) 5731.

[7] J.R. Höhner, R.A. Gumerov, I.I. Potemkin, C. Rodriguez-Emmenegger, N.Y. Kostina, A. Mourran, J.R. Englert, D. Schröter, L. Janke, M. Möller, Globular Hydrophilic Poly (acrylate) s by an Arborescent Grafting-from Synthesis, Macromolecules, 55(2022) 2222.

[8] P.D. Gujrati, Polydisperse solution of randomly branched homopolymers, inversion symmetry and critical and theta states, The Journal of chemical physics, 108 (1998) 5089.

[9] D. Hayward, R.A. Pethrick, B. Eling, E. Colbourn, Prediction of the rheological properties of reactive polymer systems, Polymer international, 44 (1997) 248.

[10] J.H. Daly, D. Hayward, R.A. Pethrick, 2013. Prediction of the rheological properties of a curing thermoset system, Macromolecules, 46(2013) 3621.

[11] H. Stutz, K.H. Illers, J. Mertes, A generalized theory for the glass transition temperature of crosslinked and uncrosslinked polymers, Journal of Polymer Science Part B: Polymer Physics, 28 (1990) 1483.

[12] M.C. Righetti, M.L. Di Lorenzo, D. Cavallo, A.J. Müller, M. Gazzano, Structural evolution of poly (butylene succinate) crystals on heating with the formation of a dual lamellar population, as monitored by temperature-dependent WAXS/SAXS analysis, Polymer, 268 (2023) 125711.

[13] B.J. Factor, T.P. Russell, B.A. Smith, L.J. Fetters, B.J. Bauer, C.C. Han, Phase-separation kinetics of mixtures of linear and star-shaped polymers, Macromolecules, 23 (1990) 4452.

[14] O. Kalyuzhnyi, J.M. Ilnytskyi, Y. Holovatch, C. Von Ferber, Universal shape characteristics for the mesoscopic star-shaped polymer via dissipative particle dynamics simulations, Journal of Physics: Condensed Matter, 30 (2018) 215101.

[15] J. Hadar, S. Skidmore, J. Garner, H. Park, K. Park, Y. Wang, B. Qin, X. Jiang, Characterization of branched poly (lactide-co-glycolide) polymers used in injectable, long-acting formulations, Journal of Controlled Release, 304 (2019) 75.

[16] J. Hadar, S. Skidmore, J. Garner, H. Park, K. Park, Y. Wang, B. Qin, X.J. Jiang, D. Kozak, Method matters: Development of characterization techniques for branched and glucose-poly (lactide-co-glycolide) polymers, Journal of Controlled Release, 320 (2020) 484.

[17] B.H. Zimm, W.H. Stockmayer, The dimensions of chain molecules containing branches and rings, The Journal of Chemical Physics, 17 (1949) 1301.

[18] B.H. Zimm, R.W. Kilb, Dynamics of branched polymer molecules in dilute solution, ournal of Polymer Science, 37 (1959) 19.

[19] J. Douglas, J. Roovers, K. Freed, Characterization of branching architecture through" universal" ratios of polymer solution properties, Macromolecules, 23 (1990) 4168.

[20] J. Roovers, In Star and Hyperbranched Polymers, M.K. Mishra, S. Kobayashi, (Eds.), Marcel Dekker, New York, NY, 1999, pp. 285-341.

[21] R.W. Simms, M.F. Cunningham, High molecular weight poly (butyl methacrylate) by reverse atom transfer radical polymerization in miniemulsion initiated by a redox system, Macromolecules, 40 (2007) 860.

[22] A.M. Striegel, Specific refractive index increment (∂ n/∂ c) of polymers at 660 nm and 690 nm, Chromatographia, 80 (2017) 989.

[23] S. Podzimek, T. Vlcek, C. Johann, Characterization of branched polymers by size exclusion chromatography coupled with multiangle light scattering detector. I. Size exclusion chromatography elution behavior of branched polymers, Journal of Applied Polymer Science, 81 (2001) 1588.

[24] L. Mandelkern, In Physical Properties of Polymers, 2nd ed., J.E. Mark, (Eds.), American Chemical Society, Washington, DC, 1993, Ch. 4.

[25] I.M. Ward, Mechanical Properties of Solid Polymers, 2nd ed., J. Wiley & Sons: New York, 1983.

[26] T. Sun, P. Brant, R.R. Chance, W.W. Graessley, Effect of short chain branching on the coil dimensions of polyolefins in dilute solution, Macromolecules, 34(2001) 6812.

[27] M. Chanda, Introduction to Polymer Science and Chemistry: A Problem-Solving Approach, second ed., CRC Press, Boca Raton, FL, 2013, pp.1820.

[28] R.J. Young, P.A. Lovell, Introduction to Polymers, third ed., CRC Press, Boca Raton, FL, 2011, pp. 56.

[29] X. Zhu, Y. Zhou, D. Yan, Influence of branching architecture on polymer properties, Journal of Polymer Science Part B: Polymer Physics, 49 (2011) 1277.

[30] S. Sant, S. Poulin, P. Hildgen, Effect of polymer architecture on surface properties, plasma protein adsorption, and cellular interactions of pegylated nanoparticles, Journal of Biomedical Materials Research Part A, 87 (2008) 885.

[31] K. Inoue, S. Horibe, M. Fukae, T. Muraki, E. Ihara, H. Kayama, Synthesis and Conformation of Star-Shaped Poly (γ-benzyl-l-glutamate) s on a Cyclotriphosphazene Core, Macromolecular Bioscience, 3 (2003) 26.

[32] N. Hadjichristidis, M. Pitsikalis, H. Iatrou, Polymers with Star-Related Structures, Macromolecular Engineering, Wiley-VCH Verlag GmbH & Co. KGaA, 2007, pp. 909–972

[33] A. Duro-Castano, R.M. England, D. Razola, E. Romero, M. Oteo-Vives, M.A. Morcillo, M.J. Vicent, Well-defined star-shaped polyglutamates with improved pharmacokinetic profiles as excellent candidates for biomedical applications, Molecular Pharmaceutics, 12 (2015) 3639.

[34] Q. Chen, Y. Xu, X. Cao, L. Qin, Z. An, Core cross-linked star (CCS) polymers with temperature and salt dual responsiveness: synthesis, formation of high internal phase emulsions (HIPEs) and triggered demulsification, Polymer Chemistry, 5 (2014) 175.

[35] Q. Chen, X. Cao, Y. Xu, Z. An, Emerging Synthetic Strategies for Core Cross-Linked Star (CCS) Polymers and Applications as Interfacial Stabilizers: Bridging Linear Polymers and Nanoparticles. Macromolecular rapid communications, 34 (2013) 1507.

[36] R.O. Ebewele, Polymer Science and Technology, CRC Press, Boca Raton, FL, 2000.

[37] P. Ghosh, Polymer Science and Technology: Plastics, Rubbers, Blends and Composites, second ed., Tata McGraw-Hill, New York, 2002, pp. 6667.

[38] G.S. Mishra, Introductory Polymer Chemistry, New Age International Publishers, New Delhi, 2005, pp. 847.

[39] F.P. Boettcher, I.B. Dicker, R.C. Ebersole, W.R. Hertler, US Patent 4940760A, Group Transfer Polymerization Process Employing Supported Initiators, DuPont 1989.

[40] E. Kassi, M.S. Constantinou, C.S. Patrickios, Group transfer polymerization of biobased monomers, European Polymer Journal 49 (2013) 761.

[41] D.Y. Sogah, W.R. Hertler, O.W. Webster, G.M. Cohen, Group transfer polymerization-polymerization of acrylic monomers, Macromolecules, 20 (1987) 1473.

[42] L. Hu, W. Zhao, J. He, Y. Zhang, Silyl ketene acetals/B (C6F5) 3 lewis pair-catalyzed living group transfer polymerization of renewable cyclic acrylic monomers, Molecules, 23 (2018) 665.

[43] O.W. Webster, The discovery and commercialization of group transfer polymerization, Journal of Polymer Science Part A: Polymer Chemistry, 38 (2000) 2855.

[44] O.W. Webster, W.R. Hertler, D.Y. Sogah, W.B. Farnham, T.V. RajanBabu, Group-transfer polymerization. 1. A new concept for addition polymerization with organosilicon initiators, Journal of the American Chemical Society, 105 (1983) 5706.

[45] Y. Chen, K. Fuchise, T. Satoh, T. Kakuchi, Group transfer polymerization of acrylic monomers. Anionic Polymerization: Principles, Practice, Strength, Consequences and Applications, 2015 pp.451-94.

[46] K. Knoll, N. Nießner, Styrolux+ and styroflex+ - from transparent high impact polystyrene to new thermoplastic elastomers: Syntheses, applications and blends with other styrene based polymers, Macromolecular Symposia, 132 (1998) 231.

[47] L. Xue, U.S. Agarwal, P.J. Lemstra, Shear Degradation Resistance of Star Polymers during Elongational Flow, Macromolecules, 38 (2005) 8825.

[48] D.C. Forman, F. Wieberger, A. Gröschel, A.H. Müller, H.W. Schmidt, C.K. Ober, Comparison of star and linear ArF resists, In Advances in Resist Materials and Processing Technology XXVII, 7639 (2001) 225. International Society for Optics and Photonics.

[49] K. Khanna, S. Varshney, A. Kakkar, Miktoarm star polymers: advances in synthesis, self-assembly, and application, Polymer Chemistry, 1 (2010) 1171.

[50] N. Hadjichristidis, M. Pitsikalis,H. Iatrou, P. Driva, G. Sakellariou, M. Chatzichristidi, 6.03-Polymers with Star-Related Structures: Synthesis, Properties, and Applications, in: K. Matyjaszewski, M. Möller, (Eds.), Polymer science: a comprehensive reference, 2012, pp.29-111.

[51] S. Podzimek, M. Hermannova, H. Bilerova, Z. Bezakova, V. Velebny, Solution Properties of Hyaluronic Acid and Comparison ofSEC-MALS-VIS Data with Off-Line Capillary Viscometry, Journal of Applied Polymer Science,, 116 (2010) 3013.

[52] J.C. Moore, Gel permeation chromatography. I. A new method for molecular weight distribution of high polymers, Journal of Polymer Science Part A: General Papers, 2 (1964) 835.

[53] D. Berek, Size exclusion chromatography–a blessing and a curse of science and technology of synthetic polymers, Journal of separation science, 33 (2010) 315.

[54] H.G. Barth, F.J. Carlin Jr, A review of polymer shear degradation in size-exclusion chromatography, Journal of liquid chromatography, 7 (1984), 1717.

[55] S. Podzimek, C. Johann, Asymmetric flow field-flow fractionation: Current status, possibilities, analytical limitations and future trends, Chromatographia, 84 (2021) 531.

[56] S. Podzimek, Asymmetric flow field flow fractionation In. Encyclopedia of Analytical Chemistry, John Wiley & Sons, Ltd, 2006.

[57] B.H. Zimm, Apparatus and methods for measurement and interpretation of the angular variation of light scattering; preliminary results on polystyrene solutions, The Journal of Chemical Physics, 16 (1948) 1093.

[58] M.A. Haney, The differential viscometer. I. A new approach to the measurement of specific viscosities of polymer solutions, Journal of applied polymer science, 30 (1985) 3023.

[59] S. Podzimek, Molar mass distribution by size exclusion chromatography: Comparison of multi-angle light scattering and universal calibration, Journal of Applied Polymer Science, 136 (2019) 47561.

[60] S. Podzimek, Size Exclusion Chromatography, In Encyclopedia of Polymer Science and Technology, 2022, DOI: 10.1002/0471440264.pst058.pub2.

[61] R. Pinto, G. Monastyreckis, H.M. Aboelanin, V. Spacek, D. Zeleniakiene, Mechanical properties of carbon fibre reinforced composites modified with star-shaped butyl methacrylate, Journal of Composite Materials, 56 (2022) 951.

CHAPTER 2

MONITRING THE CHEMICAL COMPOSITION OF POLYOLEFINS

2.1. Introduction

Polyolefins constitute about 60% of the annual polymer production worldwide [1]. Polyolefins (PO) are of enormous economic importance and the most important ones, polypropylene, and polyethylene, by volume represent most of the total polymer market. Most PO of industrial interest are copolymers, comonomers like (ethylene-propylene-diene-monomer (EPDM), Polypropylene (PP), High-density polyethylene (HDPE), α-olefins [1-3] etc.) are introduced to modify the final material properties from that of the homopolymer [2], and present heterogeneity in their chemical composition, and therefore, they should be also described by their chemical composition distribution (CCD) along with their molar mass distribution (MMD) [4]. Studying the molar mass distribution (MMD), long chain branching, and short chain branching distribution of polyolefins is very important to understand their chemical and physical properties during processing and applications. The catalyst type used in the preparation of polyolefins has an important effect on the final properties of polymers. Metallocene and Ziegler–Natta catalysts have been widely employed for the in-situ polymerization of polyolefins [5]. Polyolefins produced by Metallocene catalysts, also called single-site catalysts, systems have long been claimed to produce polymers with narrow MMD or copolymers with uniform comonomer distribution [6,7] while Polyolefins made with Ziegler–Natta catalysts have non-uniform distributions of molar mass and chemical composition distribution [8].

Basic macromolecular characteristics of polyolefins like molar mass distributions (MMD) information on long-chain branching, can be addressed with high-temperature size-exclusion chromatography (HT-SEC). Hyphenation of infrared detection to size exclusion chromatography (SEC) expands possibilities of SEC even more and allows to reveal comonomer incorporation across molecular weight and thus help in the study of catalytic systems used in polyolefin synthesis. Coupling HT SEC with filter-based infra-red (IR) detector gives an easy and fast access to so-called SCB distribution vs MMD.

In this chapter the new model of the filter-based infra-red (IR5) detector described by Ortin et al. [9–11] was applied for the high-temperature SEC for studying and characterization CCD along the MMD of various polyolefin copolymers.

2.2. Literature review

2.2.1. Polyolefins

Polyolefins, also called polyalkenes, are the largest class of commodity thermoplastics. They are polymers of simple alkenes such as ethylene, propylene, butenes, and pentenes, and copolymers thereof. Polyethylene (PE) and isotactic polypropylene (PP) are the most important of polyolefins and are widely used in our everyday life [12,13]. They can be processed by common forming techniques such as injection molding, blow molding, extrusion and thermoforming, using standard thermoplastic equipment. PE and PP rank as the least expensive polymers to produce and stand out because they are far less toxic compared to many other commodity plastics [14]. Polyethylene was first made as a commercial product in the late 1930s [15], but the polyolefins did not begin their rise to prominence until the 1950s, after Karl Ziegler of Germany and Giulio Natta of Italy developed a series of catalysts (now known as Ziegler-Natta (ZN) catalysts) that made it possible to manufacture the polymers to precise specifications and at low cost [16]. Polyolefins are either produced by a free radical process (Low density polyethylene: LDPE) or using coordination catalysis (Low linear density polyethylene (LLDPE), high density polyethylene (HDPE), and PP).

2.2.2. Characterization of polyolefins

Many properties of polyolefins are determined by the complicated interaction of molecular weight distribution, average chemical composition, and chemical composition distribution. The average chemical composition can be determined by spectroscopic methods (e.g., infrared (IR) and Nuclear Magnetic Resonance (NMR)) and the molecular weight distribution can be analyzed by gel permeation chromatography (GPC) [17]. GPC, also known as size exclusion chromatography (SEC), operated at high temperature, is routinely used for MMD determination, in most cases coupled to multiple on-line detectors [18,19].

Three types of coupling high temperature (HT) SEC to IR detection approaches for PO analysis have been described in literature:

(i) Off-line coupling to Fourier-transform infrared (FTIR), in which the eluent from the GPC is deposited on a rotating germanium disk, and the solid obtained after solvent evaporation is subsequently analyzed off-line by FTIR for branching content [20].

(ii) On-line coupling to FTIR where branching levels in eluent are measured in a heated flow-through cell placed inside an FTIR spectrometer [21–25].

(iii) On-line coupling to a filter-based IR detector [10, 26–28].

The on-line FTIR method mostly used because may have some advantage in sensitivity when liquid nitrogen is used to cool down the detector, although it tends to be less practical than the filter-based IR detector, because it is not fully automated, recalibration is laborious, and data treatment may be complex.

The interaction of both micro structural features (molar mass distribution and chemical composition distribution) is required to fully characterize PO resins by a bivariate MMD x CCD. The techniques based on crystallization (Temperature Rising Elution Fractionation (TREF) [29], Crystallization Analysis Fractionation (CRYSTAF) [30], and Crystallization Elution Fractionation (CEF) [31]), or more recently high temperature interaction chromatographic methods [32–35], are used for CCD analysis. Most comprehensive characterization of the bivariate MMD x CCD requires preparative fractionation, followed by analysis of the fractions by NMR, SEC, TREF, and other techniques. However, these approaches are not always convenient due to the high cost of time, equipment, and other resources [1,36].

2.2.2.1. HT SEC coupling with filter-based IR detector

When applied IR spectroscopy to the characterization of PO, some specific bands help identify and quantify different α-olefins used as a comonomers. In the filter-based IR detector specific narrow band-pass optical interference filters allow the collection of absorbance chromatograms at the methyl and methylene peaks. Even if these absorbance peaks are overlapped, the ratio of methyl over methylene detector signals is approximately proportional to the methyl group frequency in PO.

Studies comparing FTIR and filter-based IR detectors have concluded that both can be used successfully for studying chemical composition heterogeneity along the MMD in PO [25,37]. Coupling of a filter-based IR detector to HT-GPC for the analysis of SCB, as a function of molar mass, results in a very practical alternative to the use of FTIR detectors in both off-line and online modes has been described by Ortín et al [10].

2.3. Experimental

2.3.1. Polymer samples

The polymer samples were obtained from our partners working in universities, research institutes or industry. A part of these samples has been described before (see references in Tables 13–17). Where average molar masses and/or dispersities were not known from previous investigations, they were evaluated based on current SEC-IR5 measurements and are given as polyethylene-equivalent molar masses.

For determinations of reproducibility and the limit of detection, an ethylene/1-butene copolymer sample (Basell, Ludwigshafen, Germany) containing 5.2 wt. % 1-butene was used.

Table 13 Characteristics of ethylene-propylene copolymers synthetized with metallocene catalyst: average chemical composition, weight-average molar mass M_w, dispersity $Đ$.

Content of ethylene [mol %]	M_w **[kg/mol]**	$Đ$	**Reference**
18.6	180	2.0	
33.2	1405	2.1	
42.5	2270	2.0	
45.2	1160	1.9	
48.2	405	3.2	
50.1	2075	2.2	
52.8	755	2.2	[38]
57.8	1530	2.1	
60.5	290	2.2	
63.4	1585	1.9	
65.9	650	2.0	
73.7	2075	1.9	

Table 14 Characteristics of ethylene-propene copolymers synthesized with metallocene catalyst.

Content of ethylene [mol %]	M_w **[kg/mol]**	$Đ$	**Reference**
1.50	166.9	3.8	[39]
6.34	150.2	3.4	
7.90	105.0	4.7	
8.50	124.4	3.9	
13.20	92.9	4.0	
36.00	63.2	4.2	
58.70	83.1	3.8	
77.78	144.4	3.5	
90.53	198.2	3.4	
97.84	370.1	7.0	

Table 15 Characteristics of ethylene-propene copolymers synthesized with ZN catalyst.

Content of ethylene [mol %]	M_w **[kg/mol]**	$Đ$	**Reference**
0.00	652.1	7.4	[39]
5.63	557.3	5.5	
20.57	465.6	6.9	
30.07	503.8	8.4	
43.34	456.9	9.1	

Table 16 Characteristics of ethylene-1-hexene copolymers.

Content of 1-hexene [mol %]	M_w **[kg/mol]**	$Đ$	**Reference**
1.0	160	2.0	[40]
1.2	56	2.0	
1.4	278	2.0	
2.8	58	2.2	
4.3	123	2.2	
5.8	112	2.0	
6.2	280	2.0	
7.0	52	2.1	
8.4	223	2.2	
12.8	24	2.0	

Table 17 Characteristics of ethylene-propylene-2-ethylidene-5-norbornene terpolymers.

ENB [wt. %]	**ethylene [wt. %]**	**propylene [wt. %]**	M_w **[kg/mol]**	$Đ$	**Reference**
0.0	49.2	50.8	332	2.4	[41]
5.2	47.9	46.9	353	2.6	
7.1	50.6	42.3	503	2.7	
9.8	48.2	42.0	394	2.7	
14.5	47.8	37.7	395	2.6	

2.3.2. High-temperature size exclusion chromatography with a filter-based multiple band IR detector (HT SEC-IR5)

HT SEC-IR5 measurements were performed using a PolymerChar GPC-IR® (PolymerChar, Valencia, Spain), equipped with a 200 µL sample loop, at 150 °C. The mobile phase was 1,2,4-trichlorobenzene (TCB) (Across Organics, Schwerte, Germany) containing 0.5 g/L butylhydroxytoluene (BHT, Merck, Darmstadt, Germany). The mobile phase flow rate was 1 mL/min. Three POLEFIN linear XL analytical columns, 300 x 8.0 mm (Polymer Standards Service, Mainz, Germany) were used for the analysis. Detection was performed with a filter-based multiple band IR detector (model IR5-MTC, PolymerChar, Valencia, Spain) featuring a thermoelectrically cooled mercury-cadmium-telluride (MCT) sensor (see Figure 24). The IR5 detector includes two narrow band filters tuned to the adsorption region assigned to $-CH_3$ (at 2960 cm^{-1}) and $-CH_2-$ (2920 cm^{-1}) groups, as well as a broader filter used to collect absorbance from all C-H bonds in a polymer [9,10,26]. The heated flow-through cell volume and the path-length are 13 µL and 1.8 mm, respectively. The cell is equipped with sapphire windows.

The MMD was evaluated using a polystyrene (PS) calibration (EasiCal PS-1, Agilent, Waldbronn, Germany) and WinGPC software version 8 (Polymer Standards Service GmbH, Mainz, Germany). The molar masses of PS standards were transferred to polyethylene (PE) equivalents using the following Mark-Houwink coefficients from the literature: K: 3.8 x 10^{-2} mL/g, α: 0.73 for polyethylene and K: 1.26 x 10^{-2} mL/g, α: 0.702 for poly styrene [42].

For each measurement, approx. 12 mg polymer were automatically mixed with 6 mL mobile phase. Simultaneously, the vials were flushed with nitrogen. Each sample was dissolved under shaking in the autosampler for 1 h at 150 °C before injection.

Figure 24 Photo of high-temperature size exclusion chromatography coupled with a filter-based multiple band IR detector (IR5).

2.4. Results and discussion

2.4.1. SEC-IR5 of ethylene-alkene copolymers

The IR5 detector monitors the presence of methyl and methylene groups, as well as the overall polymer concentration in the eluate [9,26]. The corresponding absorbances change with the elution volume in SEC (Figure 25) and thus with the molar mass of the sample.

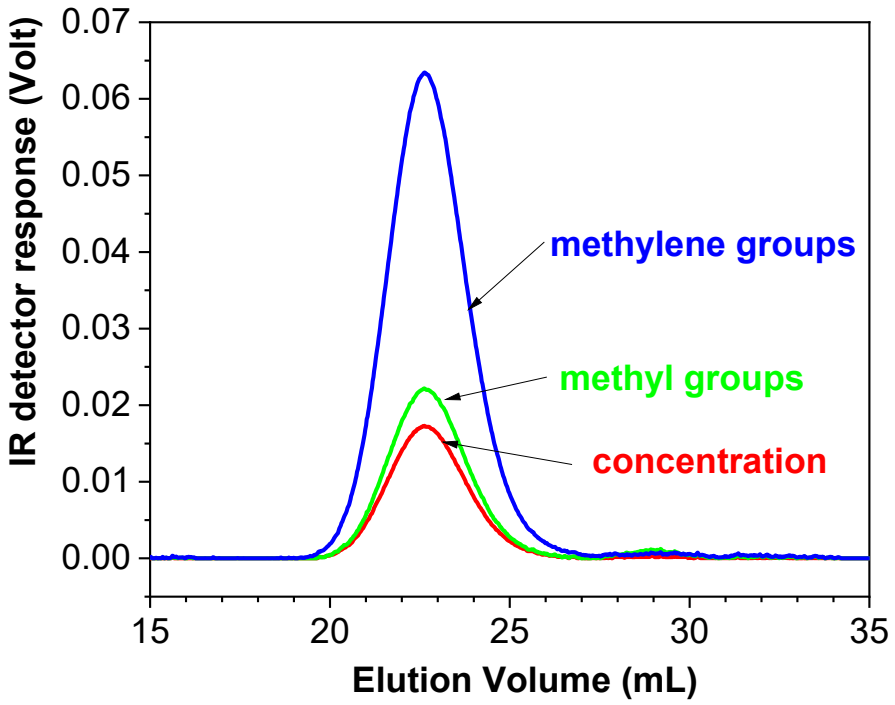

Figure 25 Chromatograms of an ethylene/propylene copolymer containing 52.8 mol % ethylene (Table 13).

The CH_3/CH_2 ratio reflects changes in the chemical composition of a polymer with the elution volume as is illustrated in Figure 26a and b, i.e., it reflects CCD of the polymer along its molar axis (Figure 26c and d). As shown in Figure 26, the baseline and both edges of the peaks yield scattered values CH_3/CH_2 because the signal intensity in these regions is very low (i.e., it is the noise of measurement). Most of the ethylene/propylene (EP) samples (Table 13) exhibit a constant CH_3/CH_2 ratio along the molar mass axis (Figure 26c and d), indicating that most of these samples (Table 13) are chemically homogeneous along the molar mass axis. The EP sample containing 48.2 mol % ethylene shows the largest decrease in the CH_3/CH_2 ratio with increasing molar mass.

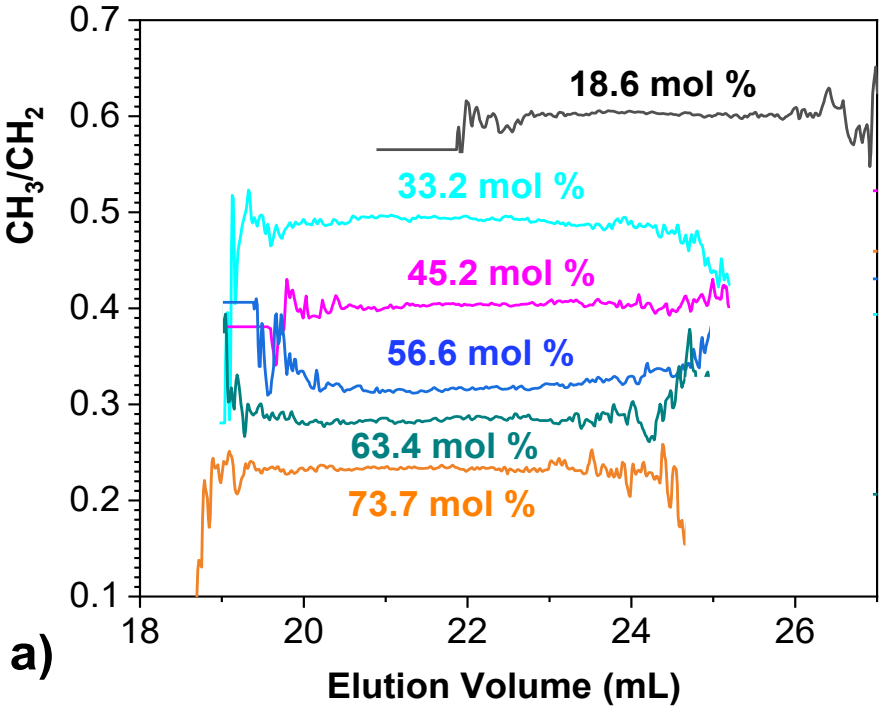
0.7
0.6
0.5
0.4
0.3
0.2
0.1
CH_3/CH_2
18.6 mol %
33.2 mol %
45.2 mol %
56.6 mol %
63.4 mol %
73.7 mol %
18
20
22
24
26
Elution Volume (mL)
a)

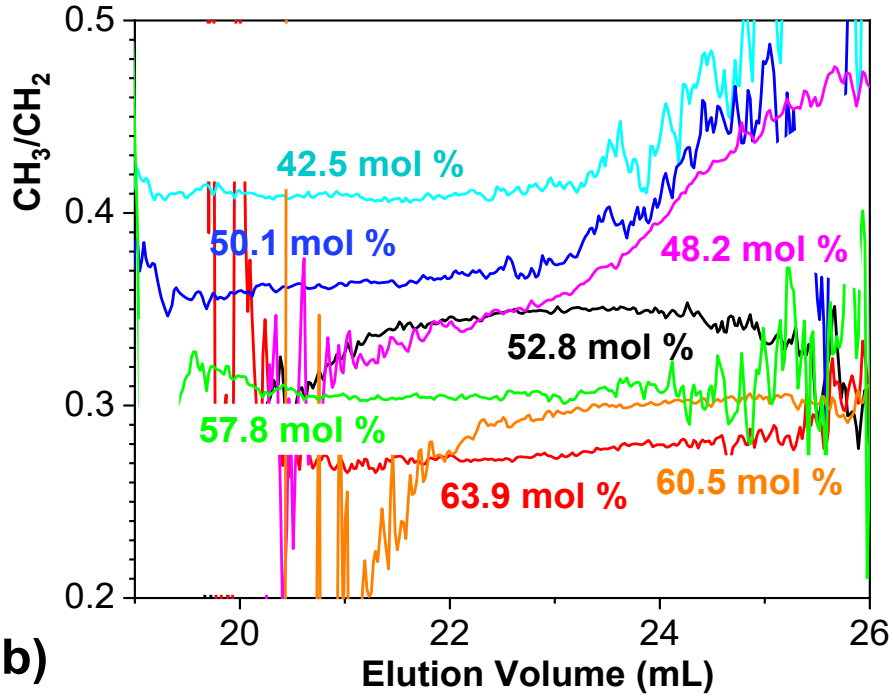
0.5
0.4
0.3
0.2
CH_3/CH_2
42.5 mol %
50.1 mol %
48.2 mol %
52.8 mol %
57.8 mol %
63.9 mol %
60.5 mol %
20
22
24
26
Elution Volume (mL)
b)

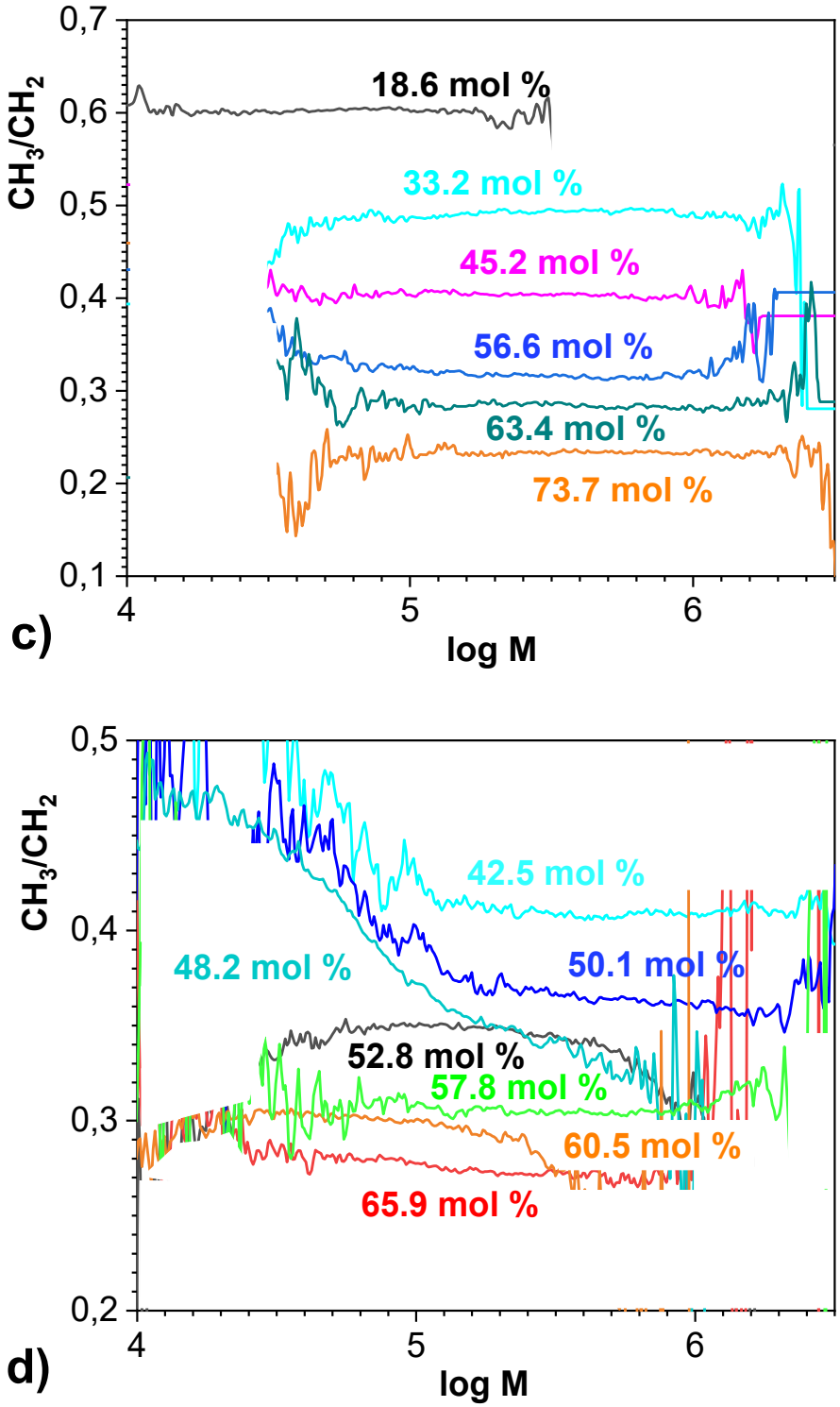

Figure 26 a,b) CH_3/CH_2 ratios as a function of elution volume of ethylene/propylene copolymers (Table 13). c,d) CH_3/CH_2 ratios as a function of equivalent polyethylene (PE) molar mass.

Plotting the CH_3/CH_2 ratios which correspond to the top of the peaks of the elugram against the average chemical composition of the samples enables to obtain a calibration line (Figure 27). The quality of any calibration depends on the chemical homogeneity of the samples. We have deliberately not removed any samples from the series, which were outliers according to the SEC-IR results. In difference to the paper by T. Frijns-Bruls et al. [11], this work will focus on differences in the shape of the CH_3/CH_2 relation.

Surprisingly, the point corresponding to the most chemically nonhomogeneous sample (48.2 mol %, Figure 26b) in this series fits into the linear calibration (Figure 27) quite well. Although the concentration of components was the primary changed parameter in the synthesis, several of the sample's manifest inhomogeneity (especially sample 48.2 mol %) - probably an experimental parameter was not controlled enough throughout the synthesis.

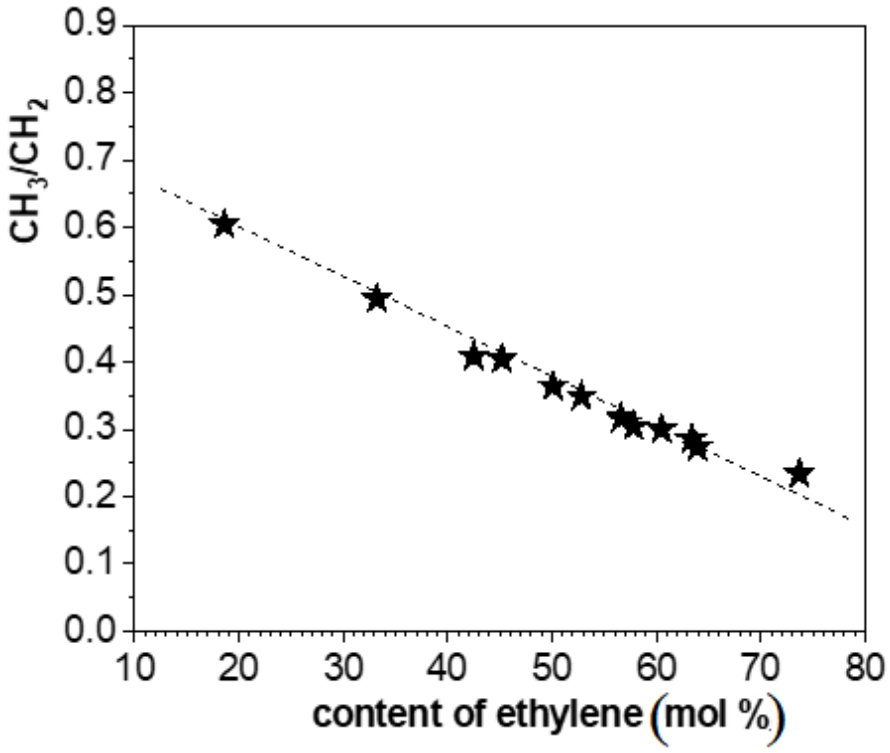

Figure 27 Dependence of CH_3/CH_2 ratio on the average content of ethylene in EP copolymers (Table 13).

Such a calibration line may be used to evaluate changes in the chemical composition distribution. It shows that the chemical composition of the sample with 48.2 mol % ethylene decreases from 59 to 39 mol % with increasing molar mass (Figure 26d), i.e., considerably.

Another type of CH_3/CH_2 profile was found in another series of EP copolymers (Table 14) synthesized also with a metallocene catalyst (Figure 28).

While the EP sample containing 58.3 mol% ethylene shows a substantial decrease in the CH_3/CH_2 ratio with increasing molar mass, the EP sample with 13.2 mol% shows an increasing CH_3/CH_2 ratio (Figure 28). According to the calibration for these copolymer samples (Figure 29), the content of ethylene in the sample with 58.3 mol % decreased from 73 mol % to 52 mol %, while in the sample with 13.2 mol% it increased from 13 mol % to 16 mol% ethylene.

Samples with increasing or decreasing CH_3/CH_2 ratios were found also in other series of EP copolymers as shown in Figure 30a synthesized with metallocene catalysts. While the majority of samples showed a constant or almost constant CH_3/CH_2 ratio, similar deviations were found, as described previously. On the other hand, in some series of EP copolymers synthesized with metallocene catalysts (Figure 30b) all samples had constant or nearly constant CH_3/CH_2 ratios. The CH_3/CH_2 profiles of EP copolymers synthesized with ZN catalysts (Table 15) are shown in Figure 31.

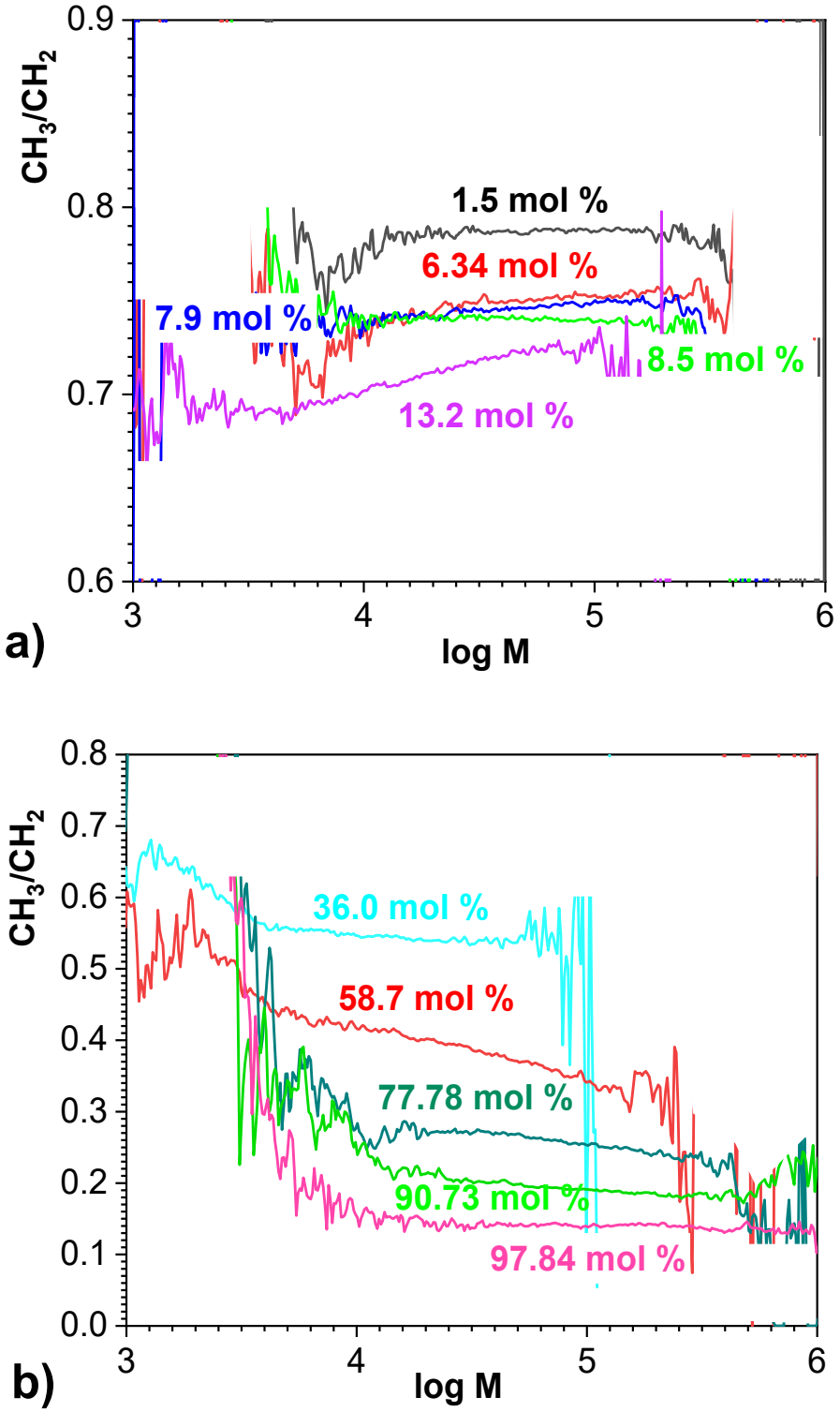

Figure 28 CH_3/CH_2 ratio as a function of equivalent PE molar mass of EP copolymers (Table 14).

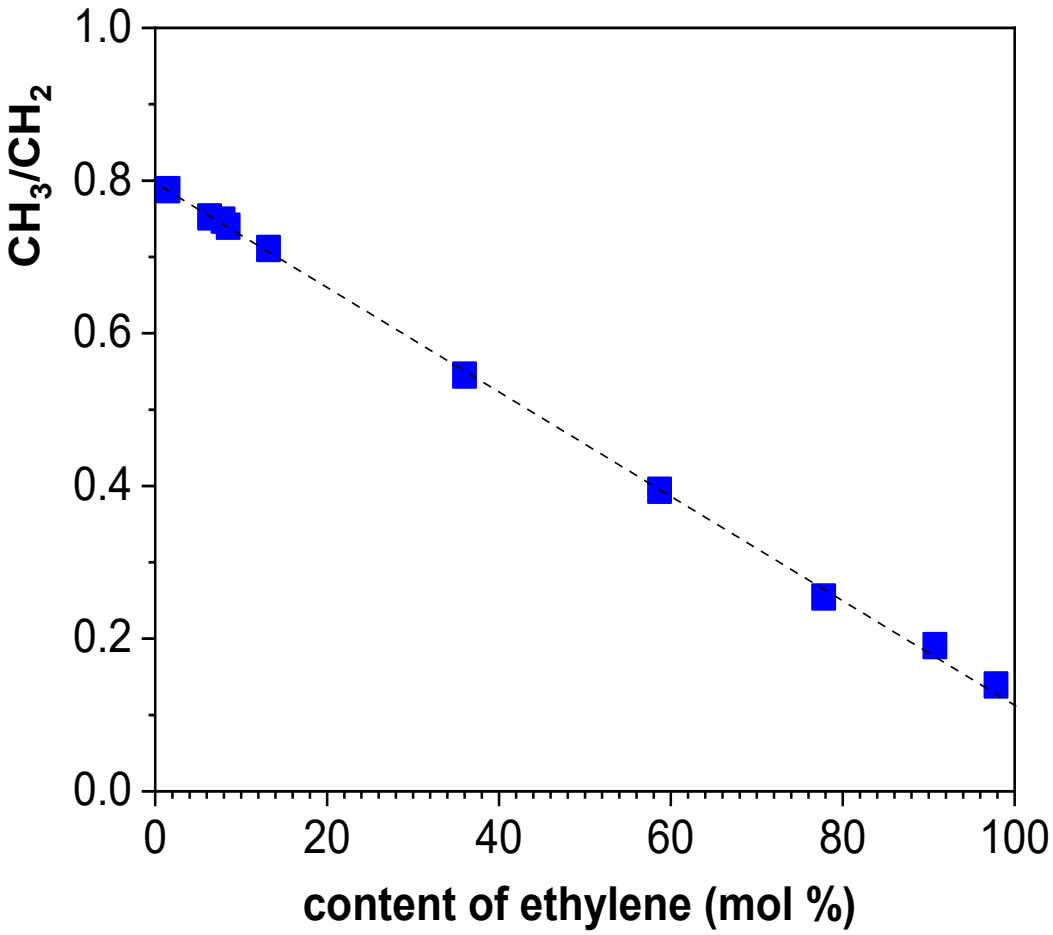

Figure 29 CH_3/CH_2 ratio as function of the average content of ethylene in EP copolymers (Table 14).

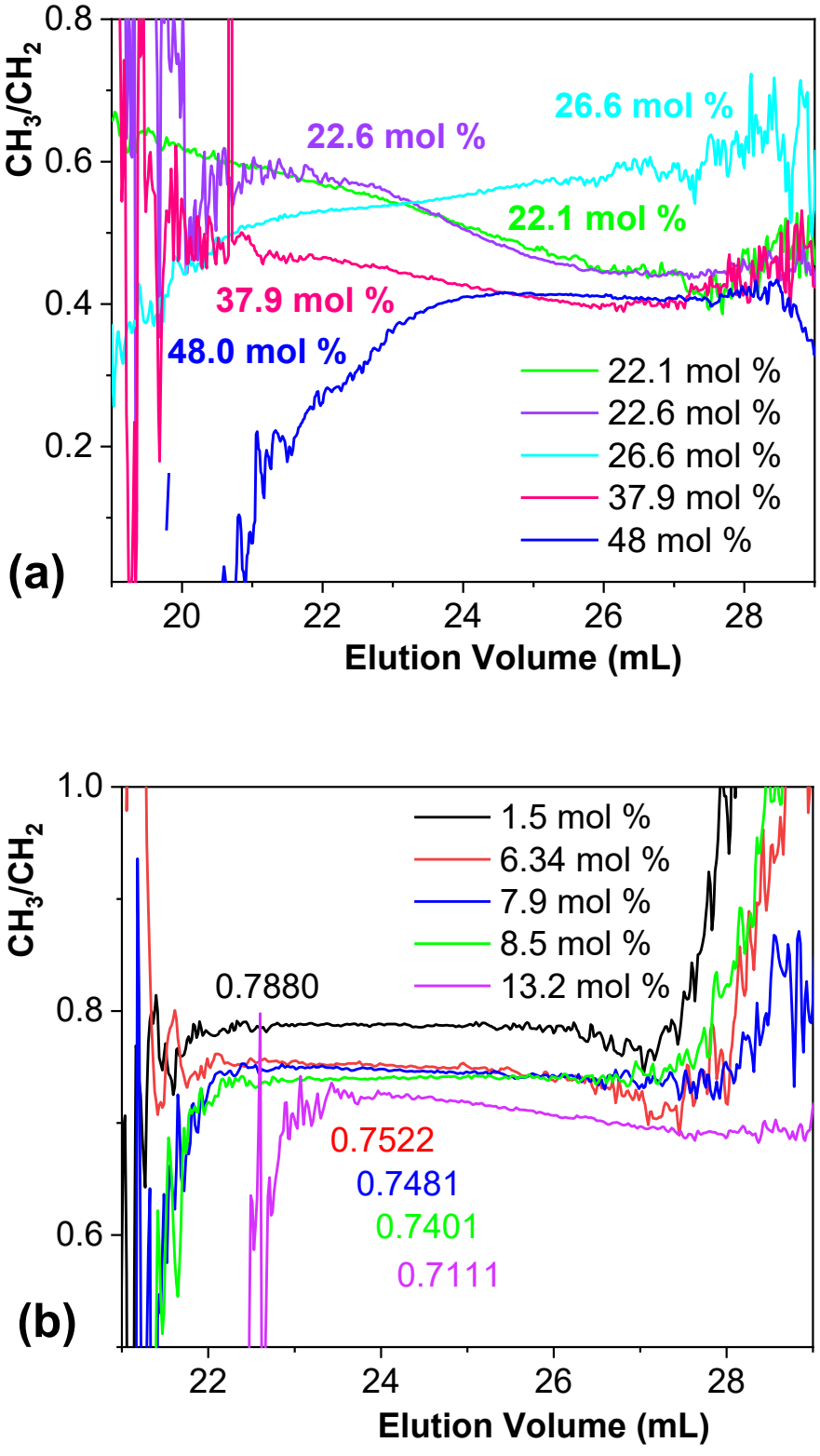

Figure 30 CH_3/CH_2 ratios as a function of elution volume of ethylene/propylene copolymers with a different content of ethylene (mol%) synthesized with metallocene catalysts.

Two samples exhibit almost constant CH_3/CH_2 ratios, the CH_3/CH_2 rations of two samples are decreasing and the EP sample containing 43 wt.% ethylene shows a pronounced increase as well as a decrease of the CH_3/CH_2 ratio. Taking the corresponding calibration (Figure 31b) into account, the ethylene content in the samples with 20 wt. % and 30 wt. % varies in the range of 15 wt. %, while it varies in the range of 25 wt. % in the sample with 43 wt. % ethylene.

Various trends in CH_3/CH_2 profiles were found also for ethylene/1-butene, ethylene/1-hexene and propylene/4-methyl-pentene copolymers. For example, from the plots in Figure 32 shows that the CH_3/CH_2 ratio is decreasing for samples containing 5.8, 7.0 and 12.8 mol % hexene in EH copolymers (Table 16) while the CH_3/CH_2 ratio of the sample with 6.2 mol % hexene is increasing with increasing molar mass. The remaining samples show a homogeneous chemical composition as the CH_3/CH_2 ratio is constant along the molar mass.

Thus Figure 32 is an example of considerable diversity in the CH_3/CH_2 profiles. While samples in the range of 1 – 4 mol % 1-hexene exhibit flat profiles, the CH_3/CH_2 ratio of samples containing 6.2 and 8.4 mol % 1-hexene increases and the CH_3/CH_2 ratio of samples containing 5.8, 7.0 and 12.8 mol % 1-hexene decreases. The sample containing 12.8 mol % is the most inhomogeneous (composition between 8 and 15 mol % 1-hexene). The chemical inhomogeneity of the samples is apparently the reason for the substantial scattering of data points around the calibration line in Figure 32b. This substantially decreases the quality of the calibration curves in comparison to previously reported ones (e.g., Frijns-Bruls et al. [11]). Considering the calibration line, the ethylene content in the sample containing 12.8 mol % ethylene decreases from 20 mol % to 9 mol % with increasing molar mass, while in the sample containing 6.2 mol % ethylene it increases from 7 mol % to 17 mol %. These are substantial changes in the 1-hexene content along the molar mass axis.

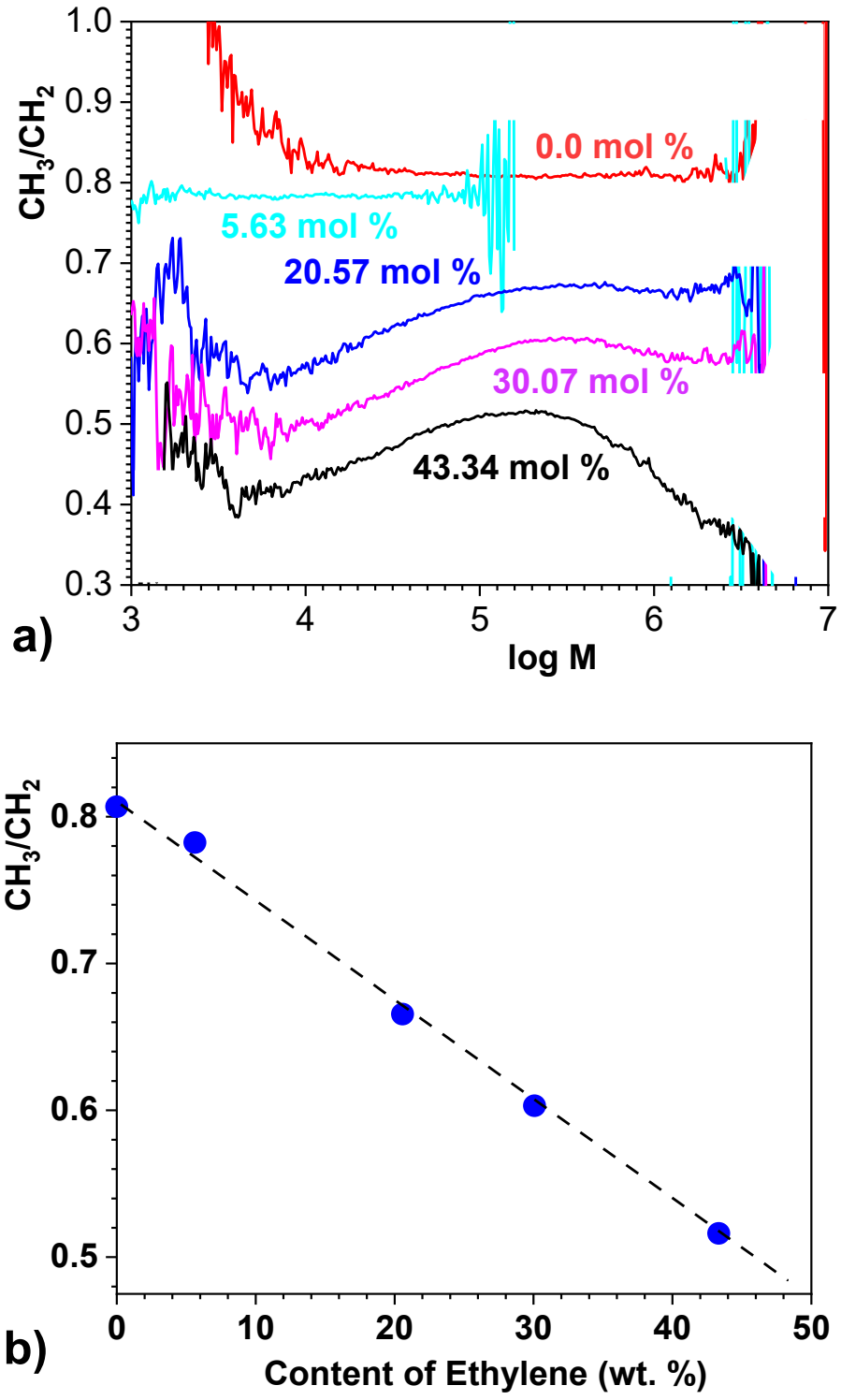

Figure 31 a) CH_3/CH_2 ratio as function of equivalent PE molar mass, b) CH_3/CH_2 ratio as function of the average content of ethylene in EP copolymers (Table 15).

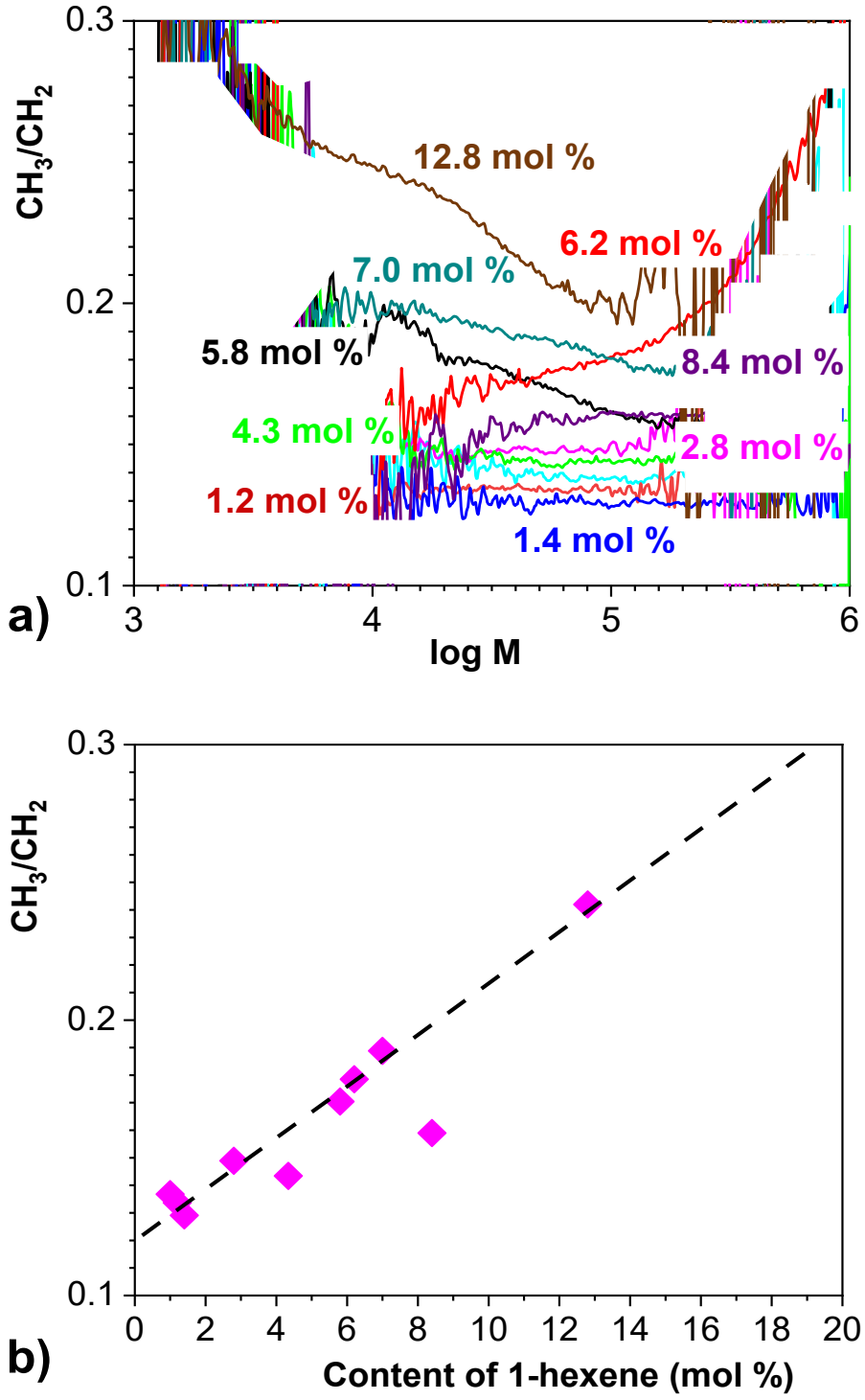

Figure 32 a) CH_3/CH_2 ratio as function of equivalent PE molar mass. b) CH_3/CH_2 ratio of the top of peaks as function of the average content of ethylene in ethylene/1-hexene copolymers (Table 16).

An overlay of calibrations, as created from the provided data regarding the average composition of EP and EH samples, is shown in Figure 33.

The majority of points fall onto the same line, but the calibration line of one set of EP copolymers is shifted. A disagreement found in the past for other series of copolymers when data were provided by different laboratories. Due to significant differences in ethylene content for the same CH_3/CH_2 ratio (a difference of 10 mol % ethylene) the ethylene content presented by Chitta et al. [43] should be evaluated again.

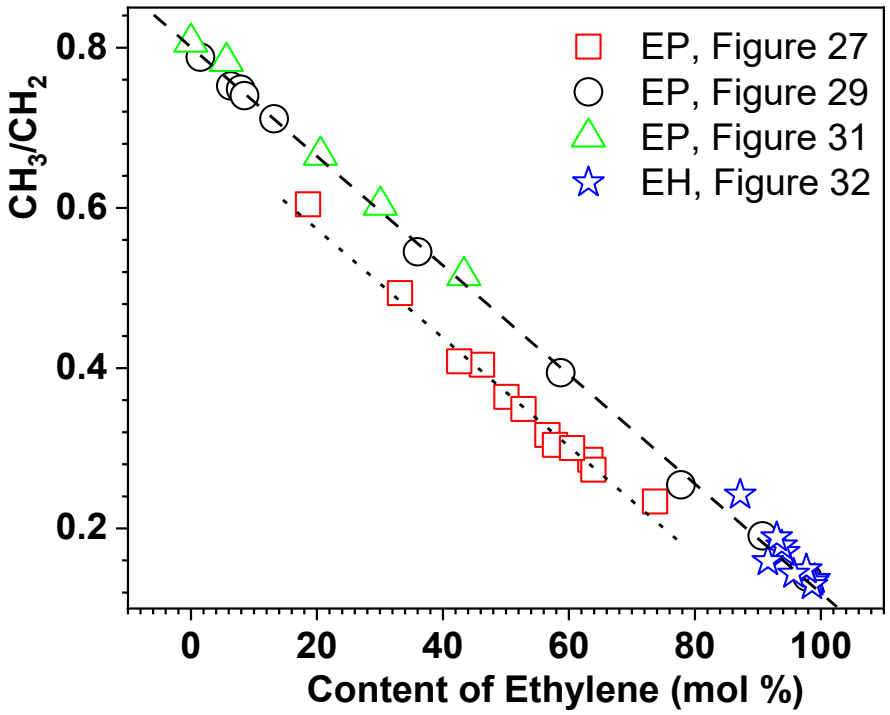

Figure 33 CH_3/CH_2 ratio at the top of the peaks as a function of the average content of ethylene in ethylene/propene and ethylene/1-hexene copolymers.

The conclusion is that EP copolymers prepared with metallocene catalysts yield more homogeneous CH_3/CH_2 profiles than EP samples prepared with ZN catalysts. However, in both groups, examples of profiles indicating SCB distribution inhomogeneity along the molar mass axis were found. Similarly, CH_3/CH_2 profiles were constant or increased or decreased with the increase of molar mass for series of EB and EH copolymers. Such nonhomogeneous samples may mix randomly with homogeneous samples or there may be a systematic trend, this may be related to experimental parameters, which were eventually not sufficiently controlled during the synthesis of the samples. Consequentially, the incorporation of comonomers changed with the molar mass of the copolymers – as shown, often substantially. When CH_3/CH_2 ratios are

not monitored, then these trends may not be recognized. If they were recognized, it could help to increase the quality (homogeneity) of the synthesized copolymers.

2.4.2. SEC-IR5 of ethylene-propylene-diene terpolymers

Tackx and Bremmers [44] have shown that SEC-FTIR using the LC-Transform approach enables profiling the distribution of methyl and diene along the molar mass in ethylene-propylene-diene (EPDM) samples. SEC-IR5 was applied for the analysis of 6 EPDM samples (Table 17) and the ratios of CH_3/CH_2 of ethylene-propene-ethylidene-norbornene are shown in Figure 34a. An almost constant ratio of CH_3/CH_2 indicates homogeneity in most of these polymer samples. Only the EPDM sample containing 5.2 wt. % ENB manifests a drift in composition along the molar mass axis (Figure 34a).

Although the plot in Figure 34a indicates that the majority of the samples is chemically homogeneous (except with the one containing 5.2 wt.% ENB), the CH_3/CH_2 ratio corresponding to the top of the peaks did not correlate linearly with either the average chemical composition of the EPDM (Figure 34b) nor with the average ethylene or propylene content. Apparently, the specific IR response of the diene must be taken into account, because the CH_3/CH_2 ratio does not reflect the presence of any monomer in EPDM alone. Thus, a linear calibration could not be established. However, the chemical inhomogeneity of the sample with 5.2 wt.% ENB is reflected in the CH_3/CH_2 profile. An independent HPLC measurement showed [45] that just this particular sample exhibits a bimodal CCD. As shown, SEC-IR5 may reveal such a sample.

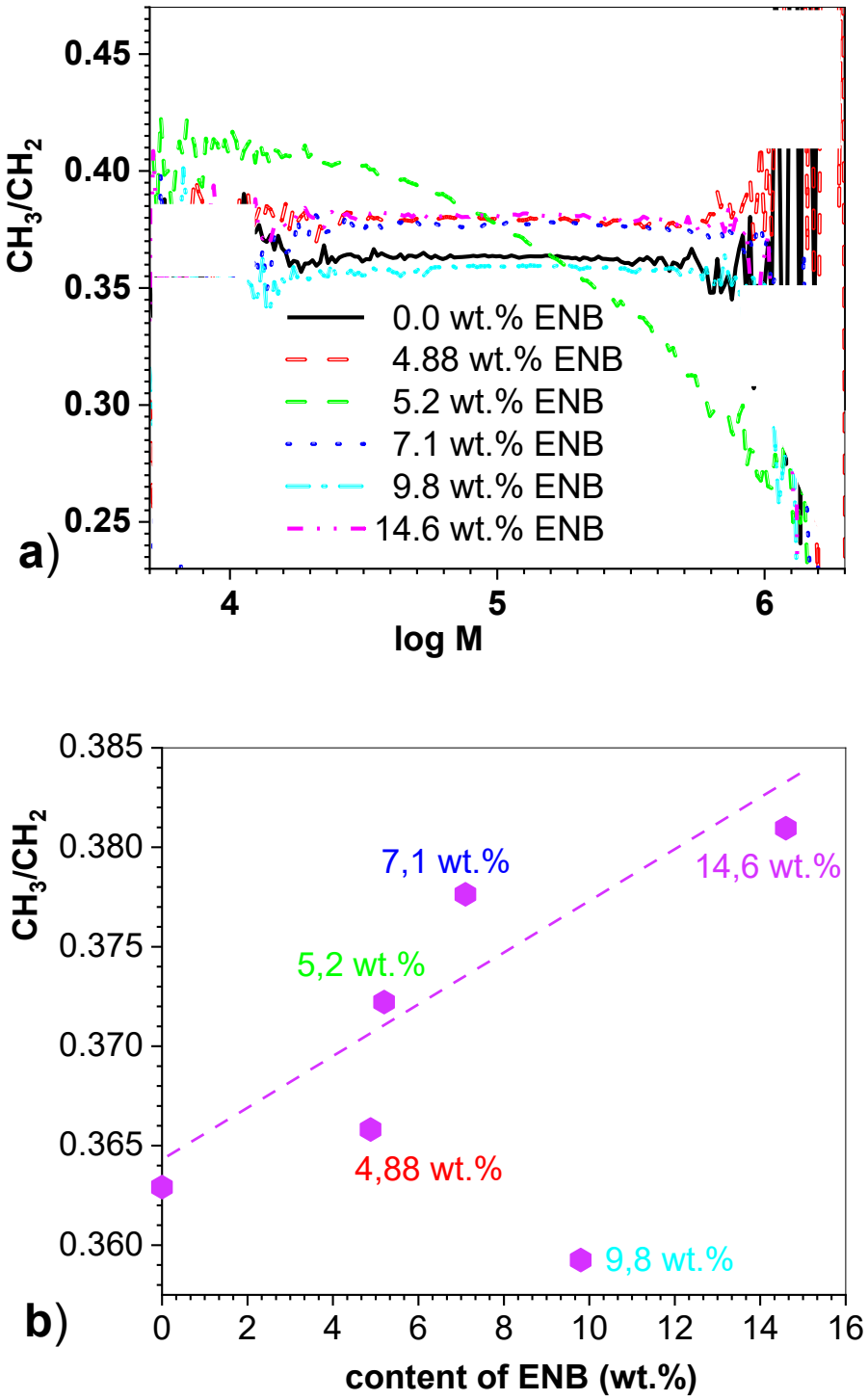

Figure 34 a) CH_3/CH_2 ratio of EPDM terpolymers (Table 5) as a function of the equivalent PE molar mass). b) Relation between CH_3/CH_2 ratio of EPDM terpolymers and the average content of ENB.

2.4.3. Repeatability, dependence on concentration and limit of detection

With the aim to check the quality of measurements with the IR5-detector, 10 solutions of an ethylene/1-butene copolymer sample were prepared and. The solutions were prepared in similar concentrations (~1.0 and ~5.0 mg/mL). Moreover, solutions with the identical concentration (1 and 5 mg/mL) were injected. The CH_3/CH_2 ratios corresponding to all measurements were calculated and the results are illustrated in Figure 35.

Figure 35 shows that reproducibility of the measurements was smaller at smaller concentration and increased with increasing concentration. The noise in the data influences reproducibility of the IR5-measurements to a larger extent at smaller concentrations compared to larger concentrations. That is because the signal-to-noise ratio increases at higher concentrations. A comparison of Figure 26a–d confirm that small variations of the concentration do not influence the reproducibility substantially.

Injections of 10 solutions with different concentrations of the ethylene/1-butene sample exhibited linear dependences between the IR response and the polymer concentration, as illustrated in Figure 36.

Taking the base line noise of the recorded IR5-concentration signal into account, the limit of detection (defined as 3 x noise) was calculated for the tested polymer sample (Table 18). The obtained results confirm high reproducibility, linear response, and suitable detection limit of the IR5-detector. The obtained results are similar to those obtained with different polymer samples by Ortin et al. [9]. Data confirm that changes in the CH_3/CH_2 profiles, which were described above, are many times larger than errors connected to the SEC-IR5 measurements.

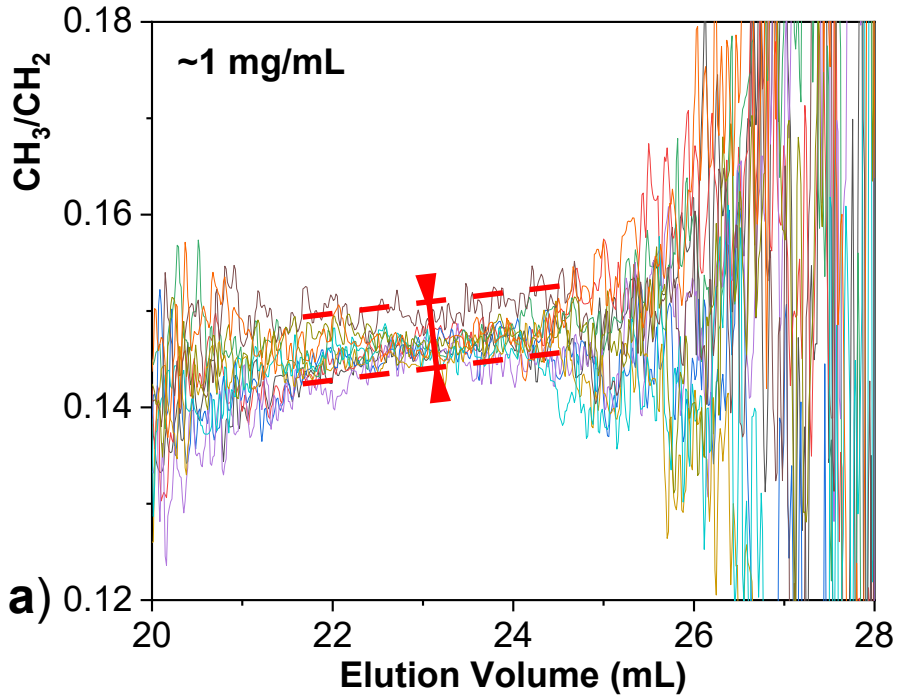
~1 mg/mL
CH_3/CH_2
0.18
0.16
0.14
0.12
a)
20
22
24
26
28
Elution Volume (mL)

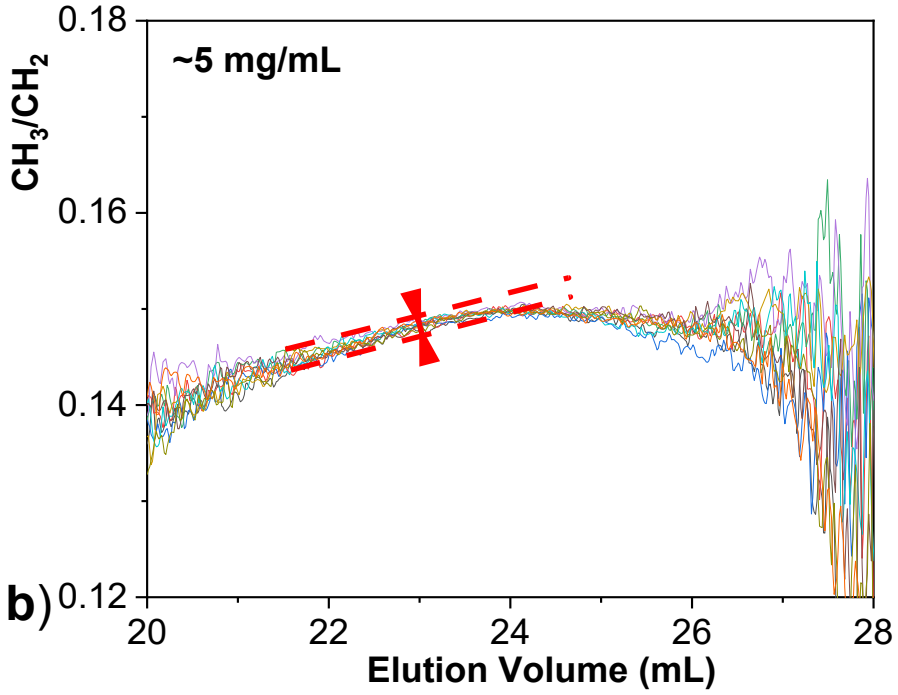
~5 mg/mL
CH_3/CH_2
0.18
0.16
0.14
0.12
b)
20
22
24
26
28
Elution Volume (mL)

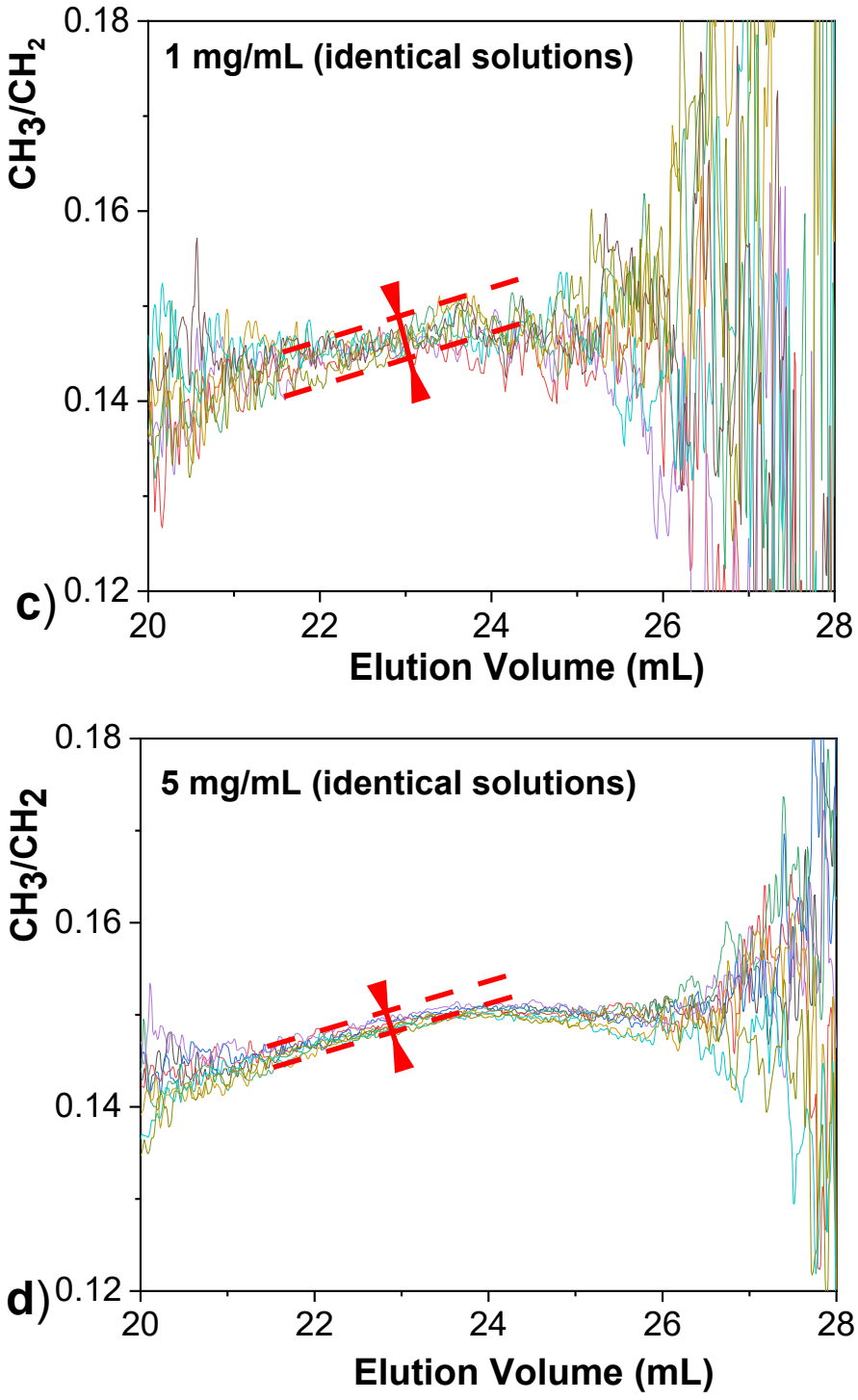

Figure 35 Ratio CH_3/CH_2 obtained after SEC-IR5 analysis of 10 solutions of ethylene/1-butene containing 5.2 wt.% of 1-butene.

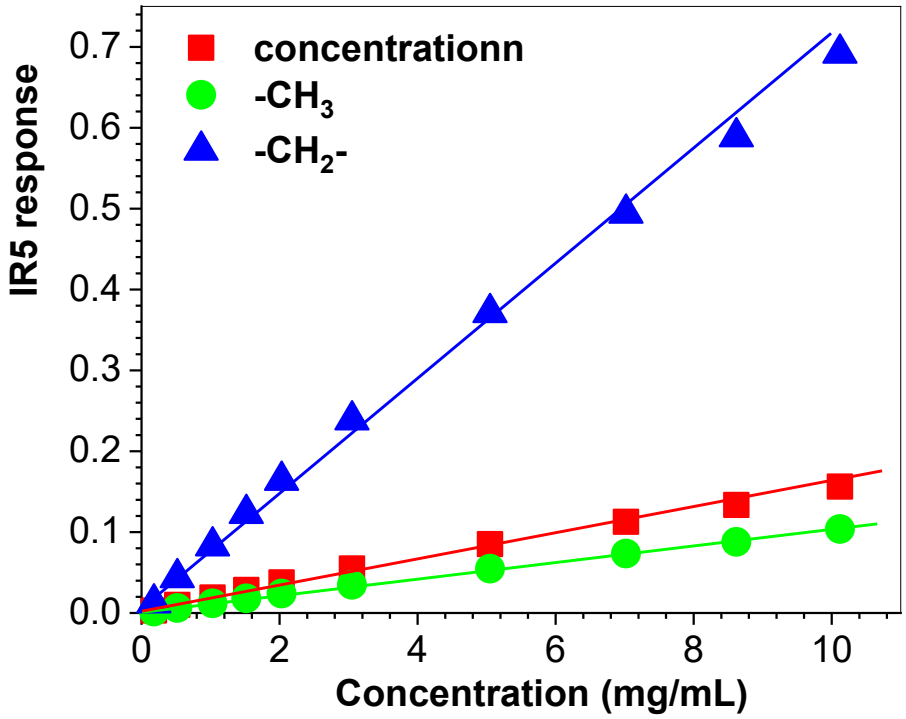

Figure 36 IR5 responses obtained after SEC-IR5 analysis of 10 solutions of EB (5.2 wt.% 1-butene) with different concentrations.

Table 18 Reproducibility and limit of detection data for the IR5.

Sample	Mean (CH_3/CH_2)	Standard deviation (CH_3/CH_2)	Limit of detection (mg/ mL)	Linearity (R^2) of concentration dependence
EB (5.2 wt. % 1-butene)	0.14483	0.000638	0.09	0.997

2.5. Conclusion

This chapter shows that the high temperature SEC-IR (with a filter-based infrared detector model IR5, PolymerChar, Valencia, Spain) technique is a powerful tool for monitoring the CCD as a function of the molar mass of various polyolefins. The monitoring of methyl and methylene groups can be performed as part of routine SEC measurements. Thus, in addition to the MMD, the CCD along the molar mass axis can be determined for many polyolefin materials.

It was found that the ratio of the IR signals that correspond to methyl and methylene groups (CH_3/CH_2 ratio) along the molar mass axis of a polymer sample may be constant, increasing or decreasing with increasing molar mass. In some samples, first an increase and at lower molar masses a decrease was found. Such variations in CH_3/CH_2 profiles were found even within individual series of copolymers that were prepared with the same catalyst, including metallocene catalysts, which usually produce chemically very homogeneous polymers. It is hypothesized that one or several experimental parameters, which were eventually not strictly controlled during polymer synthesis, may cause such changes in CCD along the molar mass axis. Consequentially, some samples in a series exhibit different CH_3/CH_2 profiles. Monitoring the CH_3/CH_2 ratio through SEC measurements was, however, seldom performed in the past. That means the modern instrumentation can even change the generally accepted idea of molecular structure of industrial polyolefins.

As it is illustrated in this work, the advanced HT SEC-IR5 instrument enables to reveal inhomogeneities in CCD of polyolefins and thus the HT SEC-IR technique is a useful tool for evaluating and understanding the molecular structure of polyolefins.

2.6. References

[1] T.J. Hutley, M. Ouederni, Polyolefin compounds and materials: fundamentals and industrial applications "Polyolefins—The History and Economic Impact", M. Al-Ali AlMa'adeed, I. Krupa (Eds.), Springer International Publishing, 2016, ch2. https://doi.org/10.1007/978-3-319-25982-6_2

[2] A. Faldi, J.B.P. Soares, Characterization of the combined molecular weight and composition distribution of industrial ethylene/a-olefin copolymers, Polymer, 42 (2001) 3057.

[3] N. Luruli, T. Pijpers, R. brüll, V. Grumel, H. Pasch, V. Mathot, Fractionation of Ethylene/1-Pentene Copolymers Using a Combination of SEC-FTIR and SEC-HPer DSC, Journal of Polymer Science: Part B: Polymer Physics, 45 (2007) 2956.

[4] S. Anantawaraskul, J.B.P. Soares, P.M. Wood-Adams, Chemical composition distribution of multicomponent copolymer chains, Macromolecular Symposia, 206 (2004) 69.

[5] C. Vasile [Ed.], Handbook of polyolefins, CRC press, 2000.

[6] W. Kaminsky, The discovery of metallocene catalysts and their present state of the art, Journal of Polymer Science Part A: Polymer Chemistry, 42 (2004) 3911.

[7] W. Kaminsky, G. Schupfner, Defined synthesis of copolymers using metallocene catalysis, Macromolecular Symposia, 177 (2002) 61.

[8] A.A. Alghyamah, J.B.P. Soares, Simultaneous deconvolution of the bivariate distribution of molecular weight and chemical composition of polyolefins made with Ziegler-Natta catalysts, Macromolecular rapid communications, 30 (2009) 384.

[9] A. Ortín, E. Lopez, B. Monrabal, J.R. Torres-Lapasió, M.C. García-Álvarez-Coque, Filter-based infrared detectors for high temperature size exclusion chromatography analysis of polyolefins: Calibration with a small number of standards and error analysis, Journal of Chromatography A, 1257 (2012) 66.

[10] A. Ortín, J. Montesinos, E. López, P. del Hierro, B. Monrabal, J.R. Torres-Lapasió, M.C. García-Álvarez-Coque, Characterization of Chemical Composition along the Molar Mass Distribution in Polyolefin Copolymers by GPC Using a Modern Filter-B ased IR Detector, Macromolecular Symposia, 330 (2013) 63.

[11] T. Frijns-Bruls, A. Ortin, J. Weusten, E. Gelade, Studies on the use of filter-based IR detector for short-chain branching characterization of polyolefin copolymers with high temperature size exclusion chromatography, Polymer, 180 (2019) 121600.

[12] C. Vasile, (Ed.), Handbook of polyolefins, CRC press, 2000.

[13] J.R. Severn, J.C. Chadwick, (Eds.) Tailor-Made Polymers: via immobilization of alpha-olefin polymerization catalysts, Wiley-VCH Verlag GmbH & Co. KGaA: Weinheim, Germany, 2008.

[14] M.D. Tabone, J.J. Cregg, E.J. Beckman, A.E. Landis, Sustainability metrics: life cycle assessment and green design in polymers, Environmental science & technology, 44 (2010) 8264.

[15] K.S. Whiteley T.G. Heggs, H. Koch, R.L. Mawer, W. Immel, (Eds.), Ullmann's Encyclopedia Ind. Chem., Polyolefins, Wiley-VCH Verlag GmbH & Co. KGaA, Weinheim, 2005. DOI:10.1002/14356007.a21487.

[16] W. Kaminsky, Polyolefins: 50 Years After Ziegler and Natta. II., Berlin Heidelberg: Springer, 258, 2013.

[17] S.M. Graef, R. Brüll, H. Pasch, U.M. Wahner, Monitoring the chemical heterogeneity of metallocenecatalysed copolymers of ethylene and higher 1-olefins using CRYSTAF and SEC-FTIR, e-Polymers, 3 (2003) 005.

[18] A.M. Striegel, W.W. Yau, J.J. Kirkland, D.D. Bly, Modern Size-Exclusion Liquid Chromatography, 2nd ed., Wiley, New York, 2009.

[19] A.M. Striegel, [Ed.], Multiple Detection in Size Exclusion Chromatography, American Chemical Society, Washington, 2004.

[20] J.N. Willis, J.L. Dwyer, X. Liu, W.A. Dark, In: Chromatography of Polymers: Hyphenated and Multidimensional Techniques, T. Provder, [Ed.], ACS Symposium Series, Vol. 731, American Chemical Society, Washington, 1999, pp. 226–231.

[21] T. Housaki, K. Satoh, K. Nishikida, M. Morimoto, Gel permeation chromatography—Fourier transform infrared study of some synthetic polymers: II. Instrumentation for the characterization of polyethylene, Journal of Chromatography A, 517 (1990) 209.

[22] P.J. DesLauriers, D.C. Rohlfing, E.T. Hsieh, Quantifying short chain branching microstructures in ethylene 1-olefin copolymers using size exclusion chromatography and Fourier transform infrared spectroscopy (SEC–FTIR), 43 (2002) 159.

[23] P.J. DesLauriers, In: Multiple Detection in Size Exclusion Chromatography, A.M. Striegel, (Ed.), ACS Symposium Series, Vol. 893, American Chemical Society, Washington, 2005, pp. 210–229.

[24] Z. Zhang, R. Saetre, Characterization of styrene copolymers using size-exclusion chromatography with on-line FT-IR viscometer detectors, International Journal of Polymer Analysis and Characterization, 12 (2007) 185.

[25] C. Piel, A. Albrecht, C. Neubauer, C. W. Klampfl, J. Reussner, Improved SEC-FTIR method for the characterization of multimodal high-density polyethylenes, Analytical and bioanalytical chemistry, 400 (2011) 2607.

[26] A. Ortín, B. Monrabal, J. Montesinos, M.P. del Hierro, Application of a Multiple Linear Regression Model to Fixed Bands IR Detector Data in GPC-IR Analysis of Polyolefins, Macromolecular symposia, 282 (2009) 65.

[27] I. Suárez, B. Coto, GPC-VIS-MALS study of EVA copolymers: Quantification and interactions of SCB and LCB, Polymer Testing, 52 (2016)265.

[28] I. Suárez, M.J. Caballero, B. Coto, A fast and reliable procedure to determine the copolymer composition by GPC-IR: Application to ethylene/propylene copolymers and comparison with 13C NMR, Polymer Engineering & Science, 51 (2011) 317.

[29] B. Monrabal, In Encyclopedia of Analytical Chemistry, A. Robert Meyers, (Eds.), Wiley, New York, 2000, pp. 8074–8094.

[30] B. Monrabal, Crystallization analysis fractionation: a new technique for the analysis of branching distribution in polyolefins, Journal of applied polymer science, 52 (1994) 491.

[31] B. Monrabal, J. Sancho-Tello, N. Mayo, L. Romero, Crystallization elution fractionation. A new separation process for polyolefin resins, Macromolecular symposia, 257 (2007) 71.

[32] T. Macko, R. Brüll, R.G. Alamo, Y. Thomann, V. Grumel, Separation of propene/1-alkene and ethylene/1-alkene copolymers by high-temperature adsorption liquid chromatography, Polymer, 50 (2009) 5443.

[33] T. Macko, R. Brüll, Y. Zhu, Y. Wang, A review on the development of liquid chromatography systems for polyolefins." Journal of Separation Science, 33 (2010) 3446.

[34] R. Cong, A.W. DeGroot, A. Parrott, W. Yau, L. Hazlitt, R. Brown, M. Miller, Z. Zhou, A new technique for characterizing comonomer distribution in polyolefins: high-temperature thermal gradient interaction chromatography (HT-TGIC), Macromolecules, 44 (2011) 3062.

[35] B. Monrabal, N. Mayo, R. Cong, Crystallization elution fractionation and thermal gradient interaction chromatography. Techniques comparison, Macromolecular Symposia, 312 (2012) 115.

[36] M. Vadlamudi, G. Subramanian, S. Shanbhag, R.G. Alamo, M. Varma-Nair, D.M. Fiscus, G.M. Brown, C. Lu, C.J. Ruff, Molecular Weight and Branching Distribution of a High Performance Metallocene Ethylene 1-Hexene Copolymer Film-Grade Resin, Macromolecular symposia, 282 (2009) 1.

[37] S. Deshmukh, J.H. Arndt, T. Macko, R. Brüll, Characterization of Unsaturated Polymers Using High-Temperature Size Exclusion Chromatography Coupled with Ultraviolet-Evaporative Light Scattering Dual Detection, Macromolecular Symposia, 409 (2023) 2200159.

[38] R. Chitta, T. Macko, R. Brüll, G. van Doremaele, L.C. Heinz, Separation of ethylene-propylene copolymers and ethylene-propylene-diene terpolymers using high-temperature interactive liquid chromatography, Journal of Polymer Science Part A: Polymer Chemistry, 49 (2011) 1840.

[39] Data obtained from Dr. B. Coto, University of Madrid, Spain.

[40] T. Macko, R. Brüll, R. G. Alamo, F.J. Stadler, S. Losio, Separation of short-chain branched polyolefins by high-temperature gradient adsorption liquid chromatography. Analytical and bioanalytical chemistry, 399 (2010) 1547.

[41] S. Deshmukh, T. Macko, J.H. Arndt, B. Barton, R. Bernardo, G. van Doremaele, R. Brüll, Solvent Selection for Liquid Adsorption Chromatography of Ethylene–Propylene–Diene Terpolymers by Combining Structure–Retention Relationships and Hansen Solubility Parameters, Industrial & Engineering Chemistry Research, 61 (2022) 5672.

[42] S. Mori, H.G. Barth, Size Exclusion Chromatography, Springer, Berlin, 1999.

[43] R. Chitta, T. Macko, R. Brüll, G. van Doremaele, L.C. Heinz, Separation of ethylene-propylene copolymers and ethylene-propylene-diene terpolymers using high-temperature

interactive liquid chromatography, Journal of Polymer Science Part A: Polymer Chemistry, 49 (2011) 1840.

[44] P. Tackx, S. Bremmers, Chemical composition disribution of polyolefins by SEC-FTIR, Polymeric Materials Science and Engineering (USA), 78 (1998) 50.

[45] S. Deshmukh, T. Macko, J.H. Arndt, F. Malz, R. Bernardo, S. Niessen, G. van Doremaele, R. Brüll, Critical conditions for liquid chromatography of statistical polyolefins: Evaluation of diene distribution in EPDM terpolymers, Analytica Chimica Acta, 1246 (2023) 340856.